In vitro metabolism and drug-drug interaction potential of irosustat, a steroidal sulfatase inhibitor

Verònica Ventura Ventanachs

FACULTAT DE FARMÀCIA

DEPARTAMENT DE BIOQUÍMICA I BIOLOGIA MOL·LECULAR

IN VITRO METABOLISM AND DRUG-DRUG INTERACTION POTENTIAL OF IROSUSTAT, A STEROIDAL SULFATASE INHIBITOR

VERÒNICA VENTURA VENTANACHS, 2013

FACULTAT DE FARMÀCIA

DEPARTAMENT DE BIOQUÍMICA I BIOLOGIA MOL·LECULAR

PROGRAMA DE DOCTORAT DE BIOTECNOLOGIA

IN VITRO METABOLISM AND DRUG-DRUG INTERACTION POTENTIAL OF IROSUSTAT, A STEROIDAL SULFATASE INHIBITOR

Memòria presentada per Verònica Ventura Ventanachs per optar al títol de doctor per la Universitat de Barcelona

Directors de Tesi:

Dr. Josep Solà Vidal Dra. Concepció Peraire Guitart

Doctoranda: Verònica Ventura Ventanachs

VERÒNICA VENTURA VENTANACHS, 2013

Vull expressar el meu agraïment als meus directors de tesi. Al Josep, pel seu suport i per haver-me ensenyat tot el que hi ha en aquesta tesi i molt més. I a la Conxita, pel seu recolzament i ajuda en tot el que he necessitat.

Als laboratoris Ipsen Pharma, S.A., on he pogut realitzar tota aquesta feina rodejada de gent estupenda i amb una gran qualitat tant professional com personal. Especialment als meus companys de feina, i sobretot a la Mari i la Cristina, pel seu ajut tècnic i la seva amistat.

A Ipsen Group per autoritzar-me a presentar aquesta tesi i a publicar els articles relacionats.

També al departament de Bioquímica i Biologia Molecular de la Facultat de Farmàcia, especialment a la Pepita Badia, on tot i haver realitzat la tesi fora del departament, sempre he trobat el suport que he necessitat.

I per suposat, vull expressar també el meu agraïment:

Als meus pares, pel seu gran amor incondicional i per saber educar-me tan bé amb l'esperit de responsabilitat, treball, constància i superació que m'ha ajudat tant en tots els aspectes de la meva vida, incloent la presentació d'aquesta tesi.

Al Juan, l'amor de la meva vida, qui m'ha ensenyat a estimar i a ser estimada. Gràcies per entendre'm i recolzar-me sempre tant a nivell personal com professional.

A la Isona, la meva vida, el millor que he pogut fer fins ara. Espero que algun dia es senti orgullosa de la seva mare.

A la resta de la família, tot i que diuen que no es pot triar, no em podria haver tocat cap de millor.

I també als meus amics, que encara que últimament cada vegada tenim menys temps per reunir-nos sempre trobem un forat per quedar i xerrar. Gràcies per fer-me sempre costat.

TABLE OF CONTENTS

ABBREVIATIONS

17β-HSD	17β-hydroxysteroid dehydrogenase
ß-NADP	ß-Nicotinamide adenine dinucleotide phosphate
ACN	Acetonitrile
AhR	Aryl hydrocarbon receptor
AI	Aromatase inhibitor
AIC	Akaike criteria
AUC	Area under the curve
BLQ	Below limit of quantification
BSA	Bovine serum albumin
cDNA	Complementary desoxyribonucleic acid
$C_{max, ss}$	Maximal concentration at steady-state
CA II	Carbonic anhydrase II
CAR	Constitutive androstane receptor
$Cl_{int, app}$	Apparent intrinsic clearance
C_T	Threshold cycle
CV	Coefficient of variation
CYP	Cytochrome P450
DDI	Drug-drug interaction
DHEA	Dehydroepiandrosterone
DHEAS	Dehydroepiandrosterone sulfate
DMA	N,N-dimethylacetamide
DMPK	Drug metabolism and pharmacokinetics
DMSO	Dimethylsulfoxide
DTT	Dithiothreitol
E1	Estrone
E1S	Estrone sulphate
EMA	European Medicines Agency
ER	Estrogen receptor
ESI	Electrospray ionization
FA	Formic Acid
FDA	Food and Drug Administration
FGly	Cα-formylglycine
FMO	Flavin-containing monooxygenase

G6P-DH	Glucose 6-phosphate dehydrogenase
GLP	Good laboratory practices
GSH	Reduced glutathione
HLM	Human liver microsomes
HPLC	High performance liquid chromatography
IC_{50}	Inhibitor concentration which causes 50% inhibition
IS	Internal standard
K_i	Inhibition constant
K_M	Michaelis Menten constant
LC	Liquid chromatography
LOQ	Limit of quantification
mRNA	Messenger ribonucleic acid
MBI	Mechanism-based inhibition
MEM	Minimum essential medium
MRM	Multiple reaction monitoring
MS	Mass spectrometry
MW	Molecular weight
NADPH	Nicotinamide adenine dinucleotide phosphate (reduced form)
NMR	Nuclear magnetic resonance spectroscopy
P450	Cytochrome P450
PAPS	3'-phosphoadenosine-5'-phosphosulfate
PBS	Phosphate buffer saline
PEG	Polyethylene glycol
PXR	Pregnane X receptor
qPCR	Real time quantitative polymerase chain reaction
RT	Reverse transcription
SAM	S-Adenosyl methionine
SBC	Schwarz´s Bayesian criteria
SD	Standard deviation
SPE	Solid-phase extraction
STS	Steroid sulfatase
SULT	Sulfotransferase
TCA	Trichloroacetic acid
TDI	Time-dependent inhibition

TFA	Trifluoroacetic acid
UDPGA	UDP-glucuronic acid
UGT	UDP-glucuronosyltransferase
UV	Ultraviolet
$\mathbf{V_{max}}$	Maximum enzymatic velocity

1. INTRODUCTION

INTRODUCTION I:
DRUG METABOLISM

DRUG METABOLISM

The metabolism of a drug is understood as a set of biochemical reactions that produce changes on drug chemical structure to facilitate its elimination. These metabolic changes can occur in several body tissues, mainly in the liver, but also in the kidney, intestine, etc. Metabolism can affect drug clearance and a broad spectrum of consequences of drug action including both the desired therapeutic effects and undesired/toxic effects. During the early stages of drug development, metabolism-based experimental strategies allow scientists to improve the pharmacokinetic properties of a lead compound by either blocking or inserting sites of facile metabolism. During the clinical phases and post-marketing stages, metabolism data can be used to promote safe use of a drug, including dosing adjustments or warnings about drug-drug interactions.

The most common fate of metabolism is the formation of inactive products (metabolites having no physiological effect). If the drug is converted to inactive metabolites pre-systemically or too quickly for the desired action, then analogues can be developed with these sites of metabolism blocked, thereby slowing metabolic clearance. A second possible consequence of drug metabolism is the formation of active metabolites (those having the desired activity to an extent similar to/or greater than the parent drug). In some of these cases, the drug is called prodrug and the clearance of all active metabolites needs to be considered. A third possible fate of drug metabolism is the formation of toxic metabolites, which are undesirable and analogues can be developed with some sites blocked to prevent their formation. And finally, the formation of metabolites with physiological action unrelated to the desired mechanism of action is also possible. These metabolic derivatives can lead to new indications of the drug or to the development of drug metabolites (Nassar et al., 2009).

Phase I and Phase II Reactions

The routes by which drugs may be metabolized are many and varied. From a biochemical point of view, most of these changes can be divided in two types of reactions called phase I and phase II reactions.

Phase I reactions are most commonly described as “functionalization” reactions and include oxidations, reductions and hydrolyses. These reactions introduce a new polar functional group to the parent drug (oxidations); modify an existing functional

group to be more polar (reductions); or unmask existing polar functional groups (hydrolyses).

Phase II reactions are most commonly described as conjugation reactions, and include glucuronidation, sulfation, glycine/glutamine conjugation, acetylation, methylation and glutathione conjugation. These are substitution-type reactions and they link a new group either to the parent compound or to a phase I metabolite. Some conjugations cause a dramatic increase in the polarity and generally leading to a water-soluble product which can be excreted in bile or urine.

Cytochrome P450

Cytochrome P450 (CYP) is the terminal oxidase component of an electron transfer system present in the endoplasmic reticulum responsible for the oxidation of most drugs, and is classified as a haem-containing enzyme (a haemoprotein) with iron protoporphyrin IX as the prosthetic group (Gibson and Skett, 2001).

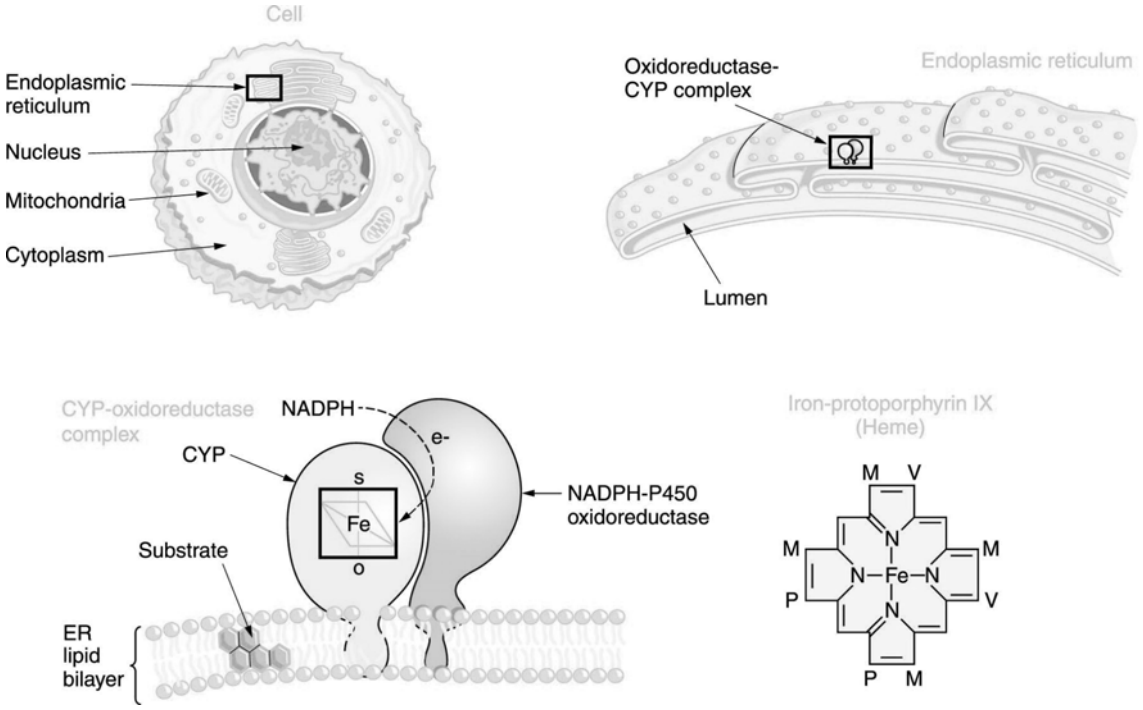

Figure 1. Location of CYPs in the cell. The figure shows increasingly microscopic levels of detail, sequentially expanding the areas within the black boxes. (Figure from books.mcgraw-hill.com/medical/goodmanandgilman/pdfs/CHAPTER3.pdf)

Cytochrome P450 is not a single enzyme, but rather consists of a family of closely related isoforms embedded in the membrane of the endoplasmic reticulum (see Figure 1). The haem group of cytochrome P450 is not covalently bound to the

apoprotein and the name "cytochrome P450" is derived from the fact that the cytochrome (or pigment) exhibits a spectral absorbance maximum at 450 nm when reduced and complexed with carbon monoxide. The haemoprotein serves as the locus for oxygen binding/activation (and the binding site for some drugs) and in conjuction with its associated flavoprotein reductase (NADPH-cytochrome P450 reductase) undergoes cyclic reduction/oxidation of the haem iron that is mandatory for its catalytic activity (see Figure 2).

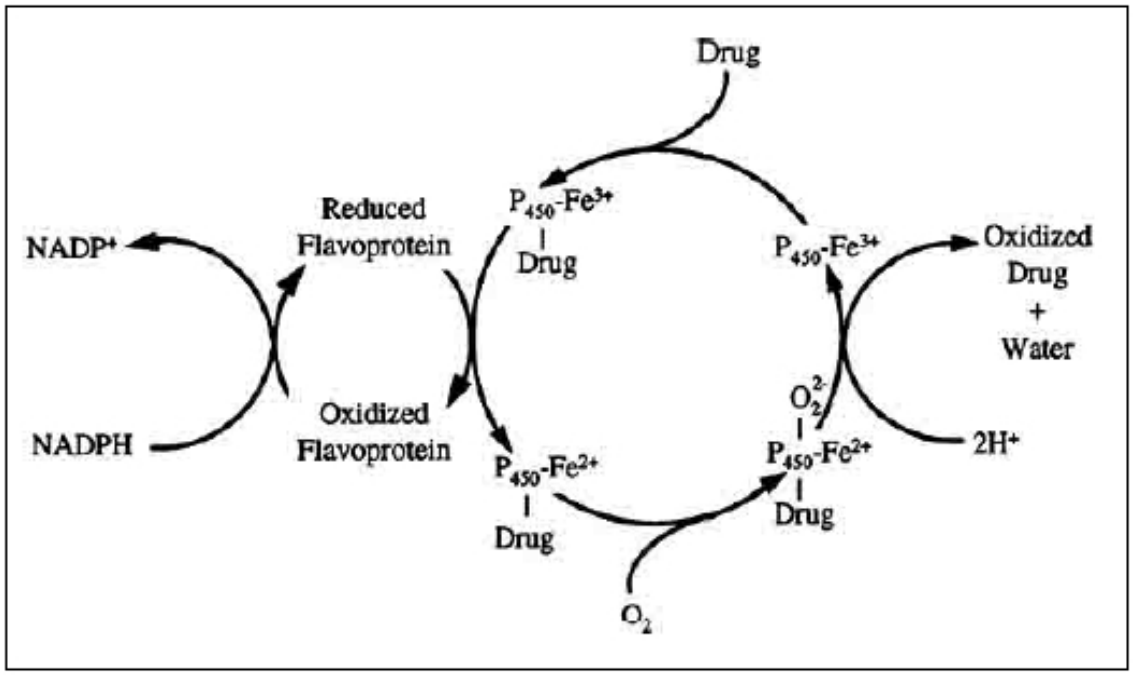

Figure 2. The catalytic cycle of cytochrome P450 (Figure from www.biology-online.org).

Oxidations comprise the bulk of phase I metabolism reactions, and members of the cytochrome P450 superfamily catalyze the majority of these drug oxidation reactions. Individual members are coded by separate genes, and the members are grouped and named according to amino acid sequence similarity of the gene product. Within each CYP gene family (i.e. CYP1, CYP2), the members have more than 40% sequence identity. Each family is divided into subfamilies indicated by a capital letter (i.e. CYP2C, CYP3A). Each subfamily contains members with more than 55% amino acid sequence identity but coded by separate genes. Members can be further subdivided into allele or variant categories. Alleles are responsible for hereditary variation and are defined as alternative versions of a gene resulting from mutation or duplication/deletion events. Genetic polymorphism is used to describe genes that contain an alternative allele

present in >1% of a given population (i.e. CYP2C9 which includes a wild-type allele (CYP2C9*1) and several alternative alleles (CYP2C9*2, CYP2C9*3).

Of the nearly 60 human CYP members currently identified, only about 10 contribute significantly to metabolism of marketed drugs (see Figure 3). The most important isoforms participating in drug metabolism in humans are: CYP1A2, CYP2A6, CYP2B6, CYP2C8, CYP2C9, CYP2C19, CYP2D6, CYP2E1, CYP3A4 and CYP3A5. Most of these CYP members are present in the human liver at different proportions (see Figure 4). For instance, the CYP3A is quantitatively the major sub-family expressed in the majority of human livers (approximately 30% of the total) and consist of three forms, namely CYP3A4, CYP3A5 and CYP3A7. CYP3A7 is the major foetal form and its expression is essentially switched off after birth, whereas CYP3A4 is the major form expressed thereafter (in all age groups and gender). CYP3A5 is polymorphically expressed in approximately 50% of human livers and its substrate specificity is similar to CYP3A4 but generally less active in oxidation (Gibson and Skett, 2001).

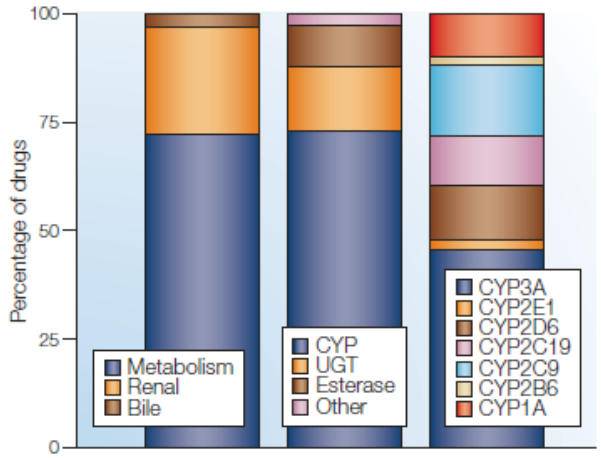

Figure 1 | **Routes of elimination of the top 200 most prescribed drugs in 2002.** Metabolism represents the listed clearance mechanism for ~73% of the top 200 drugs. Of the drugs cleared via metabolism, about three-quarters are metabolized by members of the cytochrome P450 (CYP) superfamily. For the CYP-mediated clearance mechanisms, the majority of drug oxidations (46%) were carried out by members of the CYP3A family; followed by 16% by CYP2C9; 12% for both CYP2C19 and CYP2D6; 9% for members of the CYP1A family; and 2% for both CYP2B6 and CYP2E1 (REF. 9). UGT, uridine diphosphate glucuronyl transferase.

Figure 3. Routes of elimination of the top 200 most prescribed drugs in 2002 (Figure from Wienkers and Heath, 2005).

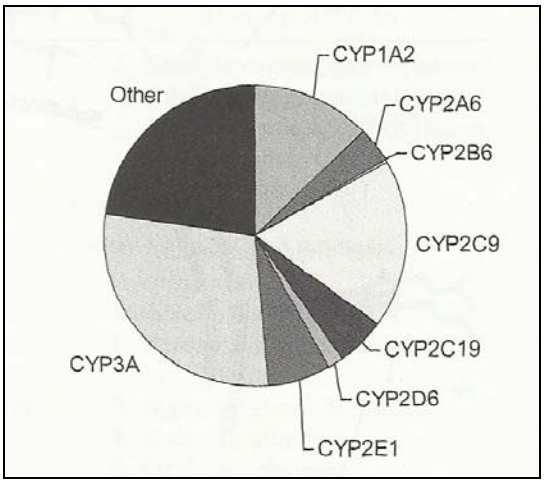

Figure 4. Average relative proportions of CYPs present in human liver (Figure from Nassar et al., 2009).

Subcellular Locations of Metabolizing Enzymes

Both hepatic and extrahepatic cells contain a great amount of metabolizing enzymes that are usually located in specific organelles within the cell or in the cytosol (see Table 1), although some of these enzymes may also be expressed in an organ-specific manner.

Table 1. Characteristics of Major Phase I and Phase II Enzymes (Table from Pearson and Wienkers, 2009).

Characteristics of Major Phase I Enzymes

Enzyme	Reaction	Cofactor	Location
Cytochromes P450	Oxidation Reduction	NADPH	Endoplasmic reticulum
Flavin-containig monooxygenase	Oxidation	NADPH	Endoplasmic reticulum
Monoamine oxidases	Oxidation		Mitochondria
Alcohol or aldehide dehydrogenases	Oxidation	NAD	Cytosol
Reductases	Reduction		Cytosol
Esterases and amidases	Hydrolysis		Cytosol Endoplasmic reticulum
Epoxide hydrolase	Hydration		Cytosol Endoplasmic reticulum

Characteristics of Major Phase II Enzymes

Enzyme	Reaction	Cofactor	Location
UDP-glucuronosyltranferases	Transferase	UDPGA	Endoplasmic reticulum
Sulfotransferases	Transferase	PAPS	Cytosol
Methyltransferases	Transferase	SAM	Endoplasmic reticulum Cytosol
N-acetyltransferase	Transferase	Acetyl CoA	Cytosol
Glutathione S-transferase	Transferase	GSH	Cytosol Endoplasmic reticulum

Subcellular fractions can be thought of as highly concentrated enzyme sources, with the cytosol, microsomes and mitochondria containing most drug-metabolizing enzymes. The major enzymes involved in drug metabolism: P450s and UDP-glucuronosyltransferases (UGTs), along with flavin-containing monooxygenases (FMOs), carboxylesterases and epoxide hydrolases, are predominantly localized within the endoplasmic reticulum. Consequently, microsomes isolated from multiple organs and species are the most popular subcellular fractions for use in in vitro metabolism studies (Pearson and Wienkers, 2009).

Isolation of the different subcellular fractions requires disruption of the cells by homogenization, followed by differential centrifugation (see Figure 5).

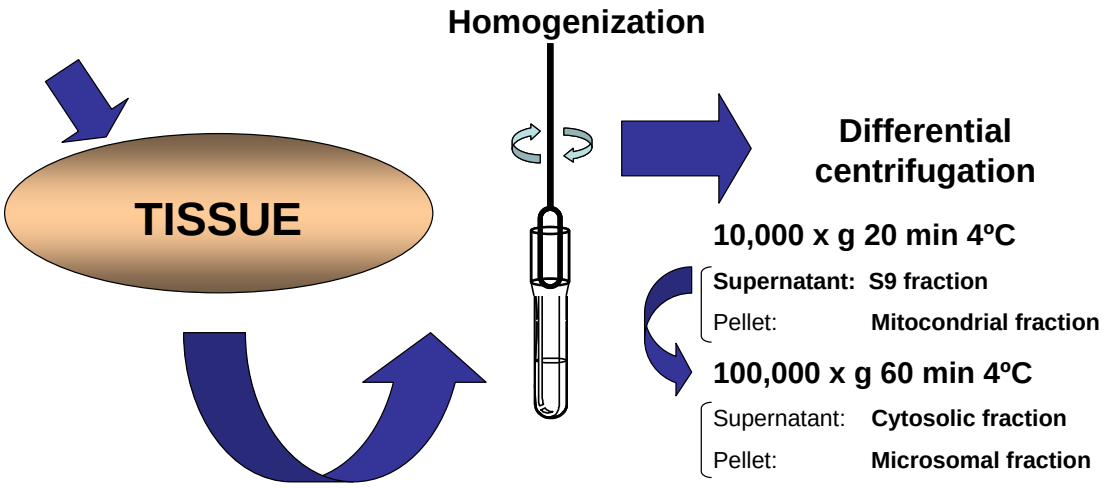

Figure 5. Scheme of isolation of the different subcellular fractions from tissues by homogenization and differential centrifugation.

In the present work, the use of liver microsomes (subcellular fraction derived from the endoplasmic reticulum of hepatocytes) let us to study phase I metabolism, while the use of hepatocytes let us to study both phase I and phase II metabolism.

P450 Enzyme Inhibition

The inhibition of the metabolism of one drug caused by another drug concurrently administered to a patient has been demonstrated to be a highly important cause of adverse drug reactions. When the activity of a given drug-metabolizing enzyme is modified by inhibition, this modification may change the pharmacokinetics of the drug whose metabolism is inhibited by leading to an increase in exposure to the parent drug. However, where more than one enzyme may be responsible for the metabolism of a drug and the different enzymes may result in the formation of different products, the inhibition of a drug-metabolizing enzyme may result in a significant change in the profile of the metabolites formed. If any of the different metabolites have significantly enhanced or decreased biological and/or toxicological properties, this may lead to significantly altered biological activity or toxic response (Nassar et al., 2009).

Since many of the drug-metabolizing enzymes are relatively non-specific in their substrate affinity, it is not surprising that two or more drugs can compete for metabolism by the same enzyme resulting in inhibition of the metabolism of one or both

of the drugs. As a consequence, unexpected increases in the plasma concentrations may occur that can ultimately result in a variety of adverse effects (Nassar et al., 2009).

The inhibition of P450 enzymes can be reversible or time-dependent (TDI). Reversible inhibition involves rapid association and dissociation of drugs and enzymes and may be competitive, noncompetitive, or uncompetitive:

- Competitive inhibition occurs when the inhibitor binds reversibly to the enzyme and prevents the binding of the substrate to the catalytically active site of the enzyme. The inhibitor may or may not be metabolized by the enzymes that it inhibits. In some cases, a competitive inhibitor may bind reversibly to a site other than the active site and block substrate binding to the active site. In this case, the K_M value for the reaction of the substrate under study will increase in the presence of inhibitor while the V_{max} does not change (Nassar et al., 2009).

- A noncompetitive inhibitor binds to a site on the enzyme that is distinct from that of the substrate and thus, it is not metabolized by that enzyme and does not alter substrate binding and vice versa. The substrate and the inhibitor bind reversibly and independently. Although the bound inhibitor has the effect of apparently decreasing the amount of enzyme (decrease in V_{max} with no change in K_M), it does not inactivate the enzyme. In this case, the enzyme-substrate-inhibitor complex is formed; however, it is unable to function catalytically. This type of inhibition is relatively uncommon and is not routinely encountered in studies of the drug-metabolizing enzymes.

- In the uncompetitive inhibition type, the inhibitor does not bind to the free enzyme but only binds to the enzyme that already has substrate bound and prevents subsequent metabolism. Therefore, both the V_{max} and K_M decrease proportionately so that the ratio (V_{max}/K_M) remains constant. Uncompetitive inhibition is also rarely observed (Nassar et al., 2009).

TDI often results from irreversible covalent binding or quasi-irreversible noncovalent binding of a chemically reactive intermediate to the enzyme that catalyzes its formation, resulting in loss of enzyme function. However, in some cases, TDI can be produced by reversible inhibition of a metabolite(s) generated in situ. Experimentally, TDI is defined as an inhibitor that increases its inhibition extent when it is incubated with the enzyme before addition of the substrate, and it is different from the mechanism-based inactivation (MBI) (Grimm et al., 2009). MBI refers to a subset of TDI in which the enzyme acts upon the substrate to form a chemically reactive

metabolite that subsequently inactivates the enzyme. The biochemical mechanisms by which compounds function as MBI of P450 can be divided into three categories: quasi-irreversible or metabolite-intermediate complex (MIC) formation, heme alkylation, and protein alkylation (Grimm et al., 2009).

P450 Enzyme Induction

Unlike CYP inhibition, which is an almost immediate response, CYP induction is a slow regulatory process, meaning it takes time to reach a higher steady-state enzyme concentration as a result of a new balance between the rate of biosynthesis and degradation. Similarly, the return to the enzyme basal levels after discontinuing the treatment with an inducer is a time-dependent process. Because of its time-dependent nature, CYP induction may complicate drug-dosing regimens in chronic drug therapies. Addition of any potent inducer to or withdrawal of a potent inducer from an existing drug-dosing regimen may cause pronounced changes of exposure to drugs that can lead to failure of drug therapy or adverse effects. The addition or withdrawal of an inducer should be performed gradually with appropriate monitoring for therapeutic efficacy and adverse events. Because CYP induction is a metabolic liability in drug therapy, it is highly desirable to develop new drug candidates that are not potent CYP inducer. Ideally, the information on whether a new drug candidate is a potent CYP inducer should be obtained at the drug discovery stage before the drug candidate is selected for clinical development.

Several in vitro models have been established to assess the potential of a drug to induce P450 enzymes, including liver slices, immortalized cell lines, reporter gene assays and primary hepatocytes. Among these models, primary culture of human hepatocytes is probably the current most predictive model for evaluating CYP induction.

Activity of CYP enzymes is affected by increasing the expression of the corresponding genes responsible for their formation. Expression of these genes is mainly regulated by the nuclear receptors: PXR (pregnane X receptor), CAR (constitutive androstane receptor) and AhR (aryl hydrocarbon receptor). The activity of a molecule towards these receptors is often used as an indirect indicator of its induction properties. Both CAR and PXR belong to the same gene family (family NR1) and share a common heterodimerization partner, retinoid X receptor. On the other hand, AhR

belongs to the Per-Arnt-Sim (PAS) family of transcription factors and require AhR nuclear translocator (Arnt) as its heterodimerization partner.

In humans, AhR regulates mainly CYP1-family (CYP1A2), PXR is involved in the expression of CYP2A, CYP2B, CYP2C and CYP3A-families, and CAR is most often connected to regulation of CYP2B subfamily, even though it regulates also members of the CYP2C and CYP3A families.

One of the intriguing aspects of CYP induction is the overlapping induction profiles of CYP2B, CYP2C, and CYP3A enzymes with respect to one single inducing agent. Rifampicin is known to be a good inducer of CYP2B6, CYP2C9, and CYP3A4 genes in humans. Similar to the overlapping induction profiles of CYP enzymes, accumulating evidence from in vitro studies indicates that there is a remarkable redundancy between CAR and PXR with regard to the overlapping ligand spectrum. In addition, there is also a significant overlapping affinity between the binding of CAR and PXR to the DNA response elements of many genes. The process that individual gene can be activated by more than one nuclear receptor is often referred to as “cross talk”. In fact, the cross talk (interplay) between CAR and PXR becomes one of the central topics in the field of CYP induction.

UDP-Glucuronosyltransferases and Sulfotransferases

Glucuronidation is the most widespread conjugation reaction probably due to the relative high abundance of the cofactor for the reaction, UDP-glucuronic acid (UDPGA) and to the ubiquitous nature of the enzymes (UDP-glucuronosyltransferases, UGTs). UDPGA is found in all tissues of the body and UGTs are membrane-bound enzymes located in the endoplasmic reticulum of the cells.

UGTs catalyze the transfer of the glucuronic acid moiety from UDPGA to an acceptor molecule. Glucuronidation is an important step in the elimination of many important endogenous substances from the body, including bilirrubin, bile acids, steroid hormones, thyroid hormones, etc. The UGTs are expressed in many tissues although interactions between drugs at the enzymatic level are most likely to occur during the absorption phase in the intestine and liver or systemically in the liver, kidney or intestine (Gibson and Skett, 2001).

Glucuronide formation is quantitatively the most important form of conjugation for drugs and endogenous compounds and can occur with alcohols, phenols, carboxylic

acids, hydroxylamines, amines, sulfonamides and thiols, forming O-, N- or S-glucuronides. The O-glucuronides are often excreted in bile and thus released into the gut where they can be broken down to the parent compound by intestinal microflora and potentially reabsorbed. This is the basis for the "enterohepatic circulation" of drugs.

There are multiple UGTs with a broad array of substrates. The UGTs have been divided into two families (UGT1 and UGT2) on the basis of their sequence homology. All members of a family have at least 50% sequence identity to one another. The UGT1A family is encoded by a gene complex located on chromosome 2. The large gene complex contains 13 variable region exons that are spliced onto four constant region exons that encode for amino-acids on the C-terminus of the enzyme (UDPGA binding site). Several human UGT2B have been characterized for a variety of substrates. The nomenclature for the UGT2B genes has been assigned to the basis of the order of their discovery (Pearson and Wienkers, 2009).

Inhibitory interactions involving glucuronidation have been described in a number of clinical and in vitro studies. Apparent decreases in the amount of glucuronide excreted in urine or bile or apparent increases in the AUC (decreased clearance) have been demonstrated in clinical studies (Pearson and Wienkers, 2009).

Sulfation is the major conjugation pathway for phenols but can also occur for alcohols, amines and thiols. As with sugar conjugation, an energy-rich donor is required: 3'-phosphoadenosine-5'-phosphosulfate (PAPS). Sulfation occurs by interaction of the drug and PAPS in the presence of the cytosolic enzymes, sulfotransferases (SULTs).

Most of drugs and endogenous compounds that can be glucuronidated can also be sulfated and this leads to the possibility of competition for the substrate between the two pathways. In general, sulfate conjugation predominates at low substrate concentration and glucuronide conjugation at high concentration due to the limited supply of PAPS in the cell compared to UDPGA (Gibson and Skett, 2001).

Unlike the situation with cytochrome P450, specific and selective inhibitors of individual UGT or SULT enzymes may not be available. The only method available to identify isozyme selectivity is to conduct studies with cloned, expressed enzymes. Fortunately, many of these enzymes are commercially available as microsomes

prepared from mammalian cells, insect cells or expressed in bacteria (Pearson and Wienkers, 2009).

Importance of Drug Metabolism Studies

During the early development phases of a new drug candidate, in vitro metabolism studies are performed to provide important data about the safety of a drug. The knowledge of the enzymes involved in the metabolism of a drug, and the effect of this drug on enzymes that metabolize other drugs, enables us to make predictions about possible interactions with other concomitant medications. In addition, the comparative metabolite profile in different species in respect to man helps to determine the most suitable species for further toxicological studies, and also to provide valuable foresight on metabolic pathways in humans.

To this purpose, several in vitro test systems from different species and sexes, such as liver microsomes and hepatocytes, are commonly used in drug metabolism assessments. In the present work, the metabolic profile, the metabolite identification, and the potential species differences in the in vitro metabolism of irosustat were characterized using pooled liver microsome preparations from rats, dogs, monkeys, and humans and hepatocytes from rat, dog, and humans. The use of liver microsomes and hepatocytes let us to study both phase I and phase II metabolism.

Moreover, the enzymes participating in irosustat metabolism and the inhibitory and induction potential of irosustat towards drug-metabolizing enzymes was also investigated in order to predict possible drug-drug interactions between irosustat and possible concomitant medications in the clinical setting (Pelkonen et al., 1998; Weaver, 2001). The inhibition experiments were performed on the nine major human drug metabolizing P450s: CYP1A2, CYP2A6, CYP2B6, CYP2C8, CYP2C9, CYP2C19, CYP2D6, CYP2E1, and CYP3A4/5, using human liver microsomes (HLM) and P450 probe substrates. The potential inhibitory effect of irosustat on the three main UGT enzymes involved in drug metabolism: UGT1A1, UGT1A4, and UGT2B7 (Williams et al., 2004) was also studied using recombinant enzymes. Finally, the induction potential of irosustat on the four major inducible human P450s: CYP1A2, CYP2C9, CYP2C19, and CYP3A4/5, was assessed in human hepatocytes.

Most of these metabolism studies follow regulatory purposes because they are mandatory for the submission of a drug to the market. In the present work, most of these

studies were performed in compliance with Good Laboratory Practices (GLP) regulations and following the current guidelines issued by regulatory authorities such as the European Medicines Agency (EMA) in Europe and the Food and Drug Administration (FDA) in USA (see References Section).

INTRODUCTION II: IROSUSTAT

IROSUSTAT

Irosustat (also known as BN83495, 667 COUMATE, or STX64) is an irreversible steroid sulfatase (STS) inhibitor for steroid hormone-dependent cancer therapy and is currently under clinical development.

STS inhibitors were originally developed as potential therapies for the treatment of hormone-dependent breast cancer in post-menopausal women. The highest incidence of breast cancer occurs in this group of women after the ovarian production of estrogens has ceased and estrogens are produced exclusively in peripheral tissues. In view of the important role that estrogens have in breast cancer, current therapies in postmenopausal women are aimed to either block their interaction with the estrogen receptor (ER) by the use of an antiestrogen such as tamoxifen or ER downregulators, or inhibit the conversion of androstenedione to estrone with aromatase inhibitors (e.g., letrozole, anastrozole, exemestane) (Stanway et al., 2007). However, there is a large amount of evidence indicating that the steroid sulfatase pathway is another important route by which estrogens can be synthesized in postmenopausal women (Foster et al., 2008). Irosustat is an aryl sulfamate used to inactivate STS. Inactivation is time-dependent, irreversible, and active-site directed, consistent with a covalent modification at the active site (Bojarová et al., 2008).

Steroid Sulfatase (STS)

STS is a member of a superfamily of 12 different mammalian sulfatases and it is also named as Arylsulfatase C (E.C. 3.1.6.2). STS is an integral membrane protein, predominantly associated with the endoplasmic reticulum. STS is expressed ubiquitously, its activity being encountered in almost all mammalian tissues (Nussbaumer and Billich, 2004).

The gene for the human STS is located on the distal short arm of the X-chromosome; the gene is pseudoautosomal and escapes X-inactivation. Inactivation of the STS gene results in X-linked ichthyosis, one of the most prevalent human inborn errors of metabolism (Reed et al., 2005). It is a skin disease characterized by accumulation of cholesterol sulfate in corneocyte membranes. Cholesterol sulfate may also be deposited in the cornea of the eye, leading to corneal opacity. Thus, turnover of

cholesterol sulfate as a soluble transport form of cholesterol is a major function of STS (Nussbaumer and Billich, 2004).

As shown in Figure 6, STS catalyzes the formation of estrone (E1) and dehydroepiandrosterone (DHEA) from their sulfate conjugates. Both compounds are further converted by 17β-hydroxysteroid dehydrogenase (17β-HSD) type 1 to estradiol and androstenediol, respectively, which are described to promote tumour growth (Reed et al., 2005; Foster, 2008). Androstenediol (or also called Adiol), although an androgen, can bind to the ER and stimulate the growth of hormone-dependent breast cancer cells in vitro and in carcinogen-induced mammary tumors in rodents. Although its affinity for the ER is lower than that of estradiol, it has been suggested that because of its much higher plasma and tissue concentrations, it may be equipotent to estradiol in postmenopausal women (Stanway et al., 2007).

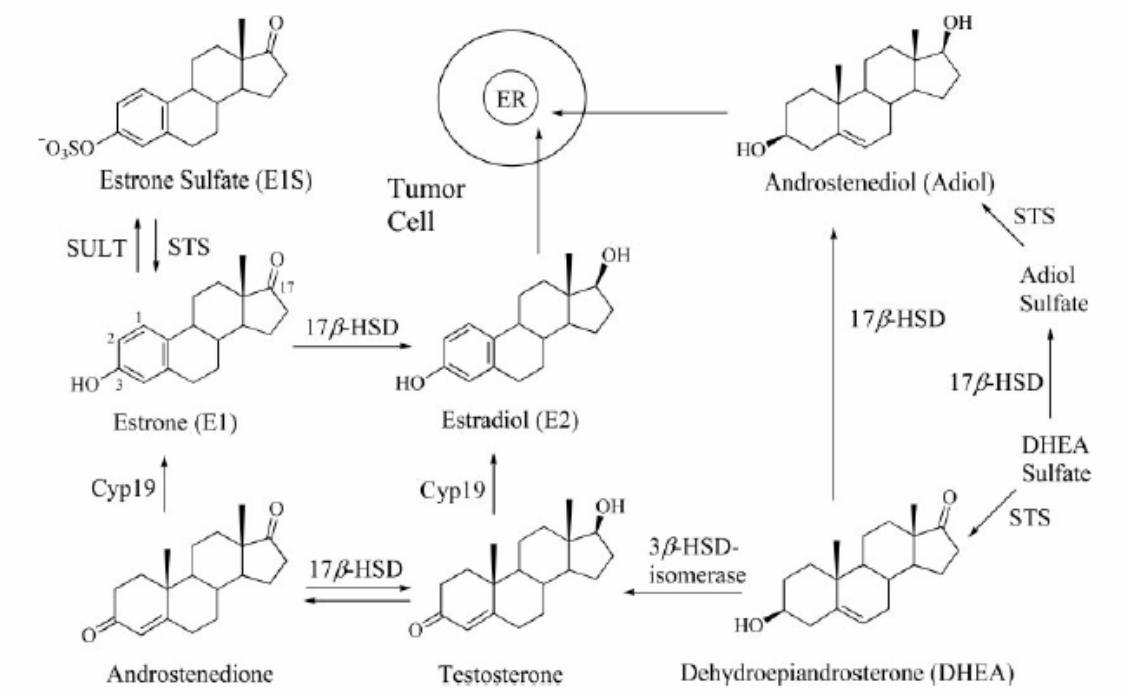

Figure 6. The origin of estrogenic steroids in postmenopausal women with hormone-dependent breast cancer (Figure from Reed et al., 2005).

Much of the estrone synthesized form androstenedione can be converted to estrone sulphate by estrone sulfotransferase and phenol sulfotransferase enzymes (SULTs) that are ubiquitously distributed throughout the body. Plasma and tissue concentrations of estrone sulphate are considerably higher than that of unconjugated

estrogens. Furthermore, the half-life of estrone sulphate (10-12 h) is considerably longer than that of unconjugated estrone and estradiol (20-30 min). Thus, it was initially postulated that the high tissue and circulating levels of estrone sulphate could act as reservoir for the formation of biologically active estrones via the action of STS (Purohit et al., 2003).

STS has been crystallized and its structure has been determined by X-ray crystallography. The architecture of the protein can be described as a featuring "mushroom-like" shape, with two anti-parallel hydrophobic α-helices capable of traversing the membrane, thus anchoring the functional domain on the membrane surface facing the lumen of the endoplasmic reticulum. The active site is buried deep in a cavity of the globular part of the "mushroom" and rests near the membrane surface. The polar globular domain of STS resembles the two known structures of the Arylsulfatases A and B which feature a unique Cα-formylglycine (FGly) residue in their active site and essential in sulfate ester hydrolysis. From the crystal structures, it had been deduced that the aldehyde function of FGly is hydrated, suggesting a catalytic mechanism involving transesterification, that is, intermediate formation of a covalent bond between the aldehyde hydrate and the released sulfate moiety. In fact, the structure of STS shows a hydrated FGly at position 75 linked to a sulfate moiety, presumably the resting state of the enzyme (Nussbaumer and Billich, 2004).

The putative mechanism of STS for the hydrolysis of estrone sulfate (E1S) to E1 is depicted in Figure 7. The first step involves the regeneration of the FGly from FGlyS via (1) desulfation, catalyzed by the nonesterified hydroxyl group, followed by the attack of a molecule of water on the FGly intermediate; or (2) a direct attack of a molecule of water on the sulfur atom of FGlyS. One of the hydroxyl groups then attacks the sulfur atom of E1S, releasing E1 and regenerating FGlyS as a consequence (Reed et al., 2005).

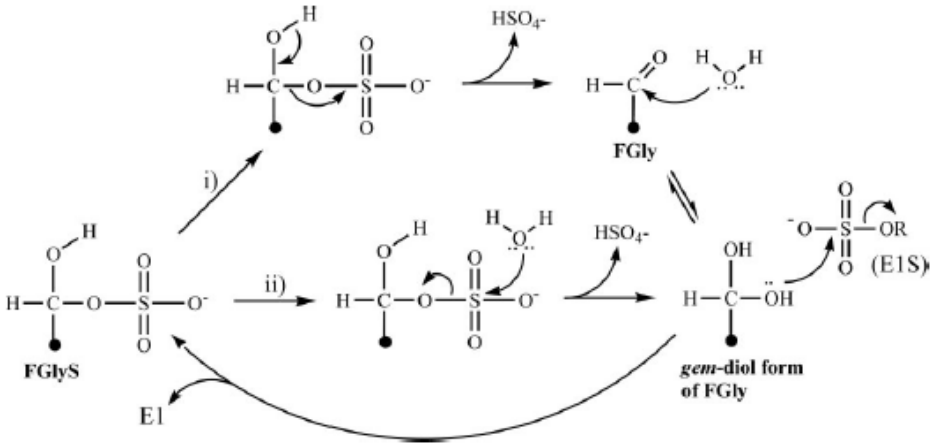

Figure 7. Proposed reaction schemes for cleavage of E1S by STS via: i) desulfation, catalyzed by the nonesterified hydroxyl group, followed by the attack of a molecule of water on FGly; and ii) a direct attack of a molecule of water on the sulfur atom of FGlyS (Figure from Reed et al., 2005).

STS and aromatase (CYP19) are considered as the key enzymes in the two main pathways of estrogen synthesis in peripheral tissues of postmenopausal women, in whom breast cancer most frequently occurs. While the aromatase pathway is already targeted in breast cancer treatment by widely prescribed AIs such as letrozole, anastrozole, and exemestane (Mouridsen et al., 2003; Nabholtz et al., 2003; Paridaens et al., 2003), increasing amounts of evidence support the role of STS as an important source of estrogens. STS activity is higher than aromatase activity in normal and malignant breast tissue (James et al., 1987), and the origin of estradiol in breast cancer tissue has been described to be predominantly estrone sulfate (Santner et al,. 1984). Besides, STS expression is an important prognostic factor in human breast carcinoma (Suzuki et al., 2003).

The pathways currently hypothesised on the local production of estrogenic steroids in breast cancer are shown in Figure 6. As already mentioned, circulating inactive hormones, such as androstenedione and E1S, are at high concentrations in the plasma. The discovery that the sulfatase pathway is an important route of the formation of steroids with estrogenic properties resulted in the development of potent STS inhibitors (Foster, 2008).

Irosustat, potent STS inhibitor

The design of first potent STS inhibitors came when the sulfate group of E1S was replaced by a sulfamate moiety ($-OSO_2NH_2$). It is thought that during irreversible inhibition the sulfamoyl group is transferred to a residue in the STS active site. [Woo et al., 2011]

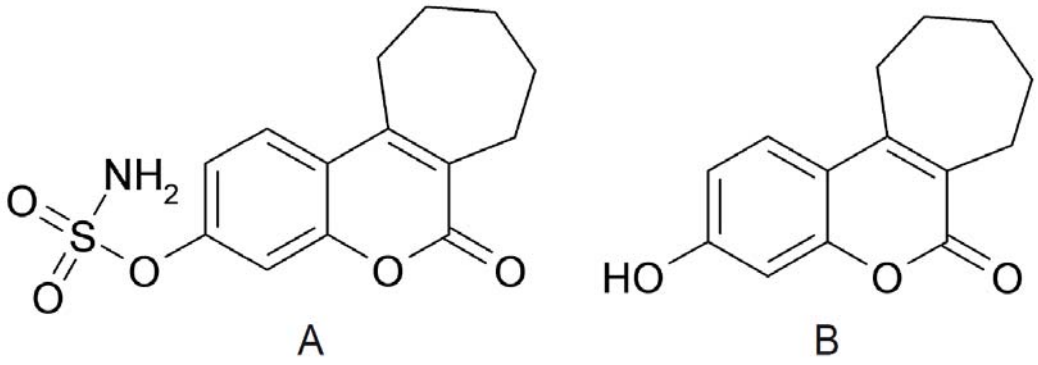

Figure 8. Chemical structures of irosustat (A) and 667-coumarin (B).

The irosustat structure is a tricyclic coumarin-based sulfamate (Figure 8A). The presence of the sulfamoyl ester group is indispensable for its STS inhibitory activity and, in addition, confers to the irosustat molecule the ability to bind and to reversibly inhibit carbonic anhydrase II (hCAII) with a IC_{50} of 25 nM (Ho et al., 2003; Lloyd et al., 2005). Irosustat undergoes spontaneous desulfamoylation in aqueous solutions at nearly physiological pH (Ireson et al., 2003) and also as a result of its mechanism of inhibition of STS (Figure 9), leading to the formation of its major degradation derivative, 667-coumarin (structure shown in Figure 8B), a process that is enhanced by increasing temperature.

Carbonic anhydrase II enzyme is highly expressed in mammalian erythrocytes and the binding to CAII induces irosustat uptake and transport by red blood cells, while preventing it from degradation (Ireson et al., 2004). This behaviour provides a structural basis for the stabilization and long half-life of irosustat in blood compared with its rapid disappearance in plasma, and suggests that reversible binding of inhibitors to CA may be a general method of delivering this type of labile drugs. (Lloyd et al., 2005).

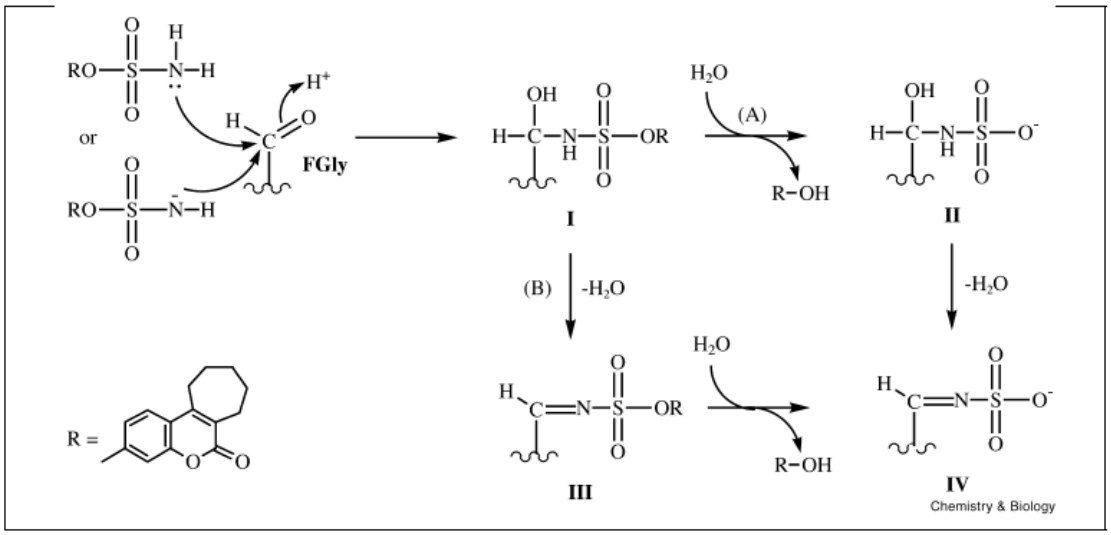

Figure 8. Proposed mechanism of steroid sulphatase inhibition by 667COUMATE involving the conserved formylglycine (FGly) residue in the enzyme active site. Structures **I**, **II**, **III** and **IV** are proposed to be 'dead-end' products.

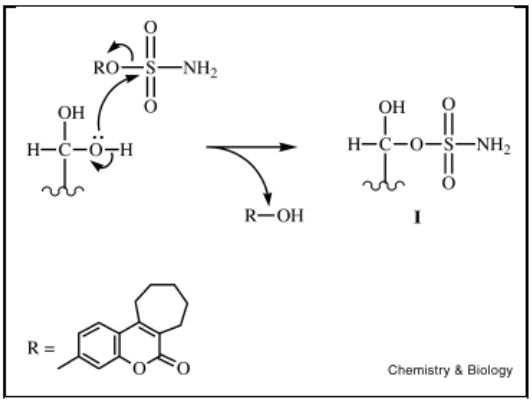

Figure 9. Proposed mechanism of steroid sulphatase inhibition by 667COUMATE via a nucleophilic attack on the sulphamoyl group by the hydrated form of formylglycine residue (aldehyde hydrate) in the enzyme active site. Structure **I** is proposed to be a 'dead-end' product.

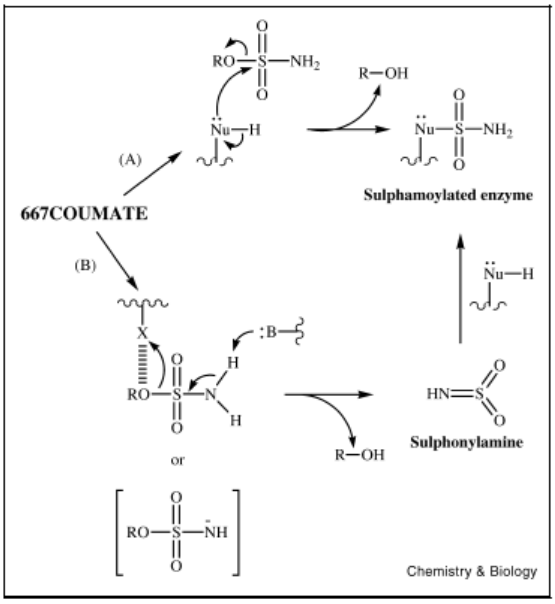

Figure 10. Proposed random specific or non-specific sulphamoylation by 667COUMATE of an essential amino acid residue in the steroid sulphatase active site. Path A: via an attack by a nucleophilic amino acid residue in the active site other than the *gem*-diol residue (:Nu-H). Path B: via the generation of a sulphonylamine species. No regeneration of the enzyme active form from the sulphamoylated intermediate is expected. :B, a proton-abstracting amino acid residue; X, a hydrogen bond-donating amino acid residue or a coordinating metal ion. Dashed line: hydrogen bonding.

Figure 9. Proposed mechanisms of steroid sulfatase inhibition by irosustat (Figures from Woo et al., 2000).

Irosustat exhibits potent STS inhibition both in vitro, showing an IC_{50} value of 8 nM in placental microsome preparations (Woo et al., 2000) and in vivo in a MCF-7 xenograft breast cancer model (Foster et al., 2006). It also causes regression of estrone sulfate-stimulated nitrosomethylurea-induced mammary tumors in ovariectomized rats (Purohit et al., 2000). In addition to breast cancer therapy, STS inhibitors may be useful for the treatment of other steroid hormone-dependent cancers such as prostate cancer (Selcer et al., 2002).

Irosustat was the first ever STS inhibitor to be placed into a Phase I clinical trial in post-menopausal women with hormone-dependent breast cancer. The results of this clinical study showed that irosustat (given as an oral solution) is a potent, well-tolerated STS inhibitor. Irosustat inhibits STS activity in peripheral blood lymphocytes and in tumor tissues (98-99% inhibition) and causes significant decreases in serum concentrations of steroids with estrogenic properties (Stanway et al, 2006). A solid pharmaceutical formulation was developed and a subsequent Phase I dose-escalation study was carried out with a continuous dosing schedule. In this study the optimal biological dose was determined to be 40 mg/day, and the safety and tolerability of irosustat was also evaluated (Palmieri et al., 2011; Coombes et al., 2013).

Data from clinical trials indicate that the mean steady state maximum plasma concentrations ($C_{max, ss}$) of irosustat and 667-coumarin are around 0.23 μM (range 0.05-0.41 μM; Coombes et al., 2013) and 0.08 μM (range 0.02-0.15 μM), respectively, following 40 mg daily irosustat oral doses. Both compounds are highly bound to plasma proteins. Irosustat and 667-coumarin plasma free fractions are 1.3 and 1.1%, respectively (unpublished data).

In both Phase I studies patients had received at least one prior line of endocrine therapy. Given the unique mechanism of action of irosustat, the study needs to first show objective clinical responses by the addition of irosustat to background aromatase inhibition (on which the breast cancer has progressed). This would support the hypothesis that the production of estrone, DHEA and adiol are important mechanisms of resistance to AI treatment. New studies are needed to explore how best to utilize sulfatase inhibition with AIs (i.e. dual sulfatase and aromatase inhibition compared with aromatase inhibition alone) (Palmieri et al., 2011).

Because AIs are potential medications for combined therapy with irosustat (Woo et al., 2011), the prediction of possible interactions between AIs and irosustat was

assessed in the present study specifically for letrozole, anastrozole, and exemestane. From published data, letrozole inhibits CYP2C19 activity (Ki = 42.2 μM) in HLM (Jeong et al., 2009), and anastrozole inhibits CYP2C9, CYP3A activities (both with a Ki of 10 μM) and CYP1A2 activity (Ki = 8 μM, Grimm and Dyroff, 1997). Exemestane does not inhibit CYP1A2, CYP2C9, CYP2D6, CYP2E1, and CYP3A4 activities (Aromasin® prescribing information, 2005); however, no information is available on its CYP2C8 inhibition potential. Therefore, the effect of the three AIs on irosustat metabolism was investigated in HLM.

2. OBJECTIVES

OBJECTIVES

The main purpose of this thesis is the study of the in vitro metabolism of irosustat and the evaluation of possible drug-drug interactions with other drugs. Irosustat is a first-generation, irreversible, steroid sulfatase inhibitor for hormone-dependent cancer therapy. Despite several publications have been published regarding its novel mechanism of action, its metabolism has not been previously studied.

The metabolism of a new drug and the prediction of possible drug-drug interactions must be studied in order to be able to bring a compound into the market; therefore, the objectives of this thesis were defined as follows:

1. Determination of the in vitro metabolite profile of irosustat in different test systems.
2. Comparison of the irosustat metabolism between preclinical animal species and humans, and comparison between sexes.
3. Identification of irosustat main metabolites.
4. Identification of the enzymes responsible for the irosustat metabolism.
5. Study of the inhibitory potential of irosustat towards the main drug-metabolizing enzymes.
6. Study of the induction potential of irosustat towards the main drug-metabolizing enzymes.
7. In vitro study of the possible interaction between irosustat and possible concomitant medication (aromatase inhibitors).

3. MATERIAL AND METHODS

SPECIFIC REAGENTS

- 1-Hydroxymidazolam, CYP3A4 metabolite reference standard, MW: 341.77 g/mol, Ultrafine Chemicals Ref. UC-430.
- 2-Acetamidophenol, CYP1A2 test internal standard, MW: 151.16 g/mol, Aldrich Ref. A7000.
- 4-Acetamidophenol (Acetaminophen, Paracetamol), CYP1A2 metabolite reference standard, MW: 151.16 g/mol, Sigma Ref. A7085.
- 4-Hydroxymephenytoin, CYP2C19 metabolite reference standard, MW: 234.25 g/mol, Sigma Ref. H146.
- 4-Hydroxytolbutamide, CYP2C9 metabolite reference standard, MW: 286.35 g/mol, Sigma Ref. T145.
- 4-Methylpyrazole, CYP2E1 inhibitor, MW: 118.56 g/mol, Sigma Ref. M1387.
- 5,5-Diphenylhydantoin, CYP2C19 test internal standard, MW: 274.25 g/mol, Sigma Ref. D4505.
- 6-Hydroxychlorzoxazone, CYP2E1 metabolite reference standard, MW: 185.56 g/mol, Sigma Ref. C188.
- 6α-Hydroxypaclitaxel, CYP2C8 metabolite reference standard, MW: 869.91 g/mol, Ultrafine Chemicals Ref. UC-998.
- 6β-Hydroxytestosterone, CYP3A4 metabolite reference standard, MW: 304.42 g/mol, Sigma Ref. H2898.
- 7-Hydroxycoumarin (Umbelliferone), CYP2A6 metabolite reference standard, UGT1A1 and UGT2B7 test internal standard, MW: 162.14 g/mol, Sigma Ref. U7626.
- 7-Hydroxy-4-methylcoumarin (4-Methylumbelliferone), UGT1A1 and UGT2B7 substrate, CYP2A6 test internal standard, MW: 176.17 g/mol, Sigma Ref. M1381.
- 7-Hydroxy-4-methylcoumarin glucuronide (4-methylumbelliferone glucuronide), UGT1A1 and UGT2B7 metabolite reference standard, MW: 352.30 g/mol, Alfa Aesar Ref. B21190.
- 667-Coumarin (IDP-17619), MW: 230.3 g/mol, from Panchim (Evry Cedex, France).

- Anastrozole (Arimidex®), aromatase inhibitor, MW: 293.4 g/mol, Sequoia Research Products Ref. SRP05647a.
- Bupropion hydrochloride, CYP2B6 substrate, MW: 276.2 g/mol, Sigma Ref. B102.
- Chlorpropamide, CYP2C9 test internal standard, MW: 276.74 g/mol, Sigma Ref. C1290.
- Chlorzoxazone, CYP2E1 substrate, MW: 169.57 g/mol, Sigma Ref. C4397.
- Coumarin, CYP2A6 substrate, MW: 146.14 g/mol, Sigma Ref. C4261.
- Dextromethorphan monohydrate, CYP2D6 substrate, MW: 370.32 g/mol, Sigma Ref. D2531.
- Dextrorphan tartrate, CYP2D6 metabolite reference standard, MW: 407.46 g/mol, Sigma Ref. D127.
- Diclofenac, UGT1A1 and UGT2B7 inhibitor, MW: 318.13 g/mol, Sigma Ref. D6899.
- Disulfiram, CYP2E1 inhibitor, MW: 296.54 g/mol, Sigma Ref. T1132.
- Exemestane (Aromasin®), aromatase inhibitor, MW: 296.4 g/mol, Selleck Chemicals Ref. S1196.
- Furafylline, CYP1A2 inhibitor, MW: 260.25 g/mol, Sigma Ref. F124.
- Hydroxybupropion, CYP2B6 metabolite reference standard, MW: 255.7 g/mol, BD Ref. 451711.
- Irosustat (BN83495, STX-64, 667-COUMATE), MW: 309.3 g/mol, from Micron Technologies (Dartford, Kent, UK).
- ^{14}C-Irosustat (^{14}C-BN83495, ^{14}C-STX-64), 1 mCi/mL (in acetonitrile) radioactive activity, 123 mCi/mmol specific activity, MW: 313.3 g/mol, was custom-labeled by GE Healthcare (Little Chalfont, Buckinghamshire, UK).
- Ketoconazole, CYP3A4/5 inhibitor, MW: 531.43 g/mol, Sigma Ref. K1003.
- Letrozole (Femara®), aromatase inhibitor, MW: 285.3 g/mol, TRC Ref. L330100.
- Levallorphan tartrate, CYP2D6 test internal standard, MW: 433.49 g/mol, Sigma Ref. L121.
- Methoxsalen (8-Methoxy-psoralen), CYP2A6 inhibitor, MW: 216.19 g/mol, Sigma Ref. M3501.
- Midazolam, CYP3A4 substrate, MW: 325.8 g/mol, European Pharmacopoeia Ref. M2200000.

- (+)-N-3-benzyl-nirvanol, CYP2C19 inhibitor, MW: 294.35 g/mol, Sigma Ref. B8686.
- Nifedipine, CYP3A4 substrate, MW: 346.33 g/mol, Sigma Ref. N7634.
- Nitrendipine, CYP3A4 test internal standard, MW: 360.36 g/mol, Sigma Ref. N144.
- (+)-Nootkatone, CYP2C19 inhibitor, MW: 218.33 g/mol, Fluka Ref. 74437.
- Omeprazole, CYP1A2 inducer, MW: 345.42 g/mol, Sigma Ref. O104.
- Orphenadrine, CYP2B6 inhibitor, MW: 305.84 g/mol, Sigma Ref. O3752.
- Oxidized nifedipine, CYP3A4 metabolism reference standard, MW: 344.32 g/mol, Ultrafine Chemicals Ref. UC-167.
- Paclitaxel, CYP2C8 substrate, MW: 853.91 g/mol, Sigma Ref. T1912.
- Phenacetin, CYP1A2 substrate, CYP3A4 test internal standard, MW: 179.22 g/mol, Sigma Ref. A2500.
- Quercetin di-hydrate, CYP2C8 inhibitor, MW: 338.27 g/mol, Fluka Ref. 83370.
- Quinidine monohydrate, CYP2D6 and UGT1A4 inhibitor, MW: 378.89 g/mol, Sigma Ref. Q0750.
- Rifampicin, CYP2C9, 2C19 and 3A4 inducer, MW: 822.94 g/mol, Sigma Ref. R3501.
- S-Mephenytoin, CYP2C19 substrate, MW: 218.25 g/mol, TRC Ref. M225000.
- Sulfaphenazole, CYP2C9 inhibitor, MW: 314.36 g/mol, Sigma Ref. S0758.
- Testosterone, CYP3A4 substrate, MW: 288.42 g/mol, Sigma Ref. T1500.
- Thio-TEPA, CYP2B6 inhibitor, MW: 189.22 g/mol, Sigma Ref. T6069.
- Tolbutamide, CYP2C9 substrate, MW: 270.35 g/mol, Sigma Ref. T0891.
- Trazodone, CYP2B6 test internal standard, MW: 408.32 g/mol, Sigma Ref. T6154.
- Trifluoperazine, UGT1A4 substrate and reference standard, MW: 480.42 g/mol, Sigma Ref. T6062.

Other reagents were of analytical grade when available.

TEST SYSTEMS[1]

- **Liver Microsomes**

- Male and female Sprague-Dawley rat liver microsomes and liver microsomes from male Beagle dogs and from male and female Cynomolgus monkeys were prepared in-house (Ipsen Pharma, S.A.).
- Female human liver microsomes (HLM), female beagle dog liver microsomes, Reaction Phenotyping Kit version 7 (consisting of HLM from 16 separate donors), and HLM (mixed-gender pool from 50 donors) were purchased from XenoTech, LLC (Lenexa, KS).
- Male HLM were purchased from BD Gentest (Woburn, MA).

- **Hepatocytes**

- Male and female Sprague-Dawley rat hepatocytes were prepared in-house (Ipsen Pharma, S.A.).
- Fresh male Beagle dog hepatocytes, fresh and cryopreserved female human hepatocytes were purchased from Biopredic (Rennes, France).

- **cDNA-Expressed Human Enzymes**

- Commercial microsomes from Baculovirus-insect cell-expressed human P450s (Supersomes) CYP1A1, 1A2, 1B1, 2A6, 2B6, 2C8, 2C9*1, 2C19, 2D6*1, 2E1, 3A4, 3A5, and non CYP-expressing control supersomes; human UDP-glucuronosyltransferases (UGTs) 1A1, 1A3, 1A4, 1A6, 1A7, 1A8, 1A9, 1A10, 2B4, 2B7, 2B15, and 2B17; and human flavin-containing monooxygenase 3 (FMO3) were all purchased from BD Gentest (Woburn, MA).
- Human sulfotransferases (SULTs) 1A1*1 and 1A3 were purchased from Cypex (Dundee, Scotland, UK), and SULTs 1A1*2 and 1A2*1 were purchased from Invitrogen (Carlsbad, CA).

[1] All liver-derived samples were obtained with permission from the ethics committees of Ipsen Pharma S.A. and the other local manufacturers.

PREPARATION OF LIVER MICROSOMES

Liver microsomes from Sprague-Dawley rats, Beagle dogs, and Cynomolgus monkeys were prepared in house. Liver samples were excised and washed in isotonic saline. All subsequent steps were performed at 4°C. The livers were placed on crushed ice, minced with scissors, and then homogenized in 50 mM Tris-HCl buffer (pH 7.4) containing 154 mM KCl, using a Potter-Elvehjem homogenizer. The homogenates were centrifuged at 10,000g at 4°C for 20 min, and the resulting pellet was discarded. The supernatants were centrifuged at 100,000g at 4°C for 1 h (Lake, 1987), and the pellets (microsomes) were resuspended in 50 mM Tris-HCl buffer pH 7.4, containing 154 mM KCl. The protein concentration was measured by the Lowry method using a protein determination kit (from Sigma). The resulting microsomal suspensions were adjusted to 20 mg/mL and aliquoted and stored at -80°C. Microsomes were characterized by determination of total content of cytochrome P450 (Omura and Sato, 1964) and by determination of cytochrome c (P450) reductase (Lake, 1987), ethoxycoumarin O-deethylase (Peters et al., 1991), and testosterone 6β-hydroxylase activities (Kawano et al., 1987).

HEPATOCYTE ISOLATION AND CULTURE

Male and female Sprague-Dawley rats (180–220 g) were anesthetized with ketamine-medetomidine (10:0.1 mg). After loss of the righting reflex, an abdominal midline incision was made, and the portal vein was cannulated. Hepatocytes were further isolated by collagenase perfusion method adapted from Seglen (1976) and Gomez-Lechon et al. (1992). After wash in a suspension medium [50% Leibovitz L-15 medium and 50% Ham's F-12 nutrient mixture, containing 5% fetal calf serum, 0.94 mg/mL D-(+)-glucose, 2 mg/mL bovine serum albumin, 2 mM L-glutamine, 10 mM $HNaCO_3$, 100 IU/mL penicillin, 100 µg/mL streptomycin, and 10^{-8} M insulin], the viability and cell density were measured by the trypan blue exclusion method using a hemocytometer. Finally, rat hepatocytes were plated in 24-well culture dishes coated with collagen substratum (cell density 25 x 10^4 viable cells/well).

Fresh male beagle dog hepatocytes were purchased already plated in 24-well culture dishes coated with collagen substratum (cell density 30 x 10^4 viable cells/well).

Female human cryopreserved hepatocytes were thawed according to the instructions provided by the supplier, and the viability and cell density were measured by the trypan

blue exclusion method. Finally, human hepatocytes were plated in 24-well culture dishes coated with collagen substratum (cell density 0.4 x 10^6 viable cells/well).

INCUBATION OF ^{14}C-IROSUSTAT WITH LIVER MICROSOMES

Liver microsomes (1 mg/mL) from Sprague-Dawley rats, beagle dogs, cynomolgus monkeys, and humans (both sexes, separately) were incubated in duplicate with 25 µM ^{14}C-irosustat at 37°C in 50 mM Tris-HCl buffer pH 7.4, containing 5 mM $MgCl_2$. Incubations were performed in the presence of a NADPH-generating system consisting of 4 mM D-glucose 6-phosphate, 2 IU/mL glucose-6-phosphate dehydrogenase and 1 mM β-NADP (0.5-mL final volume). The reactions were started by addition of β-NADP and were quenched at 0, 30, 60, and 120 min by addition of 1 volume of acetonitrile containing 10% acetic acid. Incubation mixtures without microsomes and without β-NADP incubated for 120 min were used as controls. The samples generated were either stored at -80°C until analysis or directly analyzed by HPLC after centrifugation at 20,000g at 4°C for 15 min and further dilution with HPLC mobile phase.

DETERMINATION OF APPARENT INTRINSIC CLEARANCE

For each species and sex, the apparent intrinsic clearance ($Cl_{int,\ app}$) parameter was estimated using the $t_{1/2}$ method, where the log percentage of substrate remaining versus time was plotted. For calculation, data from incubations up to 30 min were selected. Because 667-coumarin is formed by degradation during the incubations and both irosustat and 667-coumarin actually act as a substrate, the percentage remaining included both compounds, enabling the estimation of the P450-mediated $Cl_{int,\ app}$. The slope of the resulting linear regression (-*k*) was used to obtain in vitro $t_{1/2}$ as described in Equation 1 :

Equation 1 $$\textit{in vitro } t_{1/2} = 0.693 / k$$

The in vitro $t_{1/2}$ was further converted to $Cl_{int,\ app}$ using the Equation 2:

Equation 2 $$Cl_{int,\ app} = [(0.693 / \text{in vitro } t_{1/2}) * (\text{mL of incubation / mg of microsomes}) * (45 \text{ mg of microsomes / g liver}) * (X \text{ g of liver / kg body weight})]$$

where $X = 45$ for rat, 25 for dog, 30 for monkey, and 20 for human (Bohnert and Gan, 2010).

INCUBATION OF UNLABELED IROSUSTAT AND 667-COUMARIN WITH RAT LIVER MICROSOMES AND RAT HEPATOCYTES.

Liver microsomes (1 mg/mL) and hepatocytes from female Sprague-Dawley rats were incubated either with 50 μM irosustat or with 50 μM 667-coumarin for 120 min (liver microsomes) and 3 h (hepatocytes), under the same conditions as described previously.

INCUBATION OF UNLABELED IROSUSTAT WITH HEPATOCYTES

Cultured hepatocytes from male and female Sprague-Dawley rats, male Beagle dogs, and women, were incubated in duplicate with 50 μM unlabeled irosustat at 37°C in a humidified atmosphere containing 95% air and 5% CO_2. The incubation volume was 0.5 mL, and the incubation time period was 3 h. The incubations were quenched by addition of 1 volume of acetonitrile containing 3% acetic acid. The samples generated were either stored at -80°C until analysis or directly analyzed by HPLC after centrifugation at 20,000g and 4°C for 15 min and dilution with HPLC mobile phase.

ESTIMATION OF THE APPARENT K_M AND V_{MAX} FOR IROSUSTAT METABOLISM IN HLM

The microsomal incubations were conducted with final ^{14}C-irosustat concentrations of 0, 5, 10, 25, 50, 80, 110, 150 and 250 μM (n=4 for each concentration, except for 110 and 150 μM, which were n=2) under previous selected linear conditions: 1 mg microsomal protein per mL and 40 minutes incubation (data not shown). Reactions were quenched by addition of acetonitrile containing 10% acetic acid, and samples analysed by HPLC with on-line radioactivity detection as described below. Apparent K_M and V_{max} were estimated after fitting the Michaelis-Menten equation (Equation 3, [Michaelis and Menten, 1913]) to the obtained data, using the WinNonlin version 3.3 software (Pharsight, Mountain View, CA).

Equation 3 $$v = \frac{V_{max} \cdot [S]}{K_M + [S]}$$

where, v and V_{max} are the observed and maximal enzymatic activity respectively, K_M is the Michaelis-Menten constant and [S] the substrate concentration.

DETERMINATION OF IROSUSTAT METABOLITE PROFILE BY HPLC ANALYSIS

^{14}C-Irosustat and its metabolites were separated by HPLC using a Waters 600 solvent delivery system or Alliance 2695 separations module from Waters (Milford, MA, USA) equipped with a reversed-phase column Sunfire C_{18}, 150 x 4.6 mm, 5 µm particle size from Waters at 30ºC. The mobile phase consisted of 50 mM ammonium formate pH 5.0 (solvent A) and methanol (solvent B), and the flow rate was 1 mL/min. The initial mobile phase contained 25% solvent B and was maintained at this composition for 2 min. The percentage of solvent B was increased linearly up to 53% over the next 24 min, and further increased to 70% in the following 7 min. The percentage of solvent B was rapidly changed to 100% in 0.1 min, and maintained at this composition for 5 min. Finally, the percentage of solvent B was returned to 25% for the last 7 min. On-line radiochemical detection was performed using a LB508 radioflow detector equipped with 150 µl-solid scintillation cell (YG-150) from Berthold Technologies (Bad Wildbad, Germany). When using non-radiolabeled irosustat, peak detection was made using a 486 variable wavelength UV or 2487 dual λ absorbance detectors (Waters) at 312 nm.

Occasionally, the column was replaced by a Symmetry C_{18}, 250 x 4.6 mm, 5 µm particle size or a Sunfire C_{18}, 100 x 4.6 mm, 3.5 µm particle size (both from Waters), the gradient times and the flow rate were adjusted to the column dimensions when necessary.

MASS SPECTROMETRIC CHARACTERIZATION

Metabolites in representative incubate samples were selected for LC-MS characterization. Monitoring of metabolite ions was conducted using a ZQ2000 mass

spectrometer (Waters) over the regions where HPLC peaks were present. The mass spectrometer operated with an electrospray ion source in positive ionization mode. Data were captured by means of full scan mass spectra (*m/z* 150 to 600). The capillary and extractor voltages were set at 3 kV and 3 V, respectively; the radiofrequency lens voltage was set at 0.5 V; source and desolvation temperatures were set at 120ºC and 250°C, respectively; and the desolvation and cone gas flow rates were 400 and 50 L/h, respectively. Two cone voltages (30V and 60V) were used in order to determine the fragmentation pattern of the compounds. The spectra obtained in chromatograms from incubates with irosustat or 667-coumarin were compared to blank samples. Data were acquired by Masslynx 4.0 software (Waters).

PHASE I METABOLITE ISOLATION

The main phase I metabolites of irosustat were produced by incubating 50 μM irosustat or 667-coumarin with rat liver microsomes (2 mg/mL protein concentration) over 120 minutes as described previously. Incubates were centrifuged and the supernatants were first diluted with 50 mM ammonium formate pH 5.0. The metabolites were purified by solid phase extraction (SPE) using Sep-Pak Plus C-18 cartridges (Waters). SPE cartridges were first activated with 5 mL acetonitrile and further conditioned with 50 mM ammonium formate pH 5.0. Then, diluted supernatants (5 mL) were loaded onto each SPE cartridge, and a washing step was performed with 5 mL 50 mM ammonium formate pH 5.0. Metabolites were eluted using 2 mL acetonitrile. The SPE fractions were then pooled and dried under a stream of nitrogen. The dry residues were reconstituted into 50 mM ammonium formate pH 5.0 containing 17% acetonitrile. Metabolites were separated by HPLC using a Symmetry C_{18} column (250 x 4.6 mm, 5 μm; Waters) using the method previously described. Purification of the metabolites was performed by fraction collection of HPLC elutes based on their retention times. The isolated metabolite fractions were diluted with 50 mM ammonium formate pH 5.0 and freeze-dried on a Christ Alpha 2-4 Lyophilizer (B.Braun-Biotech, Melsungen, Germany). The freeze-drying procedure was repeated three times and the resultant residues were used for chemical characterization of the metabolites.

NMR ANALYSIS OF ISOLATED METABOLITES LACKING SULFAMOYL GROUP

The characterization of the chemical structure of isolated 667-coumarin derivatives was performed by NMR (Centres Científics i Tecnològics, University of Barcelona). NMR experiments were carried out on either a 600- or 800-MHz Avance NMR spectrometer fitted with TCI H-C/N-D-05 cryoprobes (Bruker, Wissembourg Cédex, France). Samples of the isolated metabolites were dissolved in dimethyl sulfoxide-d_6, and NMR data sets were acquired at 25°C. The experiments performed were monodimensional ^{1}H-NMR spectra, two-dimensional homonuclear ^{1}H-^{1}H correlation experiments (correlation spectroscopy and total correlation spectroscopy), and two-dimensional heteronuclear ^{1}H-^{13}C correlation experiments (heteronuclear single quantum correlation and heteronuclear multiple bond correlation).

IDENTIFICATION OF IROSUSTAT PRIMARY METABOLITES (CONTAINING SULFAMOYL GROUP)

Isolated irosustat primary metabolites were incubated in aqueous buffer at pH 7-8 at 37ºC for 2.5 h in order to induce the desulfamoylation. The resulting 667-coumarin derivatives were compared with the NMR-identified derivatives by HPLC coelution experiments.

β-GLUCURONIDASE TREATMENT

Some of the main phase II metabolites of irosustat were tentatively identified by LC-MS as glucuronides of a number of oxidised derivatives of 667-coumarin (see results section). To assess the identity of the aglycones (actually phase I metabolites), the glucuronides were obtained by incubation of irosustat with hepatocytes and purified by fraction collection of HPLC elutes. The fractions containing each metabolite were pooled and dried under a stream of nitrogen. After dilution with 50 mM ammonium formate pH 5.0, the specimens were freeze-dried. The conjugated metabolites were individually incubated with 3.75 mg/mL β-glucuronidase enzyme (from *Helix pomatia*, type H-1; Sigma-Aldrich) in 100 mM sodium acetate buffer pH 5.0, at 37ºC for 6 h. The incubations were quenched by addition of acetonitrile containing 10% acetic acid. Finally, all the samples generated were analysed by HPLC, and the resulting phase I

metabolites where compared with those already identified by HPLC coelution experiments.

DETERMINATION OF THE HUMAN P450 ENZYMES RESPONSIBLE FOR IROSUSTAT METABOLISM

The main P450 enzymes responsible for the formation of the phase I metabolites of irosustat were identified using the following three complementary approaches:

(a) Correlation Study with P450 Isoform-Specific Activities in HLM

The irosustat biotransformation rate (as metabolite formation) in incubations of the test compound with a panel of 16 individual batches of characterized HLM was correlated with the rate of 13 probe P450-specific reactions: 7-ethoxyresorufin O-dealkylation and phenacetin O-deethylation (for CYP1A2), coumarin 7-hydroxylation (for CYP2A6), S-mephenytoin N-demethylation and bupropion hydroxylation (for CYP2B6), paclitaxel 6α-hydroxylation (for CYP2C8), diclofenac 4'-hydroxylation (for CYP2C9), S-mephenytoin 4'-hydroxylation (for CYP2C19), dextromethorphan O-demethylation (for CYP2D6), chlorzoxazone 6-hydroxylation (for CYP2E1), testosterone 6β-hydroxylation and midazolam 1'-hydroxylation (for CYP3A4/5), and benzydamine N-oxidation (for FMO3). The incubations (n=2) were performed with 50 μM unlabelled irosustat and 1 mg/mL microsomal protein concentration for 40 minutes, under the conditions described previously for incubations of irosustat with liver microsomes. The results of the activity assays using specific cytochrome P450 substrates were taken from the characterization certificate supplied by the microsome manufacturer (Reaction Phenotyping Kit v7 from Xenotech, LLC). The Pearson Correlation Coefficient (r) was estimated, and the correlation was accepted as significant when the probability level was lower than 0.01 (α=0.01). NCSS 2001 software (Kaysville, UT, USA) was used for calculation.

(b) Chemical Inhibition of P450 Enzymes in Pooled HLM

Incubations of 50 μM irosustat in the presence and absence of 10 specific P450 inhibitors (n=2, except for the CYP2C19 inhibitors (+)-nootkatone and (+)-N-3-benzyl-

nirvanol, n=3) were performed using pooled HLM under the incubation conditions described above. The following chemical inhibitors and final concentrations were used (all working solutions were made in DMSO): 1 µM furafylline (CYP1A2, mechanism-based inhibitor); 0.1 µM methoxsalen (CYP2A6, mechanism-based inhibitor); 750 µM orphenadrine (CYP2B6 reversible inhibitor); 10 µM quercetin (CYP2C8, reversible inhibitor); 2 µM sulfaphenazole (CYP2C9, reversible inhibitor); 100 µM (+)-nootkatone and 5 µM (+)-N-3-benzyl-nirvanol (CYP2C19, reversible inhibitors); 0.5 µM quinidine (CYP2D6, reversible inhibitor); 15 µM 4-methylpyrazole (CYP2E1, reversible inhibitor), and 0.5 µM ketoconazole (CYP3A4/3A5, reversible inhibitor). For the mechanism-based inhibitors furafylline and methoxsalen, HLM were preincubated for 15 min in the presence of inhibitor and NADPH-generating system before addition of irosustat.

(c) Incubation with cDNA-Expressed Human Enzymes

50 µM irosustat was incubated (n=2) for 60 minutes with insect cell microsomes expressing individual human P450 enzymes (Supersomes, at 100 pmol P450/mL): CYP1A1, 1A2, 1B1, 2A6, 2B6, 2C8, 2C9*1, 2C19, 2D6*1, 2E1, 3A4, and 3A5. Irosustat was also incubated with 500 µg/mL FMO3, control nonenzyme-expressing insect cell microsomes, and with CYP2B6 at shorter incubation times (10, 20, and 40 min). The incubations were performed at 37°C as described previously.
The metabolism of 50 µM unlabeled 667-coumarin by the cDNA-expressed human enzymes was also investigated following the same incubation conditions.

INVESTIGATION OF THE ROLE OF CYP1A2 IN IROSUSTAT METABOLISM

Native pooled HLM and CYP1A2-fortified HLM showing 2-fold increased CYP1A2 activity were used for these experiments. To prepare CYP1A2-fortified HLM, phenacetin O-deethylase activity was determined in both, CYP1A2 Supersomes and pooled HLM, using 500 µM phenacetin as substrate (concentration close to V_{max} for 4-acetamidophenol formation). The data resulting from this test indicated that the concentration of recombinant human CYP1A2 necessary to increase the CYP1A2 activity in the HLM suspension by 2-fold was 20 pmol/mL. For the main experiment,

50 μM unlabeled irosustat was incubated with native pooled HLM (1 mg/mL) or CYP1A2-fortified HLM (1 mg/mL plus 20 pmol/mL CYP1A2) in the presence or absence of a mix of P450 chemical inhibitors (10 μM quercetin, 2 μM sulfaphenazole, 20 μM tranylcypromine, and 0.5 μM ketoconazole).
In all cases, incubations were performed in the presence or absence of 1 μM furafylline. The incubations (n = 2) were performed for 40 min after a 15-min preincubation with or without furafylline, under the conditions described previously.

DETERMINATION OF THE PHASE II ENZYMES RESPONSIBLE FOR THE METABOLISM OF IROSUSTAT

Human UGTs

Preliminary results indicated that cDNA-expressed human CYP1A2 is able to reproduce the metabolite profile of irosustat obtained in HLM. Therefore, irosustat was incubated with CYP1A2 Supersomes (200 pmol P450/mL). After 120 min incubation, UGT individual human enzymes (1 mg/mL final concentration, n=2): UGT1A1, 1A3, 1A4, 1A6, 1A7, 1A8, 1A9, 1A10, 2B4, 2B7, 2B15 and 2B17, were added to the incubates together with 2 mM UDP glucuronic acid, 0.025 mg/mL alamethicin and $MgCl_2$ supplementary solution (10 mM final concentration). The incubation volume was 400 μl, and the reactions were quenched after 120 min from UGT addition with one volume of acetonitrile containing 10% acetic acid.

Human SULTs

As in the case of human UGTs, unlabeled irosustat was first incubated with 200 pmol/mL CYP1A2 Supersomes. After 120 min incubation, SULT individual human enzymes (12.5 μg/mL final concentration, n=2): SULT1A1*1, SULT1A1*2, SULT1A2*1 and SULT1A3, were added to the incubates together with 50 μM adenosine 3'-phosphate 5'-phosphosulfate, 10 mM dithiothreitol and $MgCl_2$ supplementary solution (5 mM final concentration). The incubation volume was 400 μl, and the reactions were quenched after 120 min from SULT addition with one volume of acetonitrile containing 10% acetic acid.

Formation of glucuronide and sulphate conjugates of 667-coumarin

Unlabelled 667-coumarin was directly incubated (n=2) with the described human UGT and SULT enzymes, under the same conditions of incubation but without the preincubation step with CYP1A2 Supersomes.

P450 ENZYME ACTIVITY INHIBITION

The potential inhibitory effect of irosustat on the P450s CYP1A2, CYP2A6, CYP2B6, CYP2C8, CYP2C9, CYP2C19, CYP2D6, CYP2E1, and CYP3A4/5 was determined in incubations of HLMs with increasing concentrations of irosustat (working solutions in acetonitrile) and a single concentration of each P450 probe substrate (see Table 2). Three substrates were used to assess CYP3A4/5 inhibition, i.e., testosterone, midazolam, and nifedipine (Kenworthy et al., 1999; Galetin et al., 2002). Irosustat concentrations ranged from 0 to 50 μM. All incubations were performed at 37°C, as indicated in Table 2, in triplicate and using two experimental conditions:

(1) direct inhibition, i.e., simultaneous incubation of HLMs with irosustat and the P450 substrate; and

(2) time-dependent inhibition (TDI), i.e., 30-min preincubation of HLMs with irosustat in the presence of reduced NADPH (or an NADPH-generating system) before the addition of the P450 substrate.

100 mM sodium phosphate buffer pH 7.4 was used as incubation buffer in all P450 assays except for CYP2A6 assay (50 mM Tris-HCl buffer pH 7.4). Reference P450 inhibitors were incubated as positive controls at a single active concentration (see Table 2). Incubation mixtures without irosustat and reference inhibitor, without HLMs, without substrate, or without cofactor were used as controls (n = 1). The solvent composition (Table 2) was set to be constant in all assays and did not exceed 2% of the total incubation volume.

The inhibitory effects of 667-coumarin (working solutions prepared in acetonitrile) on CYP1A2 and CYP2C19 were investigated under the same incubation conditions.

Table 2. Incubation Conditions for P450 Inhibition Assays with HLMs.

P450	Marker Substrate	Protein Concentration (mg/mL)	Incubation Time (min)	Incubation Volume (mL)	Reference Inhibitor
CYP1A2	60 μM Phenacetin[1]	0.3	25	0.5	2 μM Furafylline[2]
CYP2A6	3 μM Coumarin[2]	1	10	0.5	1 μM Methoxsalen[2]
CYP2B6	50 μM Bupropion[2]	0.3	30	1	4 μM Thio-TEPA[2]
CYP2C8*	20 μM Paclitaxel[2]	1	20	0.3	30 μM Quercetin[2]
CYP2C9*	200 μM Tolbutamide[2]	0.8	20	0.2	5 μM Sulfaphenazole[2]
CYP2C19	30 μM S-Mephenytoin[1]	0.3	40	1	5 μM NBN[2]
CYP2D6	7.5 μM Dextromethorphan[1]	0.3	10	0.5	2 μM Quinidine[2]
CYP2E1*	200 μM Chlorzoxazone[3]	0.5	15	0.3	200 μM Disulfiram[3]
CYP3A4/5*	20 μM Nifedipine[2]	1	5	0.05	0.5 μM Ketoconazole[2]
CYP3A4/5*	10 μM Midazolam[2]	0.3	8	0.25	0.5 μM Ketoconazole[2]
CYP3A4/5*	50 μM Testosterone[2]	0.5	15	0.25	0.5 μM Ketoconazole[2]

Thio-TEPA : N,N',N'-triethylenethiophosphoramide; NBN : (+)-N-3-benzyl-nirvanol

* : Incubations were started with 2 mM reduced NADPH, for the remaining assays a NADPH-generating system was used.

Solvents used: (1) acetonitrile; (2) DMSO; (3) methanol

ANALYTICAL CONDITIONS TO DETERMINE P450 ENZYME ACTIVITIES

CYP1A2 Assay

At the end of the incubation period, the reaction was quenched by the addition of 150 µl of acetonitrile containing the internal standard (2-acetamidophenol) and further addition of 50 µl acetonitrile:water (50:50). Samples were kept at -80°C until analysis.

For analysis to determine phenacetin O-deethylase activity, samples were thawed and centrifuged at approximately 16,000g at 4°C for 15 min. The supernatants (100 µl) were diluted with 280 µl of 50 mM Tris-HCl buffer pH 7.4 and directly analysed by HPLC-UV equipped with a Kinetex C_{18} reversed-phase column, 100 x 4.6 mm, particle diameter 2.6 µm (Phenomenex) at 50ºC. The mobile phase was 0.1% acetic acid (solvent A) and methanol (solvent B) at a flow rate of 0.7 mL/min. The initial mobile phase contained 15% solvent B which was increased linearly up to 50% over the next 5.3 min, and further increased to 90% in 0.1 min. The percentage of solvent B was maintained at this composition for 1.6 min. Finally, the percentage of solvent B was returned to 15% for the last 10 min. The detection of the metabolite, 4-acetamidophenol, was performed at 240 nm (Lake, 1987).

CYP2A6 Assay

At the end of the incubation period, the reaction was quenched by the addition of 150 µl acetonitrile containing the internal standard (7-hydroxy-4-methylcoumarin). Samples were kept at -80°C until analysis.

For analysis to determine coumarin 7-hydroxylase activity, samples were thawed and 50 µl of acetonitrile were added into each sample. Then, the samples were centrifuged at 20,000g at 4ºC for 15 min. The supernatants were diluted with one volume of 50 mM Tris-HCl buffer pH 7.4 and these solutions were analysed by HPLC-UV equipped with a Supelcosil LC-18-DB column, 150 x 4.6 mm, particle diameter 5 µm (Supelco) with RP-18 pre-column (15 x 3.2 mm, 7 µm, Applied Biosystems). The mobile phase was 50 mM ammonium acetate pH 5.0 (solvent A) and acetonitrile (solvent B) at a flow rate of 1 mL/min. The initial mobile phase contained 25% solvent B which was increased exponentially up to 30% over the next 10 min, and further increased linearly up to 60% in the following 11 min. The percentage of solvent B was rapidly changed to 100% in 1 min, and maintained at this composition for 3 min. Finally, the percentage of solvent B

was returned to 25% for the last 7 min. The detection of the metabolite, 7-hydroxycoumarin, was performed at 325 nm (Miles et al., 1990).

CYP2B6 Assay

At the end of the incubation period, the reaction was quenched by the addition of 200 µl of 10% trichloroacetic acid and further addition of the internal standard (trazodone). Samples were kept at -80°C until analysis.

For analysis to determine bupropion hydroxylase activity, samples were thawed and centrifuged at 16,000g at 4ºC for 15 min. The supernatants were injected to the chromatographic system after an on-line solid phase extraction (SPE) process on disposable C-18 (7 µm) cartridges. Extraction was performed automatically in a programmable manifold (PROSPEKT system, Spark Holland). Briefly, the extraction cartridge was first conditioned with 2 mL methanol followed by 4 mL distilled water (both flushed at 2 mL/min). After conditioning, 1000 µl samples were injected through the loop valve into the C-18 cartridge at a flow rate of 0.5 mL/min, and the cartridge was subsequently washed with distilled water for two minutes at a flow rate of 0.5 mL/min. Elution was performed by switching the HPLC mobile phase through the cartridge which was simultaneously connected on line to the analytical column. Then, analysis was performed by HPLC-UV equipped with a Kinetex C_{18} reversed phase column, 100 x 4.6 mm, particle diameter 2.6 µm (Phenomenex) at 30ºC. The mobile phase was 50 mM ammonium acetate pH 5.0 (solvent A) and acetonitrile (solvent B) at a flow rate of 0.6 mL/min. The initial mobile phase contained 10% solvent B which was increased linearly up to 35% over the next 10 min, and further increased linearly up to 80% in the following 6 min. The percentage of solvent B was changed to 100% in 1 min, and maintained at this composition for 3 min. Finally, the percentage of solvent B was returned to 10% for the last 5 min. The detection of the metabolite, hydroxybupropion, was performed at 218 nm (Turpeinen et al., 2004).

CYP2C8 Assay

At the end of the incubation period, the reaction was quenched by the addition of 150 µl ice-chilled acetonitrile for protein precipitation and proteins were allowed to precipitate for 5 minutes at 4°C. After centrifugation at 1200g for 15 minutes, supernatants were collected and kept at -80°C until analysis.

For analysis to determine paclitaxel 6α-hydroxylase activity, samples were thawed and analysed by HPLC-UV equipped with a Nucleosil 100-5 C_{18} reversed phase column, 150 x 4.6 mm, particle diameter 5 µm (Macherey Nagel). The mobile phase was 65/35 methanol/water. Injection of sample was done at a flow rate of 1 mL/min and elution was performed in isocratic conditions. The detection of the metabolite, 6α-hydroxypaclitaxel, was performed at 230 nm (Huizing et al., 1995).

CYP2C9 Assay

At the end of the incubation period, the reaction was quenched by the addition of 200 µl 0.15 M phosphoric acid. Then, the internal standard (chlorpropamide) was added before extraction of the samples with diethyl ether. After centrifugation at 400g for 5 minutes at 4°C, the ethereal phase was withdrawn, transferred in tubes, and evaporated *in vacuo* for 30 minutes at room temperature. Residues were kept at –80°C until analysis.

For analysis to determine tolbutamide methylhydroxylase activity, thawed residues were dissolved in 10% acetonitrile in water and the resulting samples were analysed by HPLC-UV equipped with a Nucleosil 100-5 C_{18} reversed phase column, 150 x 4.6 mm, particle diameter 5 µm (Macherey Nagel). The mobile phase consisted of : A) 10 mM sodium acetate, pH adjusted to 4.3 with sulphuric acid supplemented with 25% of acetonitrile and B) acetonitrile. The flow rate was 1 mL/min and elution was performed in three phases: 1) isocratic phase with 100% A for 10.0 minutes, then 2) linear gradient from 0 to 30% B over 8.0 minutes, then 3) isocratic elution with 30% B for 2 minutes. The detection of the metabolite, hydroxytolbutamide, was performed at 230 nm (Miners et al., 1988).

CYP2C19 Assay

At the end of the incubation period, the reaction was quenched by the addition of 75 µl of 10% formic acid, and further addition of the internal standard (5,5-diphenylhydantoin) and acetonitrile (25 µl each). Samples were kept at -80°C until analysis.

For analysis to determine S-mephenytoin 4-hydroxylase activity, samples were thawed and 100 µl of 2 M NaOH were added before centrifugation at approximately 16,000g at 4°C for 15 min. The supernatants were injected to the chromatographic system after an on-line SPE process on disposable C-8 (EC-SE, Hysphere 10 µm) cartridges. Extraction

was performed automatically in a programmable manifold (PROSPEKT system). Briefly, the extraction cartridge was first conditioned with 2 mL methanol followed by 4 mL distilled water (both flushed at 2 mL/min). After conditioning, 1000 µl samples were injected through the loop valve into the C-8 (EC-SE) cartridge at a flow rate of 0.5 mL/min, and the cartridge was subsequently washed with distilled water for two minutes at a flow rate of 0.5 mL/min. Elution was performed by switching the HPLC mobile phase through the cartridge which was simultaneously connected on line to the analytical column. Then, analysis was performed by HPLC-UV equipped with a Kinetex C_{18} reversed-phase column, 100 x 4.6 mm, particle diameter 2.6 µm (Phenomenex) at 40ºC. The mobile phase was 0.1% acetic acid (solvent A) and acetonitrile (solvent B) at a flow rate of 0.8 mL/min. The initial mobile phase contained 20% solvent B which was increased linearly up to 22.5% over the next 2.5 min, and further increased linearly up to 57% in the following 5.5 min. The percentage of solvent B was rapidly changed to 90% in 1 min, and maintained at this composition for 2 min. Finally, the percentage of solvent B was returned to 20% for the last 8 min. The detection of the metabolite, 4-hydroxymephenytoin, was performed at 204 nm (up to 6 min) and 240 nm (from 6 to 20 min) (Lake, 1987).

CYP2D6 Assay

At the end of the incubation period, the reaction was quenched by the addition of 100 µl of acetonitrile for protein precipitation and further addition of 50 µl of 100 mM sodium phosphate pH 7.4 containing the internal standard (levallorphan). Samples were kept at -80°C until analysis.

For analysis to determine dextromethorphan O-demethylase activity, samples were thawed and centrifuged at approximately 16,000g at 4°C for 15 min. The supernatants were directly injected to the HPLC-Fluorescence equipped with an Atlantis dC18 reversed phase column, 150 x 4.6 mm, particle diameter 5 µm (Waters) at 40ºC. The mobile phase was 50 mM ammonium acetate pH 5.0 (solvent A) and acetonitrile (solvent B) at a flow rate of 0.7 mL/min. The initial mobile phase contained 18% solvent B which was increased linearly up to 40% over the next 6 min, further increased to 90% in 1 min, and maintained at this composition for 2 min. Finally, the percentage of solvent B was returned to 18% for the last 8 min. The detection of the metabolite, dextrorphan, was performed with a fluorescence detector set at 235 nm and 310 nm as excitation and emission wavelengths, respectively (Dayer et al., 1989).

CYP2E1 Assay

At the end of the incubation period, the reaction was quenched by the addition of 20 µl phosphoric acid 45% for protein precipitation. Specimens were kept at –80°C until analysis.

For analysis to determine chlorzoxazone 6-hydroxylase activity, samples were thawed and centrifuged at approximately 1200g for 15 minutes at 4°C. The supernatants were directly analysed by HPLC-UV equipped with a Nucleosil 100-5 C_{18} reversed phase column, 150 x 4.6 mm, particle diameter 5 µm (Macherey Nagel). The mobile phase consisted of: A) 0.5% (v/v) aqueous acetic acid, and B) acetonitrile. Injection of sample was done at a flow rate of 1 mL/min and elution was performed in three phases: 1) isocratic phase with 20% B for 8 minutes, then 2) linear gradient from 20% to 70% B over 3 minutes, then 3) isocratic elution with 70% B for 1 minute. The detection of the metabolite, 6-hydroxychlorzoxazone, was performed at 287 nm (Dekant et al., 1995).

CYP3A4/5: nifedipine oxidase assay

At the end of the incubation period, the reaction was quenched by the addition of 10 µl 1 M citric acid and 250 µl ice-chilled acetonitrile containing the internal standard (nitrendipine); proteins were allowed to precipitate for 1 h at 4°C. After centrifugation at 700g for 20 minutes at 4°C, supernatants were collected and concentrated *in vacuo* for 45 minutes at room temperature. Residues were kept at –80°C until analysis.

For analysis to determine nifedipine oxydase activity, thawed residues were dissolved in acetonitrile:water (10:90) and analysed by HPLC-UV equipped with a Lichrospher 100RP18 reversed phase column, 125 x 4 mm, particle diameter 5 µm (Interchim). The mobile phase consisted of 5 mM Tris, pH adjusted to 7.5 with sulphuric acid and B) acetonitrile/ethyl alcohol 50/50. The flow rate was 1 mL/min and elution was performed in three phases: 1) isocratic conditions with 39% B for 4 minutes then, 2) linear gradient from 39 to 80% B over 2 minutes then, 3) isocratic phase with 80% B for 4 minutes. The detection of the metabolite, oxidized nifedipine, was performed at 240 nm (Guengerich et al., 1986).

CYP3A4/5: midazolam 1-hydroxylase assay

At the end of the incubation period, the reaction was quenched by the addition of 125 µl ice-chilled acetonitrile containing the internal standard (phenacetin); proteins were allowed to precipitate for 15 minutes at 4°C. After centrifugation at 1200g for 15 minutes at 4°C, supernatants were collected, transferred in glass tubes, and kept at -80°C until analysis.

For analysis to determine midazolam 1-hydroxylase activity, thawed supernatants were directly analysed by HPLC-UV equipped with a Nucleosil 100-5 C_{18} reversed phase column, 150 x 4.6 mm, particle diameter 5 µm (Macherey Nagel). The mobile phase consisted of : A) 10 mM potassium phosphate and B) acetonitrile/methanol (375/625). Injection of sample was done at a flow rate of 1 mL/min and elution was performed in three phases: 1) isocratic phase with 45% A and 55% B for 8 minutes, then 2) linear gradient from 55% to 80% B over 1 minute, then 3) isocratic elution with 80% B for 4 minutes. The detection of the metabolite, 1'-hydroxymidazolam, was performed at 220 nm (von Moltke et al., 1996).

CYP3A4/5: testosterone 6β-hydroxylase assay

At the end of the incubation period, the reaction was quenched by the addition of 125 µl ice-chilled acetonitrile for protein precipitation. After centrifugation at 1200g for 15 minutes at 4°C, supernatants were collected and kept at –80°C until analysis.

For analysis to determine testosterone 6β-hydroxylase activity, thawed supernatants were directly analysed by HPLC-UV equipped with a Nucleosil 100-5 C_{18} reversed phase column, 150 x 4.6 mm, particle diameter 5 µm (Macherey Nagel). The mobile phase consisted of : A) water/methanol/acetonitrile (64/35/1), and B) water/methanol/acetonitrile (18/80/2). Injection of sample was done at a flow rate of 1.5 mL/min and elution was performed in four phases: 1) isocratic phase with 0% B for 10 minutes, then 2) linear gradient from 0 to 45% B over 18 minutes, then 3) linear gradient from 45% to 100% B over 1 minute, then 4) isocratic phase with 100% B for 2 minutes. The detection of the metabolite, 6β-hydroxytestosterone, was performed at 254 nm (Pearce et al., 1996; Baltes et al., 1998).

Calculation of Enzymatic Activities

The metabolites produced were quantified using calibration curve samples prepared with a range of known concentrations of each metabolite (standard) and a fixed concentration of an internal standard, except for CYP2C8, CYP2E1 and CYP3A4/5 (testosterone) assays where no internal standard were used. The peak areas of the metabolite standards or the peak area response ratios (peak area of metabolite standard/peak area of internal standard) were fitted to the nominal concentrations of the metabolite standard.

The enzymatic activities (pmol/mg/min) were calculated according to the microsomal protein concentration and the incubation time, as shown the following equation:

Equation 4 $v = MP / PC / IT$

Where, v: enzymatic activity (pmol/mg/min)
MP: Metabolite produced (pmol/mL)
PC: microsomal protein concentration (mg/mL)
IT: incubation time (min)

Percentage of Control Activity

The enzymatic activities in the presence of the test compound (or reference inhibitor) were further expressed as percent of the control activity obtained in samples incubated with the vehicle only (100% activity). It is widely agreed for this type of experiments that a decrease/increase of less than 20% of the enzymatic activity in the presence of a test compound should not be considered as relevant.

DETERMINATION OF IC_{50} VALUES

When more than 50% inhibition was found, IC_{50} values were calculated by fitting the inhibitory effect, sigmoidal, E_{max} equation (Equation 5) to the enzyme activity data by means of least-squares nonlinear regression, using WinNonlin software (Pharsight, Mountain View, CA).

Equation 5 $$V = V_0 \cdot \left(1 - \left(\frac{C^{\gamma}}{C^{\gamma} + IC_{50}{}^{\gamma}}\right)\right)$$

For CYP1A2, IC_{50} values were calculated by fitting the inhibitory effect, sigmoidal, E_{max} equation that considers residual activity that cannot be inhibited (Equation 6).

Equation 6 $$V = V_0 - (V_0 - V_{\infty}) \cdot \left(\frac{C^{\gamma}}{C^{\gamma} + IC_{50}{}^{\gamma}}\right)$$

Where, V is the enzyme activity, V_0 is the enzyme activity in the absence of test compound, V_{∞} is the remaining enzyme activity when the concentration of test compound is infinite, C is the concentration of test compound, IC_{50} is the concentration of test compound that causes 50% inhibition of V_0, and γ is the sigmoidicity factor.

NADPH DEPENDENCE AND IRREVERSIBILITY OF P450 ENZYME ACTIVITY INHIBITION

The experiments described here were conducted for the P450 enzymes for which TDI was observed, i.e., CYP1A2, CYP2B6, and CYP3A4/5 (with testosterone and midazolam). The HLM incubations were conducted with a single concentration of irosustat (5 µM for CYP1A2 and 50 µM for CYP2B6 and CYP3A4/5), 667-coumarin (0.5 µM for CYP1A2 and 5 µM for CYP2B6 and CYP3A4/5), and reference mechanism-based inhibitors (2 µM furafylline, 4 µM N,N',N'-triethylenethiophosphoramide, and 50 µM mifepristone, respectively). Appropriate controls without test compound or reference inhibitor were included. Incubations were performed at 37°C, as indicated in Table 2, in triplicate. For CYP3A4/5 assays, the following parameters were used: 10-min incubation time, 0.5-mL incubation volume, and 0.1 or 0.15 mg/mL protein concentrations for midazolam or testosterone substrates, respectively. For evaluation of the NADPH dependence of P450 activity inhibition, HLMs were preincubated at 37°C with irosustat, 667-coumarin, or reference inhibitor for 0, 15, and 30 min, in the presence or absence of an NADPH-generating system, before the addition of each P450 substrate. The irreversibility of P450 activity inhibition was assessed with preincubation of HLMs under the same conditions but with a 25-fold increase in the microsomal protein concentration (7.5 mg/mL for CYP1A2 and CYP2B6, 2.5 mg/mL for CYP3A4/5 with midazolam, and 3.75 mg/mL for CYP3A4/5

with testosterone). After preincubation, the mixtures were diluted 1/25 before the addition of each P450 substrate.

The measurement of the P450 activities was performed as previously described, except for CYP3A4/5 assays:

- *CYP3A4/5: midazolam 1-hydroxylase assay:* Samples were analysed by HPLC using an Alliance 2695 separations module (Waters) equipped with a Luna C-18(2) column (150 x 4.6 mm, particle diameter 5 µm, Phenomenex) at 50ºC. The HPLC analysis was performed with a gradient of the following mobile phases: 50 mM ammonium acetate pH 5.0 (solvent A) and acetonitrile (solvent B), flushed at 0.8 mL/min. The metabolite 1-hydroxymidazolam was quantified by UV detection using a 2487 dual λ absorbance detector (Waters) operating at 220 nm.
- *CYP3A4/5: testosterone 6-hydroxylase assay:* After on-line solid phase extraction on disposable C-2 cartridges (BondElut, Spark Holland) in a programmable manifold (PROSPEKT system, Spark Holland), samples were analysed by HPLC using a 600 solvent delivery system (Waters) equipped with a Zorbax 300SBC18 column (150 x 4.6 mm, particle diameter 5 µm, Agilent) at 30ºC. The HPLC analysis was performed with a gradient of the following mobile phases: methanol:water (25:75) containing 0.1% acetic acid (solvent A), and methanol:water:acetonitrile (64:30:6) containing 0.1% acetic acid (solvent B), flushed at 0.8 mL/min. The metabolite 6O-hydroxytestosterone was quantified by UV detection using a 2489 dual λ absorbance detector (Waters) operating at 254 nm.

DETERMINATION OF K_i VALUES

K_i values were determined for CYP1A2 and CYP2C19 activity inhibition by 667-coumarin. Incubations with HLMs were performed using five concentrations of each specific substrate [from 20 to 240 µM phenacetin or from 10 to 200 µM (S)-mephenytoin] and five concentrations of 667-coumarin (from 0 to 5 µM for CYP1A2 or from 0 to 25 µM for CYP2C19). All incubations were performed at 37°C in triplicate, with specific incubation conditions for each P450 assay (Table 2) without a preincubation step. The following equations (Cheng and Prusoff, 1973) were fitted to

the individual enzyme activity data by means of simultaneous nonlinear regression using WinNonlin software:

Equation 7 (Competitive Inhibition)

$$v = \frac{V_{max} \cdot [S]}{K_M \cdot \left(1 + \frac{[I]}{K_i}\right) + [S]}$$

Equation 8 (Non-Competitive Inhibition)

$$v = \frac{V_{max} \cdot [S]}{K_M \cdot \left(1 + \frac{[I]}{K_i}\right) + [S] \cdot \left(1 + \frac{[I]}{K_i}\right)}$$

Equation 9 (Uncompetitive Inhibition)

$$v = \frac{V_{max} \cdot [S]}{K_M + [S] \cdot \left(1 + \frac{[I]}{K_i}\right)}$$

where V and V_{max} are the observed and maximal enzymatic activities, respectively, [S] is the substrate concentration, [I] is the 667-coumarin concentration, K_M is the Michaelis-Menten constant, and K_i is the inhibition constant. The Akaike criterion and the Schwarz Bayesian criterion, together with the coefficient of variation of the K_i estimates, were considered for selection of the inhibition model. The lowest values for these parameters indicated the model that best fit the data.

UGT INHIBITION

The potential inhibitory effect of irosustat and 667-coumarin on the main UGTs involved in drug metabolism, i.e., UGT1A1, UGT1A4, and UGT2B7 (Williams et al., 2004), was investigated as follows.

Before inhibition assays for UGT1A1 and UGT2B7 activities were performed, the linearity of the 7-hydroxy-4-methylcoumarin glucuronosyltransferase activity of recombinant human UGT1A1 and UGT2B7 was evaluated as a function of protein concentration and incubation time. Linear metabolite formation was found up to 0.5 and 1 mg of protein/mL for UGT1A1 and UGT2B7, respectively, and up to 60 min for both UGTs. These incubation conditions were selected for the following experiments.

Recombinant UGT1A1 and UGT2B7 were incubated separately in triplicate with 7-hydroxy-4-methylcoumarin as a substrate (working solutions in DMSO), at a concentration close to the K_M for each enzyme (113 and 335 µM, respectively) (Uchaipichat et al., 2004), in the presence of 0 to 50 µM irosustat or 667-coumarin. The incubations were performed at 37°C in 100 mM sodium phosphate buffer pH 7.4, containing 10 mM $MgCl_2$, 2 mM UDP-glucuronic acid, and 0.025 mg/mL alamethicin (final volume, 0.4 mL). The reactions were started with the addition of UDP-glucuronic acid and were quenched by addition of acetonitrile containing 7-hydroxycoumarin (internal standard). 50 µM diclofenac was used as reference inhibitor (Uchaipichat et al., 2004).

Linear conditions for the trifluoperazine glucuronosyltransferase activity of UGT1A4 were described in the certificate of analysis of the recombinant enzyme. Recombinant human UGT1A4 (0.4 mg/mL) was incubated in triplicate with 50 µM trifluoperazine (working solutions in DMSO), which was close to its K_M value (Zhang et al., 2005), in the presence of 0 to 50 µM irosustat or 667-coumarin. The incubations were performed as described for UGT1A1 and UGT2B7 but with 50 mM Tris-HCl pH 7.4, as the incubation buffer. The reactions were quenched after 30 min by addition of one volume of acetonitrile containing 6% acetic acid. 1.6 mM quinidine was used as reference inhibitor (Uchaipichat et al., 2006). Incubation mixtures without substrate, without UDP-glucuronic acid, or without UGT were used as controls (n = 1).

MEASUREMENT OF UGT ACTIVITIES

7-Hydroxy-4-methylcoumarin Glucuronosyltransferase Enzyme Activity Assay

The incubates were centrifuged for 15 min at 16,000g at 4°C, and the supernatants were diluted with mobile phase and analyzed at room temperature with HPLC with an Alliance 2695 module (Waters) equipped with a Symmetry C18 column (150 x 4.6 mm, 5-µm particle diameter; Waters). The mobile phases were 50 mM ammonium acetate, pH 5.0 (solvent A), and acetonitrile (solvent B), which were pumped at 1 mL/min. The initial mobile phase contained 8% solvent B, which was increased linearly to 50% over the next 10 min and then increased to 90% in 1 min. The proportion of solvent B was maintained at 90% for 3 min and was set to the initial conditions for the last 8 min. UV detection of the metabolite 7-hydroxy-4-methylcoumarin glucuronide was performed with a model 2487 detector (Waters) operating at 325 nm.

Trifluoperazine Glucuronosyltransferase Enzyme Activity Assay

The incubates were centrifuged and the supernatants were diluted with mobile phase as described. Sample analyses were conducted by using the same HPLC system, detector, and column as for 7-hydroxy-4-methylcoumarin glucuronosyltransferase assays but at 45°C. The mobile phases were 0.1% trifluoroacetic acid (solvent A) and 0.1% trifluoroacetic acid in acetonitrile (solvent B), which were pumped at 1 mL/min. The initial mobile phase contained 30% solvent B, which was maintained for 1.2 min and then increased linearly to 51% over the next 8.4 min. The proportion of solvent B was set to the initial conditions for the last 5 min. UV detection of the metabolite trifluoperazine glucuronide was performed at 256 nm (Zhang et al., 2005).

P450 ENZYME INDUCTION

Irosustat at 0.25, 2.5, and 10 μM (n = 4) was incubated at 37°C, for 72 h (CYP1A2 and CYP3A4 assays) or 96 h (CYP2C9 and CYP2C19 assays), with freshly isolated human hepatocytes from four individual female donors (one of the batches, batch HEP200116, failed to provide valid data for the induction of CYP2C9). Prototypical P450 inducers, i.e., omeprazole for CYP1A2 and rifampicin for CYP2C9, CYP2C19, and CYP3A4 (both dissolved in DMSO), were incubated (n = 4) at 50 μM concentration as positive controls. Incubations without any compound but with the same organic solvent composition (0.2% acetonitrile or DMSO) were conducted as negative controls (n = 4). Hepatocytes were used as monolayer cultures in 96-well plates coated with rat type I collagen. They were seeded at a density of 50,000 cells per well and were allowed to attach at 37°C in 0.1 mL of culture medium [William's E medium with GlutaMAX I (Invitrogen) supplemented with 10% fetal calf serum, 100 IU/mL penicillin, 100 μg/mL streptomycin, and 4 μg/mL bovine insulin], in a humidified chamber with air containing 5% CO_2. After cell attachment, the culture medium was replaced with incubation medium (William's E medium with GlutaMAX I supplemented with 50 μM hydrocortisone, 100 IU/mL penicillin, 100 μg/mL streptomycin, and 4 μg/mL bovine insulin), which contained irosustat or the prototypical inducers. Because irosustat is unstable in the incubation medium at 37°C and pH 7.4, the medium was renewed every 12 h (also for positive and negative controls). Before and during incubations, cell

morphological features were evaluated through optical microscopy, to detect any sign of cytotoxicity. At the end of the incubation period, cytotoxicity was assessed with the neutral red uptake test.

Incubation Conditions for Determination of P450 Activities.

At the end of the treatment periods, incubation media were removed and cells were washed with 25 mM HEPES buffer, pH 7.4 (Sigma-Aldrich). Cells were then incubated with minimal essential Eagle's medium without phenol red in the presence of probe substrates for CYP1A2, CYP2C9, CYP2C19, and CYP3A4 [200 μM phenacetin, 1 mM tolbutamide, 200 μM (S)-mephenytoin, and 200 μM nifedipine, respectively]. At the end of each incubation period (2 h for CYP3A4/5 assays and 6 h for the remaining assays), the supernatants and the cell monolayers were stored separately at -80°C. Metabolite formation from P450 probe substrates was determined in the supernatants by HPLC as previously described, except for CYP1A2 and CYP2C19:

- *CYP1A2 assay:* Samples were analysed by HPLC using a 600 solvent delivery system (Waters) equipped with a Nucleosil C18 column (100 x 4.6 mm, particle diameter 3 μm, Macherey Nagel, Düren, Germany). The HPLC analysis was performed with a gradient of the following mobile phases: 2 mM sodium acetate pH 2.6 (solvent A) and acetonitrile (solvent B), flushed at 1.0 mL/min. The metabolite 4-acetamidophenol was quantified by UV detection using a 2487 dual λ absorbance detector (Waters) operating at 250 nm.

- *CYP2C19 assay***:** Samples were analysed by HPLC using a 420 solvent delivery system (Kontron. Watford, UK) equipped with a Lichrospher RP18 column (125 x 4 mm, particle diameter 5 μm, Interchim, Montluçon, France). The HPLC analysis was performed with a gradient of the following mobile phases: 5 mM sodium acetate pH 4 : acetonitrile (85:15) (solvent A) and acetonitrile (solvent B), flushed at 1.5 mL/min. The metabolite, 4-hydroxymephenytoin was quantified by UV detection using a 335 UV detector (Kontron) operating at 220 nm. In the second CYP induction experiment performed for mRNA expression measurement (see below), the samples for CYP2C19 enzyme activity determination were analysed by LC-MS/MS using a G1312B solvent delivery system from (Agilent Technologies, Santa Clara, CA, USA) equipped with a

Synergy Fusion C18 column (50 x 2 mm, particle diameter 2 µm, Phenomenex) at 50ºC. The HPLC analysis was performed with a gradient of the following mobile phases: 0.1% formic acid in water (solvent A) and acetonitrile:methanol (50:50) containing 0.3% formic acid (solvent B), flushed at 0.75 mL/min. The metabolite 4-hydroxymephenytoin was quantified by LC-MS/MS using an API3200 triple-quadrupole mass spectrometer with a turbo-V ionization source (Applied Biosystems, Life Technologies Corporation, Carlsbad, CA, USA) operating in multiple-reaction-monitoring mode using the mass transition *m/z* 235.1 > *m/z* 150.2, in positive polarity.

Measurement of cell protein content

Cells were lysed through heating at 37°C for 15 to 60 min in 100 µl of 0.01 N NaOH. Protein contents in cell lysates were determined by using a DC protein assay kit (Bio-Rad) and were used for the enzyme activity calculations. P450 activities were expressed as nanomoles of metabolite formed per hour per milligram of cell proteins. Induction was calculated as the fold change in enzyme activity in each batch of hepatocytes and for each treatment group, relative to vehicle control values.

Incubation Conditions for Measurement of P450 mRNA Levels.

In a separate experiment, 2.5 µM irosustat or the prototypical inducers (see above) were incubated in triplicate with two individual batches of female human hepatocytes for CYP1A2, CYP2C19, and CYP3A4 mRNA quantification. Hepatocyte monolayers were prepared in 24-well plates coated with rat type I collagen and were seeded at a density of 380,000 cells per well (0.5 mL of culture medium), under the same conditions as described above. The duration of the incubations was 48 h. In parallel, hepatocytes from both batches were incubated with 2.5 µM irosustat for 96 h for CYP2C19 enzyme activity evaluation. In both cases, the medium was renewed every 12 h. Expression of mRNA was determined by using SYBR Green I-based, real-time quantitative polymerase chain reaction (qPCR) assays after RNA extraction and reverse transcription (RT).

RNA extraction

After a 48-hour incubation with the test and reference compounds, cells were washed with PBS before to be kept at about -80°C until RNA extraction.

Total RNA was extracted from cells using RNeasy™ Mini Kit (from Qiagen). The RNA content in each extract was quantified by UV spectrophotometry at λ = 260 nm. The ratio between the optical density at λ = 260 nm and λ = 280 nm was used to evaluate the purity of the specimen.

Reverse transcription (RT)

To evaluate mRNA content of cells by qPCR, the mRNA was reversed into cDNA using the enzyme reverse transcriptase (Super Script™ II RT, from Invitrogen). The synthesis of cDNA by the Reverse Transcriptase was performed in the presence of desoxyribonuclotides triphosphate dNTPs, random hexamers 5'-phosphate, dithiothreitol, and recombinant RNasin ribonuclease inhibitor (from Promega). The reverse transcription was performed on the same amount of RNA for all specimens. The RT reaction was performed by heating specimens at 42°C for 30 min using MiniOpticon™ (BioRad).

Real time PCR (qPCR)

qPCR was performed on MiniOpticon™ (Bio-Rad) using SYBR Green I™ (from Applied Biosystems) and validated set of primers of *CYP2C19, CYP1A2* and *CYP3A4* (PrimSign™ primers from Biopredic). The three housekeeping genes, *TBP* (coding for the TATA box binding protein), *RPLP0* (P0; coding for large ribosomal protein) and *PPIA* (coding for Cyclophiline A), were analysed as the reference genes (Girault et al., 2005).

The amplification of cDNA by qPCR was performed in presence of the fluorochrome SYBR Green I™, Taq polymerase, dNTP, $MgCl_2$ and the specific primers of the screened genes. The amplification was performed on diluted RT products and in duplicate in all qPCR.

Each qPCR assay was constituted by 40 cycles. The program for one cycle was 15 seconds at +95°C for DNA denaturation, 1 minute at +65°C for amplification and a reading of fluorescence of SYBR Green I™. At the end of the qPCR, double strains of DNA were dissociated by progressive increase of temperature to obtain the melting curve specific of each set of primers to control specific amplification.

The value used to evaluate mRNA expression in a sample is the threshold cycle (C_T) which is the number of cycles necessary to accumulate enough amplified product of qPCR to yield a detectable fluorescent signal. Since C_T is determined in the exponential phase at the start of the amplification reaction, real-time PCR can be used to reliably and accurately calculate the initial amount of cDNA present in the reaction.

As first assay, qPCR on the reference gene *TBP* was done to adjust the dilution of RT products to obtain the same levels of cDNA in all specimens, i.e., the number of C_T for *TBP* had to be approximately the same. Then, analysis by qPCR of all screened genes was performed on the same dilutions of RT products.

At the end of the qPCR, the mean of the duplicate C_T values for each specimen was determined. Then, the C_T of each CYP was related to the three reference genes *TBP, PPIA and RPLP0* (i.e., ΔC_T calculation: $C_{T\ CYP} - C_{T\ Ref\ genes}$) and $2^{-\Delta CT}$ values were calculated. Analysis of the combined results was performed to determine potential difference from control data by calculation of fold induction. Fold induction is the ratio between the treated cells and the control cells incubated in the presence of the same percent of solvent.

Statistical Analyses

CYP2C19 inhibition was observed during the P450 induction experiments. The following statistical tests were performed by using SigmaStat 1.0 (SPSS Inc., Chicago, IL): one-way analysis of variance followed by Bonferroni's test or t test ($\alpha < 0.05$). These tests were performed for each hepatocyte batch, to determine whether there were statistically significant differences between the group means.

EFFECT OF AROMATASE INHIBITORS ON THE *IN VITRO* METABOLISM OF IROSUSTAT

Pooled HLMs (1 mg of protein/mL) were incubated for 40 min at 37°C, in triplicate, with 50 mM Tris-HCl buffer pH 7.4, containing 50 µM irosustat, in the presence or absence of increasing concentrations of each AI (letrozole, anastrozole, and exemestane) and with NADPH-generating system. The incubation time and microsomal protein concentration were selected to be in the linear range for irosustat metabolism in HLMs, whereas the irosustat concentration was set to be close to its K_M value in HLMs (previously calculated). Two incubation conditions were used: (1) simultaneous

incubation of irosustat with the AI and (2) 30-min preincubation of HLMs with the AI in the presence of cofactor before the addition of irosustat. AI concentrations ranged from 0 to 100 µM for letrozole and anastrozole and from 0 to 20 µM for exemestane. Incubations were quenched with 1 volume of 10% acetic acid in acetonitrile, and samples were analyzed by HPLC with UV detection to evaluate the metabolite formation from irosustat, as described previously. The following solvents were used to dissolve test compounds: acetonitrile (for irosustat); DMSO (for letrozole and anastrozole); methanol (for exemestane). The solvent composition was adjusted to be constant in all assays and did not exceed 2% of the total incubation volume. Specific reference inhibitors of the main P450s involved in irosustat phase I metabolism were used at a single active concentration to validate the experiments, i.e., 10 µM quercetin, 2 µM sulfaphenazole, and 0.5 µM ketoconazole (for CYP2C8, CYP2C9, and CYP3A4/5, respectively). Incubation mixtures without irosustat and AI, without HLMs, or without β-NADP were used as controls (n = 1). The peak area values for each irosustat metabolite were transformed into percentage of inhibition values, compared with control samples without AI (0% inhibition).

4. RESULTS

RESULTS I:
IN VITRO METABOLISM OF IROSUSTAT AND METABOLITE IDENTIFICATION

DETERMINATION OF THE IN VITRO METABOLISM OF IROSUSTAT

In Vitro Metabolite Profile of ^{14}C-Irosustat in Liver Microsomes from Different Species and Sexes.

The in vitro metabolic profile of ^{14}C-irosustat in liver microsomes, after 30, 60 and 120 minutes incubation, was compared among rats, dogs, monkeys, and humans (males and females separately). The relative percentage of peak area in the radio-HPLC profiles for each metabolite after 120-min incubations is presented in Table 3.

Table 3. Formation of phase I metabolites in the incubations of ^{14}C-irosustat with liver microsomes from rat, dog, monkey and human (males and females, separately) after 120 min incubations.

Metabolite	Relative Percentage of Peak Area in Radio-HPLC Profiles							
	Rat		Dog		Monkey		Human	
	Male	Female	Male	Female	Male	Female	Male	Female
P-14	nd	nd	2.1	0.5	1.3	2.3	nd	nd
M7	**4.5**	**3.7**	**14.7**	**8.1**	**48.5**	**58.8**	**10.1**	**10.4**
M8	**2.2**	**1.3**	**4.9**	**2.8**	**23.1**	**25.0**	**5.0**	**4.2**
M9	0.6	0.4	1.4	1.0	4.4	1.3	2.4	1.6
M10	0.5	1.0	0.5	0.3	2.5	0.6	1.6	1.1
M11	0.9	2.0	nd	nd	nd	nd	0.7	0.9
P-23	nd	nd	0.5	0.7	nd	nd	0.3	0.4
P-24	0.4	nd	1.0	0.7	1.8	1.1	0.4	1.0
M13	**3.8**	**3.7**	**6.5**	**6.1**	**9.9**	**6.9**	**9.5**	**10.9**
M14	**2.9**	**1.6**	**4.6**	**5.5**	**1.1**	**nd**	**2.5**	**2.5**
M15	2.1	1.3	1.6	1.3	nd	nd	0.4	0.8
M16	**5.4**	**4.2**	**7.2**	**7.4**	**5.0**	**3.3**	**8.1**	**9.1**
M18	0.5	0.4	0.7	0.5	*	*	3.2	3.3
^{14}C-irosustat	**58.7**	**59.2**	**35.5**	**44.8**	**2.4**	**0.7**	**44.6**	**43.3**
P-36	nd	0.6	0.9	0.7	nd	nd	1.6	1.4
667-Coumarin	**17.4**	**20.8**	**18.0**	**19.6**	*	*	**9.8**	**9.3**

nd: peak not detected.
** peak detected in samples corresponding to intermediate incubation periods.*
Results are expressed as relative percentage of ^{14}C-labelled metabolites from duplicate incubations. Bold represents main metabolites (which accounted for more than 5 % of relative percentage in some of the species).

When all species and sexes during the whole time course experiments were considered, up to 15 different labeled metabolites of ^{14}C-irosustat were detected. The radio-HPLC metabolite profiles obtained were analogous to those obtained by UV detection at 312 nm. A representative HPLC-UV profile of an HLM incubate is shown in Figure 10 Panel A. The ^{14}C-irosustat metabolites showing a percentage of radioactive peak area higher than 5% were considered as main metabolites. In liver microsomes from the different species under study, the main metabolites were M7, M8, M13, M14, M16, and 667-coumarin. They were found in all samples, except for M14, which was not detected in female monkey microsome incubates, appearing only in males. Besides these main metabolites, some minor metabolites were also detected and showed some differences among species and/or between sexes, although these differences were not considered to be relevant (minor metabolites accounting for relative percentages less than 4.4%).

Taking into account $Cl_{int, app}$ parameters (Table 4), the highest transformation rate of ^{14}C-irosustat was observed in monkey liver microsomes (faster in females than in males), followed by rat, dog, and human microsomes.

The in vitro metabolite profile of ^{14}C-irosustat in dog liver microsomes was the closest to the one obtained in HLM both qualitatively and quantitatively, except for metabolite M11, which was detected in human but not in dog microsome incubations.

Table 4. Comparison of the apparent intrinsic clearance and the percentage of 667-coumarin formed after 120-min control incubations without cofactor or without liver microsomes.

Liver Microsomes		$Cl_{int,app}$ (mL/min/kg)	Formation of 667-Coumarin (Relative %)	
Species	Sex		Without β-NADP	Without Microsomes
Rat	Male	9.9	43.3	36.5
	Female	7.5	47.3	39.1
Dog	Male	7.9	47.7	38.4
	Female	5.4	47.3	39.0
Monkey	Male	53.9	45.4	37.7
	Female	141.6	46.3	40.0
Human	Male	5.4	41.9	37.4
	Female	5.6	42.2	37.7

Results are the mean values of duplicate incubations for each batch of microsomes.

Results from control samples without microsomes demonstrated that irosustat is hydrolyzed to 667-coumarin under the incubation conditions (at 37°C and pH 7.4). However, the amount of 667-coumarin formed in these samples was lower than the amount formed in control samples containing microsomes without β-NADP (Table 4).

In Vitro Metabolite Profile of Irosustat in Hepatocytes from Different Species.

As shown in Figure 10, the pattern of irosustat metabolism by hepatocytes was remarkably different from that obtained with liver microsomes. Five main metabolites of irosustat were detected in incubations with human hepatocytes: M1, M2, M12, M17 and 667-coumarin (Figure 10 Panel B). Except for 667-coumarin, these metabolites were not formed in the microsome incubations, suggesting that most of them might be phase II metabolites. Figure 10 Panels C and D also shows the metabolite profile of irosustat in hepatocytes from rat and dog, respectively: six main peaks in addition to 667-coumarin (M2, M3, M7, M12 and M17) were detected in rat hepatocytes, and in dog, the main metabolites detected were M12, M17 and 667-coumarin.

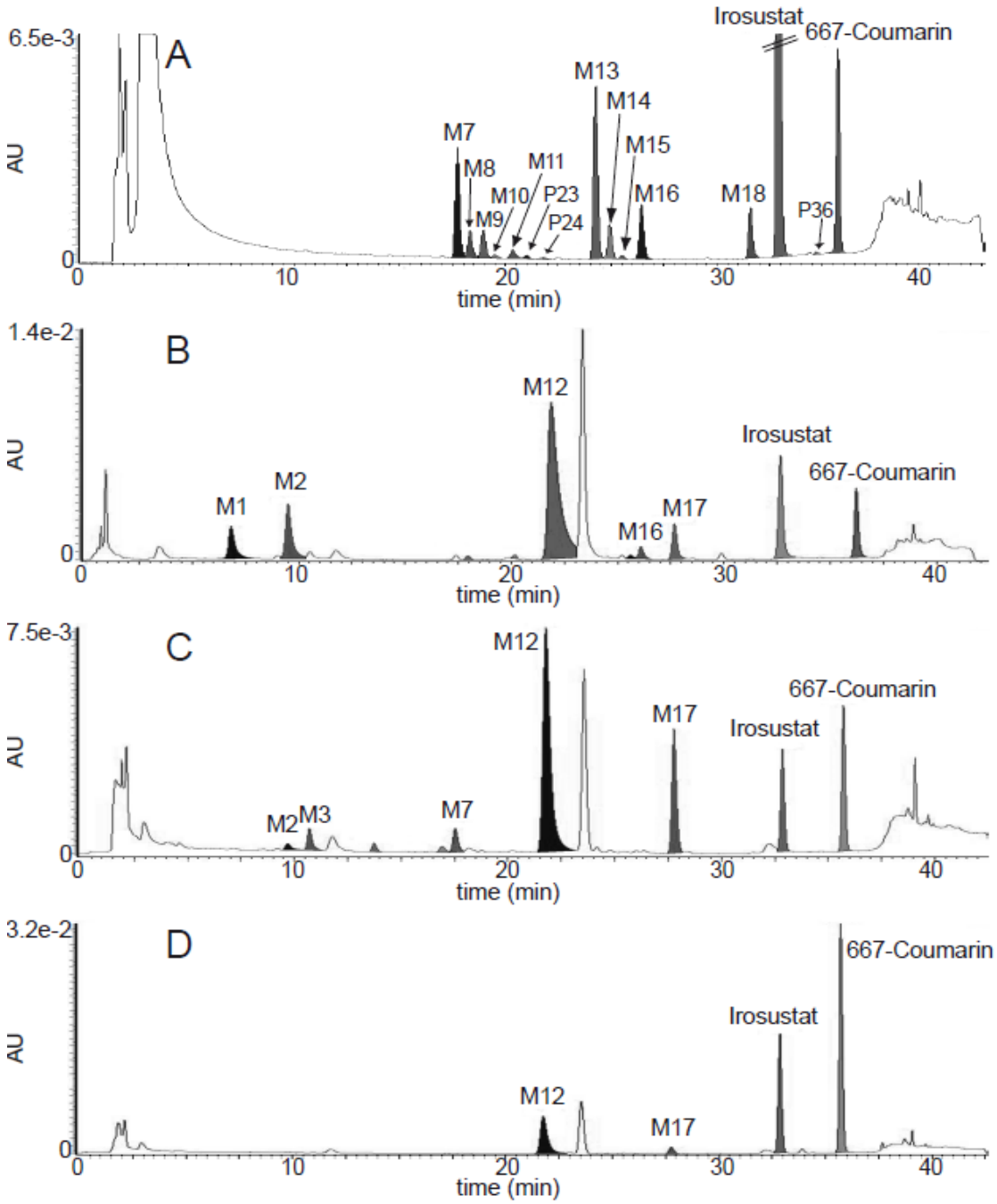

Figure 10. Comparative HPLC-UV profiles of irosustat in vitro metabolism in pooled human liver microsomes incubated with irosustat for 40 min (A) and in hepatocytes from female human (B), male rat (C), and male dog (D) incubated with irosustat for 3 hours. Peaks not shaded correspond to endogenous compounds also present in blank samples.

IDENTIFICATION OF IROSUSTAT MAIN METABOLITES

Preliminary Identification of Irosustat Main Metabolites by Mass Spectrometry.

The MS spectrum of irosustat was characterized by its protonated molecular ion of *m/z* 310 and by the formation of a main fragmentation product of *m/z* 231 (see Figure 11). This fragmentation product was consistent with the protonated molecular ion of the 667-coumarin molecule, which was produced after the loss of the 3-O-sulfamoyl group in the MS ion source. In addition to 667-coumarin, the main in vitro irosustat metabolites were identified as monooxidized derivatives, and also glucuronide and sulfate conjugates.

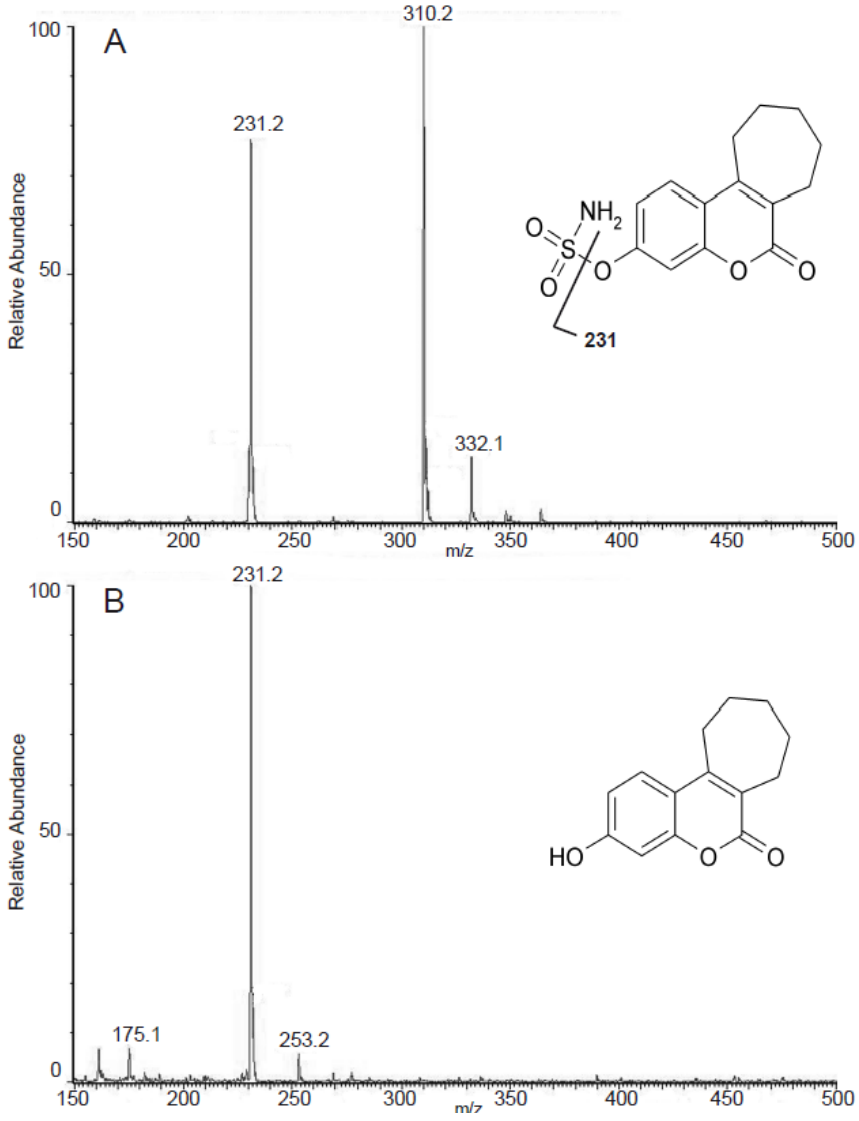

Figure 11. MS Spectra (ESI positive ion mode) of irosustat (A) and 667-coumarin (B) at 60 V cone voltage.

Monooxidized metabolites. Two groups of monooxidized metabolites were found in incubations of irosustat with microsomes: monooxidized irosustat derivatives (primary metabolites M7, M9, M13, and M14); and monooxidized 667-coumarin derivatives (secondary metabolites M8, M15, and M16). Differences in the fragmentation pattern of the metabolites at 60 V cone voltage (Figures 12 and 13) and, importantly, differences in their HPLC retention time (Figure 10 Panel A) indicated that they are probably formed by oxidation in different atoms of the irosustat or 667-coumarin structure.

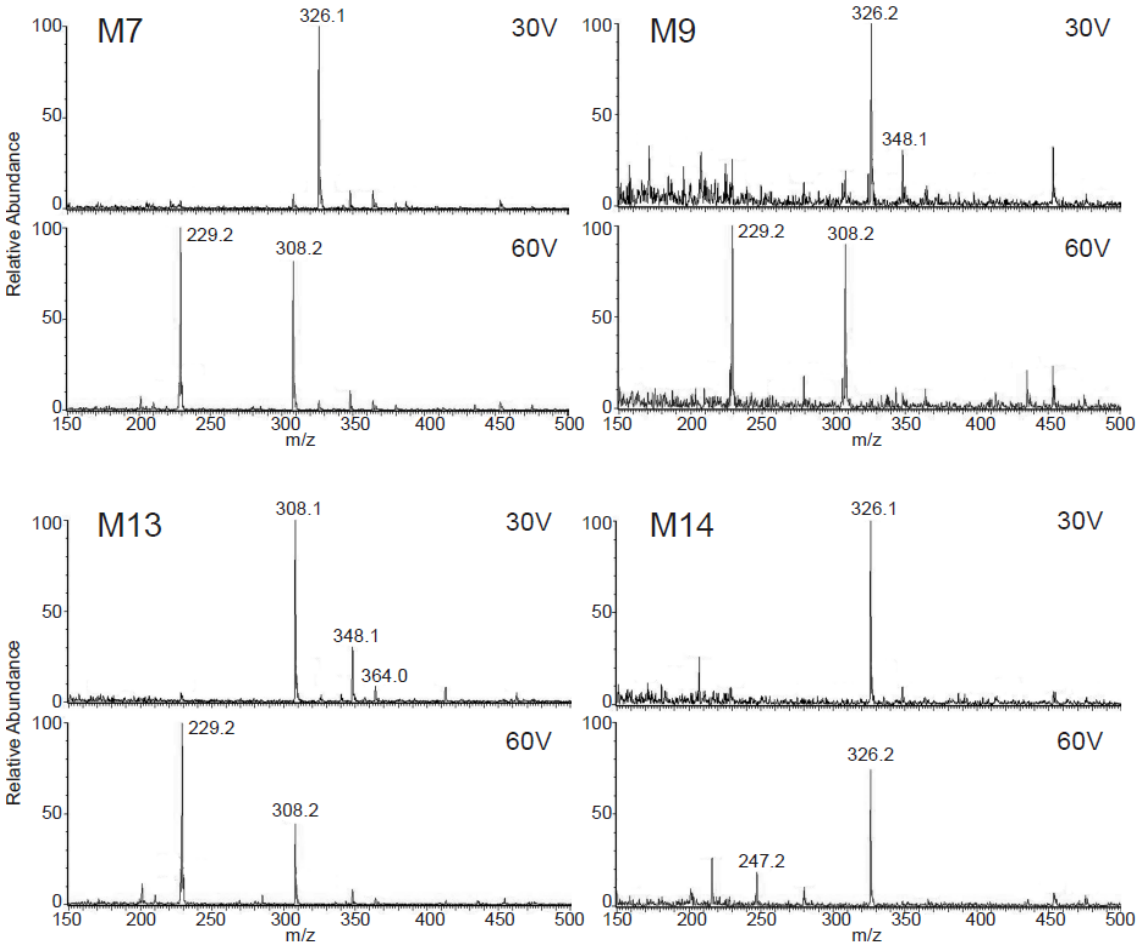

Figure 12. MS Spectra (ESI positive ion mode) of the mono-oxidised metabolites of irosustat: M7, M9, M13 and M14. Upper panel: MS spectra obtained at 30 V cone voltage; Lower panel: MS spectra obtained at 60 V cone voltage.

As depicted in Figure 12, M7, M9 and M14 showed a protonated molecular ion of *m/z* 326, representing an increase of 16 mass units from its parent compound irosustat. Although M13 showed a protonated molecular ion of *m/z* 308, the formation of ions showing *m/z* consistent with the Na^+ and K^+ adducts of *m/z* 326 using a cone

voltage of 30 V, suggested that M13 was also a mono-oxidized metabolite of irosustat, and that probably was dehydrated in the MS source, consequently losing 18 mass units.

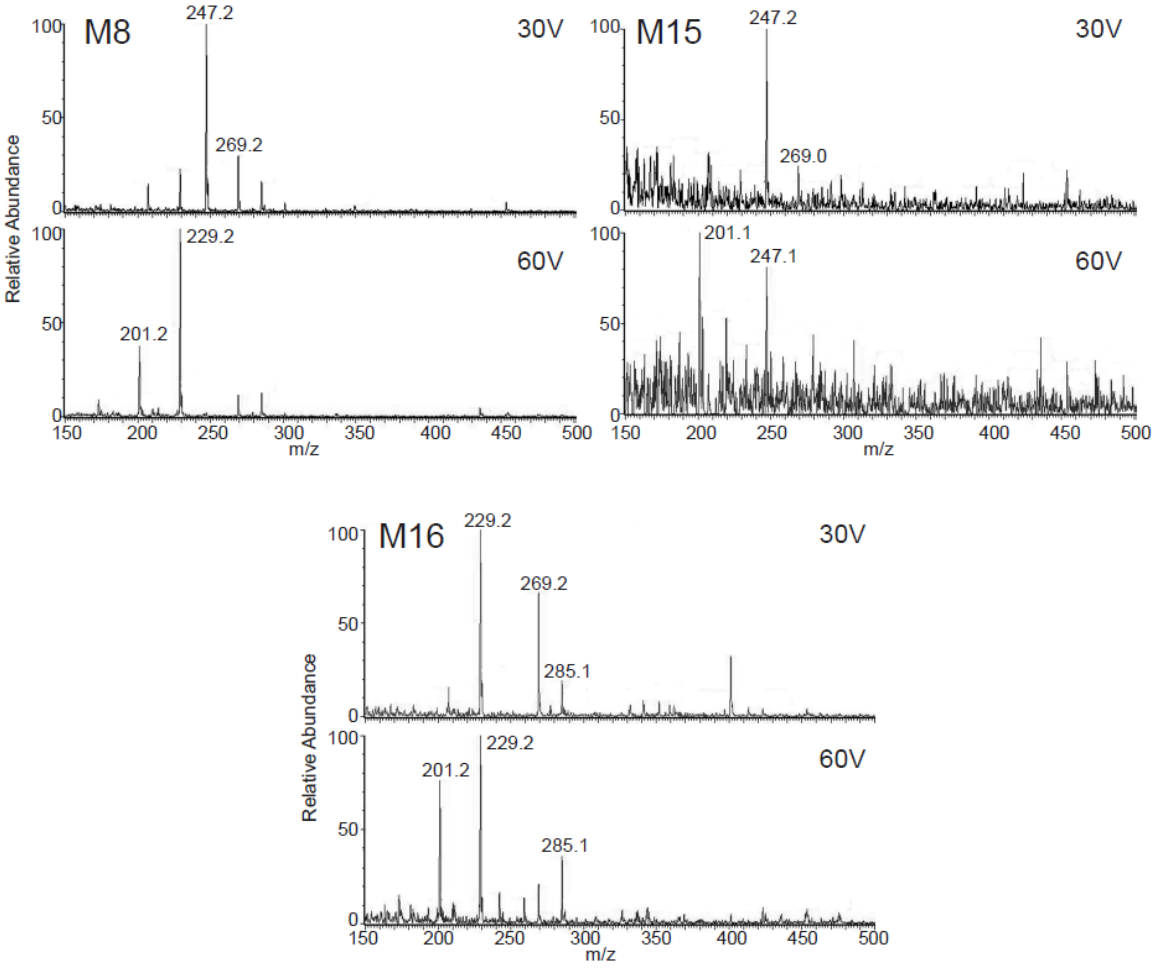

Figure 13. MS Spectra (ESI positive ion mode) of the mono-oxidised metabolites of 667-coumarin: M8, M15 and M16. Upper panel: MS spectra obtained at 30 V cone voltage; Lower panel: MS spectra obtained at 60 V cone voltage.

As illustrated in Figure 13, M8 and M15 showed a protonated molecular ion of *m/z* 247, representing an increase of 16 mass units from its parent compound 667-coumarin. Although M16 showed a protonated molecular ion of *m/z* 229 at the cone voltage of 30 V, the formation of ions showing *m/z* consistent with the Na^+ and K^+ adducts of *m/z* 247 suggested that M16 was also a mono-oxidized metabolite of 667-coumarin, and that probably was dehydrated in the MS source, consequently losing 18 mass units.

Glucuronide and Sulfate metabolites. Three glucuronide metabolites could be identified by MS in hepatocyte incubates with irosustat: one corresponding to the 667-coumarin glucuronide (M12) and two monooxidized 667-coumarin glucuronides (M1 and M2). One sulfate metabolite found in hepatocyte incubates was identified by MS as 667-coumarin sulfate and was named as M17.

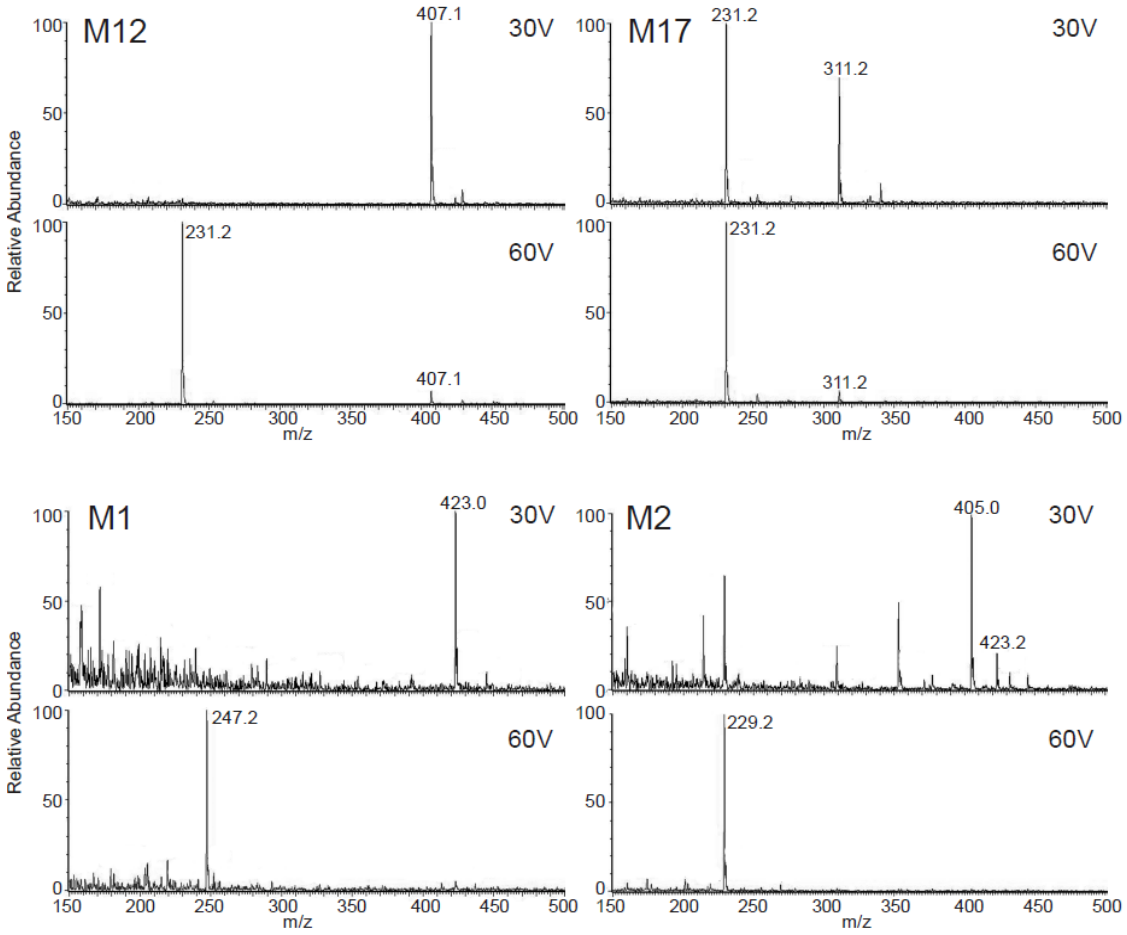

Figure 14. MS Spectra (ESI positive ion mode) of the 667-coumarin glucuronide: M12; the 667-coumarin sulfate: M17; and two glucuronides of mono-oxidized 667-coumarin metabolites: M1 (glucuronide of metabolite M11), and M2 (glucuronide of metabolite M16). Upper panel: MS spectra obtained at 30 V cone voltage; Lower panel: MS spectra obtained at 60 V cone voltage.

As shown in Figure 14, at the cone voltage of 60 V, M1 showed a fragmentation product of *m/z* 247 corresponding to the mono-oxidized 667-coumarin residue after the neutral loss of the glucuronide (i.e. 176 mass units), whereas M2 showed a fragmentation product of *m/z* 229 corresponding to the glucuronide neutral loss and to a typical fragmentation product of some mono-oxidized 667-coumarin derivatives. Metabolites M12 and M17 showed a fragmentation product of *m/z* 231 corresponding to the *m/z* of 667-coumarin residue after the neutral loss of the glucuronide or the sulphate (i.e.176 or 80 mass units, respectively).

In Vitro Incubations of 667-Coumarin with Liver Microsomes and Hepatocytes.

To help in the identification of irosustat metabolites, 667-coumarin and irosustat were incubated separately with both female rat liver microsomes and female rat hepatocytes at 37°C for 120 min and 3 h, respectively. The metabolite profiles obtained from 667-coumarin incubations were compared with those obtained with irosustat. As shown in Figure 15, M8, M11, M15, M16, M12, M17, and P-36 were formed directly from 667-coumarin; conversely, the primary metabolites M7, M9, M13, and M14 were only formed when irosustat was used as substrate. These results supported the previous metabolite identification results obtained by mass spectrometry.

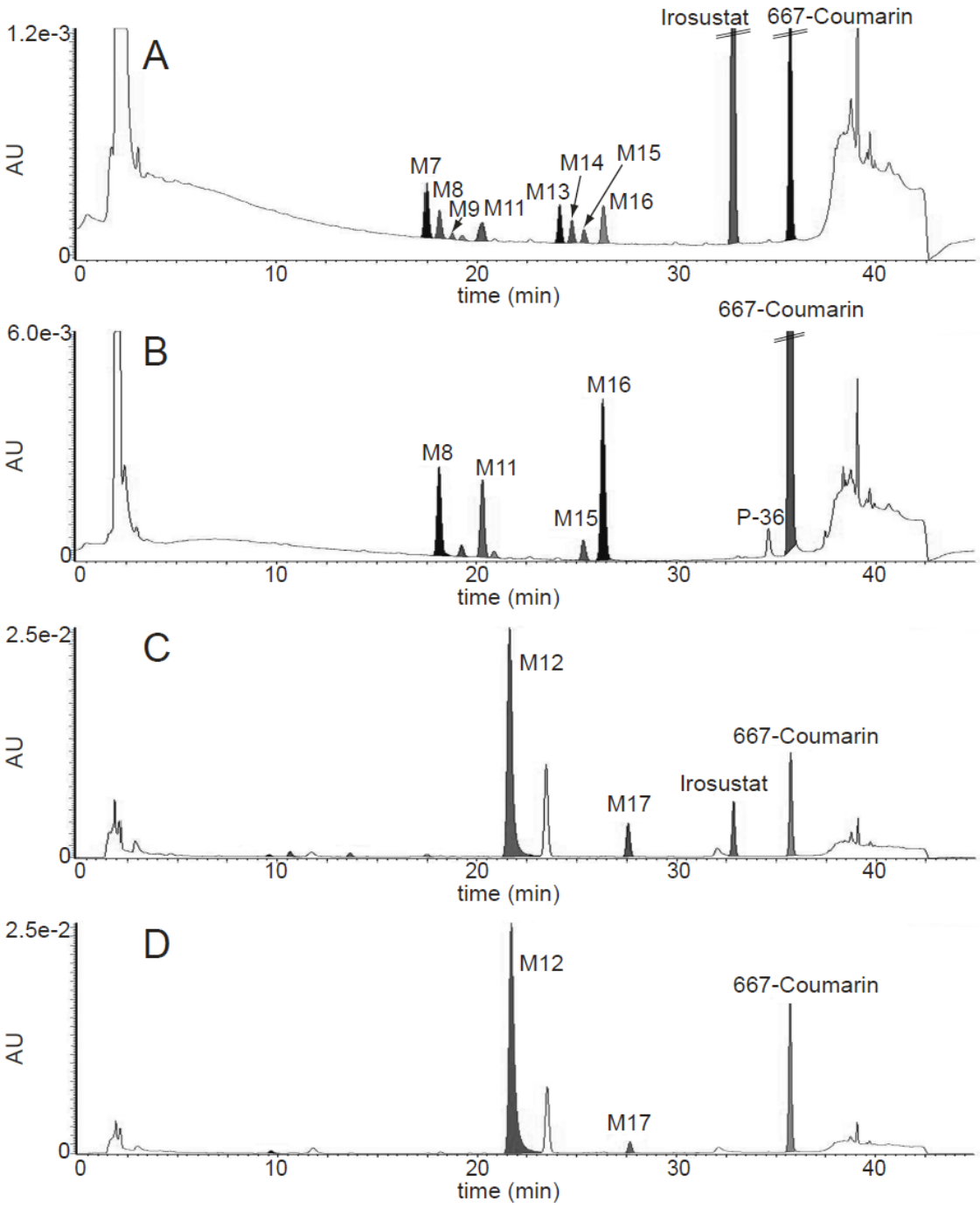

Figure 15. Representative metabolite profiles after incubation of female rat liver microsomes with irosustat (A) and 667-coumarin (B) for 120 min, and female rat hepatocytes incubated with irosustat (C) and 667-coumarin (D) for 3 h.

Structure Elucidation of Irosustat Main Metabolites.

The main phase I metabolites of irosustat were purified as described under Materials and Methods. Those compounds, corresponding to putative mono-oxidized metabolites of irosustat, were converted to their respective 667-coumarin counterparts by incubation at neutral pH and 37°C temperature to force the desulfamoylation. The resulting oxidized 667-coumarin derivatives were further characterized by its HPLC retention time. The results showed that the irosustat oxidized metabolites or primary metabolites M7, M13, M14, and M18 were the sulfamate-containing precursors of the oxidized 667-coumarin derivatives M8, M16, M15, and P-36 (secondary metabolites), respectively.

The identification of the chemical structure of the mono-oxidized 667-coumarin derivatives (indeed, the position of the oxidized atoms) was performed by NMR (Centres Científics i Tecnològics, University of Barcelona), and the identification of their respective sulfamate-containing derivatives was automatically deduced from the data described previously (see Figure 16). The monodimensional ^{1}H spectra of M8 and M16 indicated that no changes took place in the aromatic region with respect to 667-coumarin. The same conclusion was achieved for M15 after interpretation of the homonuclear ^{1}H-^{1}H correlation spectroscopy and total correlation spectroscopy and heteronuclear ^{1}H-^{13}C single quantum correlation and multiple bond correlation two-dimensional spectra. For all three cases, these spectra indicated that the hydroxyl group was located in the cycloheptane ring. The position of the hydroxyl group in the cycloheptane ring was determined from the study of the ring atoms in two-dimensional spectra. Thus, metabolites M8, M15, and M16 were hydroxylated at the C10, C12, and C8 positions, respectively, in the cycloheptane ring of the 667-coumarin molecule. It is obvious that the same hydroxylation sites corresponded to their sulfamate-containing counterparts M7, M14, and M13. The structures described in Figure 16 for these metabolites are compatible with the NMR data.

Figure 16. Structures of irosustat metabolites formed in vitro.

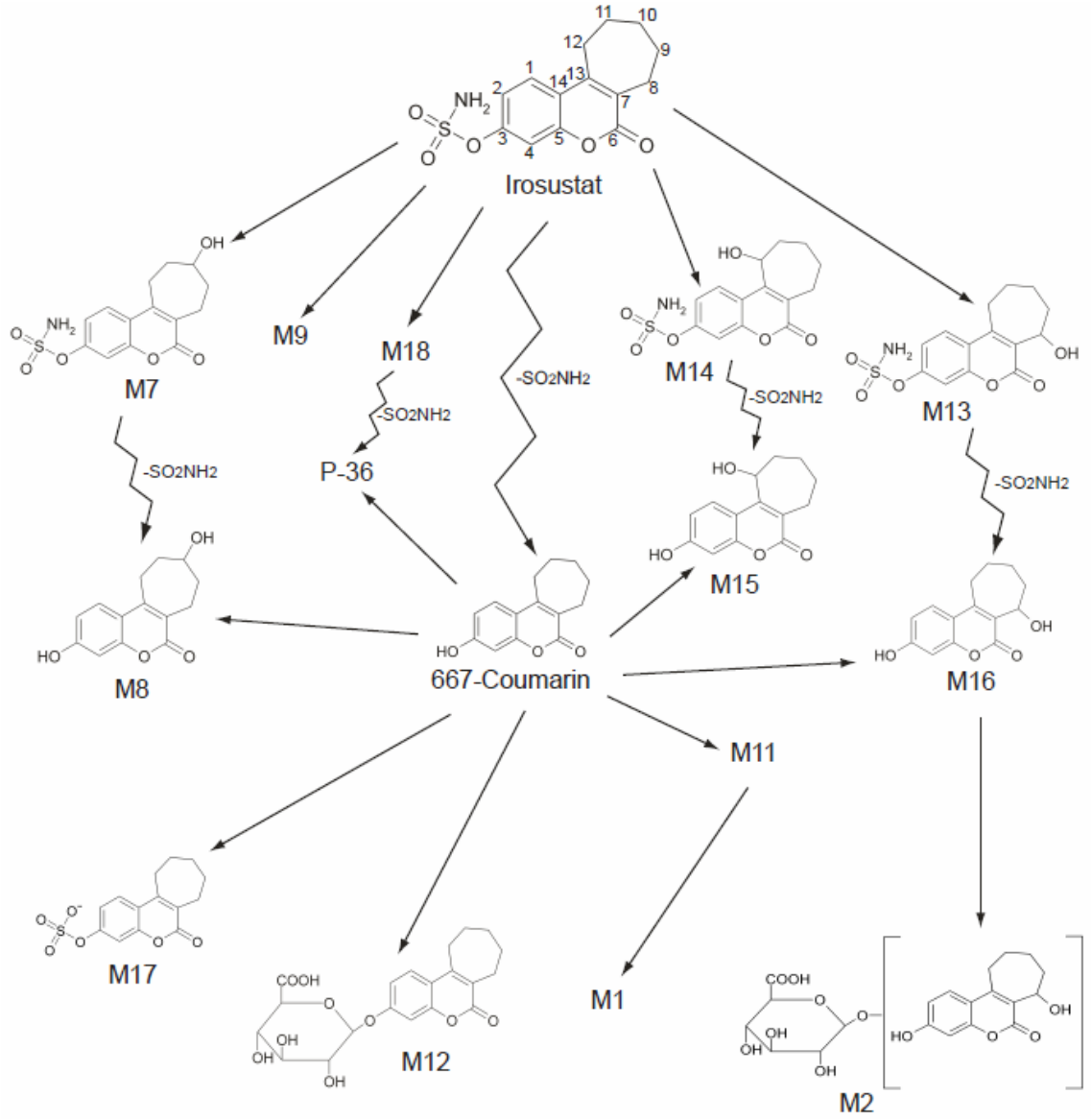

Figure 16. Structures of irosustat metabolites formed in vitro.

The glucuronidation and the sulfation of 667-coumarin may basically be produced through its unique hydroxyl group at the C3 position, yielding M12 (667-coumarin 3-O-glucuronide) and M17 (667-coumarin 3-O-sulfate), respectively (Figure 16). Metabolites M1 and M2, which were preliminarily identified by mass spectrometry as glucuronides, were purified and treated with β-glucuronidase, leading to the formation of M11 and M16, respectively (Figure 16).

RESULTS II:
IROSUSTAT DRUG-DRUG INTERACTION STUDIES

DETERMINATION OF THE HUMAN ENZYMES RESPONSIBLE FOR THE METABOLISM OF IROSUSTAT

Determination of the Human P450 Enzymes Responsible for the Metabolism of Irosustat.

As step preceding the enzyme identification experiments, the substrate concentration-dependent transformation of ^{14}C-irosustat was assessed in HLM. The kinetics showed a classic hyperbolic pattern (Figure 17), and, therefore, the Michaelis-Menten kinetics equation was fitted to the metabolite formation data, giving a K_M value of 43.4 µM and a V_{max} value of 369 pmol/mg per min. From these results and former data on linearity of ^{14}C-irosustat metabolism, the incubation conditions selected for the following phenotyping experiments were set as follows: 50 µM irosustat, 1 mg/mL microsomal protein concentration, and 40-min incubation time.

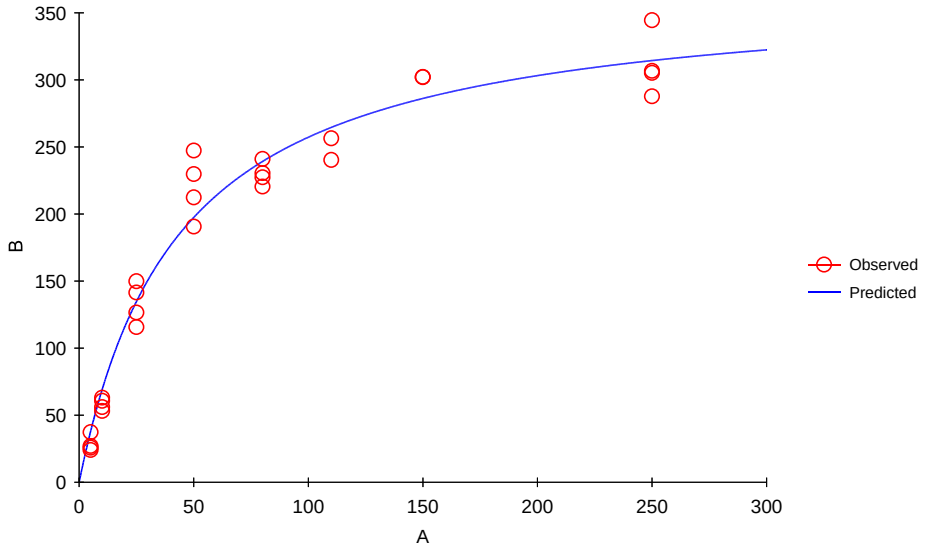

A: Irosustat concentration (µM); B: Enzyme activity (pmol/mg/min)

Figure 17. Enzyme kinetics of ^{14}C-irosustat metabolism by human liver microsomes. Michaelis-Menten model.

To identify the P450 enzymes responsible for the metabolism of irosustat, a combination of three experimental approaches was used:

(1) Correlation analysis of irosustat phase I metabolite formation rate with several P450 isoform-specific activities in a panel of 16 individual HLM;

(2) Assessment of the effect of chemical P450 isoform-specific inhibitors on irosustat metabolite formation in pooled HLM; and

(3) Formation of irosustat metabolites by cDNAexpressed human P450 enzymes.

Variable results were obtained for each approach. The correlation between specific P450 activities and irosustat metabolite formation seemed to be the most selective part of the study, and the results are shown in Table 5. Under our experimental conditions, the formation of all irosustat metabolites, except for P-36, correlated with the activity of one or more members of CYP2C family (i.e., CYP2C8, CYP2C9, and CYP2C19). For some of the metabolites, an additional correlation was found with CYP3A4/5 (M13, M14, and M16) and CYP2E1 (M7) activities. Formation of metabolite P-36 did not correlate with any of the P450s tested.

Table 5. Correlation between irosustat metabolite formation in a panel of HLM from 16 different individual donors and specific activities of individual P450 enzymes and FMO3.

Enzymes*	Pearson Correlation Coefficient (r)								
	M7	**M8**	**M9**	**M11**	**M13**	**M14**	**M16**	**M18**	**P-36**
CYP1A2[1]	0.3442	0.2113	0.1063	-0.2011	0.1428	0.1566	0.1633	0.2141	0.1036
CYP1A2[2]	0.3448	0.1842	0.1877	-0.0852	0.2512	0.3685	0.2702	0.1743	0.1871
CYP2A6	0.1461	0.1888	0.3843	0.2659	0.4432	0.4054	0.5487	0.4000	0.5040
CYP2B6[3]	0.0842	0.0561	0.4763	0.4781	0.4743	0.5963	0.6118	0.2896	0.5014
CYP2B6[4]	-0.2274	-0.2807	0.0828	0.3068	0.0793	0.2639	0.2399	-0.0511	0.3690
CYP2C8	0.5678	0.5420	**0.7748*****	**0.6891****	**0.6812****	**0.6607****	**0.7612*****	0.4732	0.5552
CYP2C9	**0.8845*****	**0.8734*****	**0.7457*****	0.2617	**0.7894*****	0.4010	**0.6400****	**0.8397*****	0.5381
CYP2C19	**0.7253****	**0.7077****	0.5973	-0.0048	**0.7237****	0.4801	**0.6592****	**0.8776*****	0.5918
CYP2D6	-0.1915	-0.0889	0.0417	-0.0502	0.1044	0.3233	0.1177	-0.0034	-0.3070
CYP2E1	**0.6430****	0.4251	0.5158	0.3324	0.3751	0.2590	0.3077	0.2424	0.3554
CYP3A4/5[5]	0.2255	0.2284	0.5628	0.1269	**0.6830****	**0.9490*****	**0.7338****	0.3922	0.3699
CYP3A4/5[6]	0.2009	0.1563	0.5147	0.1804	**0.6452****	**0.9273*****	**0.7051****	0.2731	0.4055
FMO3	-0.2383	-0.1785	-0.3982	-0.4268	-0.3530	-0.2174	-0.3755	-0.2916	-0.3942

Results are expressed as the Pearson correlation coefficient from the mean of duplicate incubations for each batch of HLM.

**Enzyme activities: 7-ethoxyresorufin O-dealkylation[1] and phenacetin O-deethylation[2] (for CYP1A2), coumarin 7-hydroxylation (for CYP2A6), S-mephenytoin N-demethylation[3] and bupropion hydroxylation[4] (for CYP2B6), paclitaxel 6α-hydroxylation (for CYP2C8), diclofenac 4'-hydroxylation (for CYP2C9), S-mephenytoin 4'-hydroxylation (for CYP2C19), dextromethorphan O-demethylation (for CYP2D6), chlorzoxazone 6-hydroxylation (for CYP2E1), testosterone 6β-hydroxylation[5] and midazolam 1'-hydroxylation[6] (for CYP3A4/5), and benzydamine N-oxidation (for FMO)*

** *Statistically significant correlation ($p < 0.01$)*
*** *Statistically significant correlation ($p < 0.001$)*

The results of the chemical inhibition phase (Table 6) showed that almost all inhibitors, except those for CYP1A2 (furafylline) and CYP2C19 [(+)-nootkatone and (+)-N-3-benzyl-nirvanol], relevantly decreased the formation of several irosustat metabolites.

Table 6. Inhibition of the formation of irosustat metabolites in incubations with HLM in the presence of P450-selective chemical inhibitors.

Chemical Inhibitors*	Inhibition (%)								
	M7	**M8**	**M9**	**M11**	**M13**	**M14**	**M16**	**M18**	**P-36**
CYP1A2	-1.9	-1.4	0.0	-22.2	-0.2	14.4	-16.1	-4.4	-4.5
CYP2A6	**45.6**	**48.0**	**22.1**	5.0	NQ	NQ	**32.9**	**53.0**	**37.1**
CYP2B6	**23.5**	**21.4**	**47.9**	**48.1**	**30.2**	**32.0**	**24.1**	**30.3**	17.7
CYP2C8	**51.5**	**49.4**	**64.9**	**50.0**	**50.9**	**33.4**	**43.3**	**61.4**	**35.8**
CYP2C9	**41.8**	**71.2**	17.7	8.9	**51.3**	-1.5	**37.7**	**65.7**	**60.5**
CYP2C19[a]	10,0	19,6	13,8	17,3	14,0	-24,8	9,4	19,8	10,9
CYP2C19[b]	-2,8	-9,3	-18,4	-17,0	-4,8	-21,2	-9,0	1,3	-3,5
CYP2D6	14.5	NQ	NQ	NQ	12.6	10.7	8.4	**22.6**	6.9
CYP2E1	**24.3**	4.5	17.5	**33.6**	9.9	4.7	7.5	**26.9**	8.8
CYP3A4/5	11.8	1.0	**36.5**	15.3	**24.0**	**55.7**	**20.3**	**23.5**	-4.1

Results are expressed as percentage of inhibition relative to control incubations (without inhibitor) and are the mean values from duplicate incubations except for CYP2C19 which were triplicate incubations. Bold numbers represent >20% inhibition.

** P450 inhibitors: 1 µM furafylline (CYP1A2); 0.1µM methoxsalen (CYP2A6); 750 µM orphenadrine (CYP2B6); 10 µM quercetin (CYP2C8); 2 µM sulfaphenazole (CYP2C9); 100 µM (+)-nootkatone[a], and 5 µM (+)-N-3-benzyl-nirvanol[b] (CYP2C19); 0.5 µM quinidine (CYP2D6);15 µM 4-methylpyrazole (CYP2E1); and 0.5 µM ketoconazole (CYP3A4/5).*

NQ: not quantified because of HPLC coelution of the inhibitor with the metabolites.

Table 7 shows the results obtained in incubations of cDNA-expressed P450 enzymes with irosustat. Recombinant CYP1A2 and CYP2C19 were able to form most of the irosustat metabolites produced in HLM incubations. CYP2A6 and FMO3 enzymes were not able to metabolize irosustat. Because CYP2B6 was able to form M16 and P-36 but not their respective sulfamoylated precursors M13 and M18, CYP2B6 was also incubated with irosustat for shorter incubation times, showing formation of M18 but not M13. 667-Coumarin was also incubated with the same cDNA-expressed P450

enzymes. The 667-coumarin metabolites M8, M16, and P-36 were formed by different enzymes. M8 was formed by the same enzymes as irosustat, M16 was formed by the same enzymes as irosustat plus CYP2A6, CYP2C8, and CYP2E1, and P-36 was formed by all P450s except for CYP2C8, CYP2C9, and CYP2E1.

Table 7. Formation of irosustat metabolites in incubations with human cDNA-expressed P450s and FMO3 enzyme.

Enzyme	Mean Peak Area								
	M7	**M8**	**M9**	**M11**	**M13**	**M14**	**M16**	**M18**	**P-36**
CYP1A1	3784	nd	nd	nd	25693	30242	30049	3196	nd
CYP1A2	39779	8781	15849	nd	105131	69618	37042	16618	nd
CYP1B1	nd	nd	nd	nd	4978	nd	15681	nd	nd
CYP2A6	nd	nd	nd	nd	nd	nd	nd	nd	nd
CYP2B6	nd	nd	nd	nd	nd	nd	3132	nd	5565
CYP2C8	nd	nd	2653	nd	2731	nd	nd	nd	nd
CYP2C9	4129	nd	nd	nd	4904	nd	2106	2648	nd
CYP2C19	15105	4528	2444	nd	22693	nd	14730	6638	8235
CYP2D6	125154	20891	3785	nd	52889	nd	12864	4213	nd
CYP2E1	10210	1923	nd	nd	2599	nd	nd	nd	nd
CYP3A4	nd	nd	7425	nd	88686	51656	26628	5335	nd
CYP3A5	1855	nd	2159	nd	12175	1915	4855	2915	nd
FMO3	nd	nd	nd	nd	nd	nd	nd	nd	nd

Results are expressed as means of metabolite peak area units from duplicate incubations.
nd: not detected

Although all three approaches have advantages and disadvantages, a combination of them was required to identify which enzyme or enzymes could potentially be responsible for irosustat metabolism. The enzymes that showed positive results in the three approaches were CYP2C8, CYP2C9, CYP2E1, and CYP3A4/5, and they were identified as the main enzymes potentially responsible for the phase I metabolism of irosustat.

Investigation of the Role of CYP1A2 in Irosustat Metabolism.

As mentioned, human cDNA-expressed CYP1A2 was able to form a metabolite profile very similar to the one obtained by HLM. However, negative results were

obtained in the correlation and inhibition approach. Therefore, investigation of the role of CYP1A2 was performed.

The effect of a combination of chemical inhibitors of the P450s involved in irosustat metabolism was assessed in native and CYP1A2-fortified HLM in the presence or absence of furafylline (CYP1A2 inhibitor). Table 8 shows the percentage of inhibition for each of the irosustat metabolites formed. Furafylline alone showed no inhibitory effect either in native or in CYP1A2-fortified HLM, except for a slight inhibition of M14 formation in the latter. The formation of all metabolites was remarkably inhibited by the combination of specific P450 inhibitors in both HLM models. Approximately the same inhibition percentages were found in irosustat incubations with native HLM when the mix of inhibitors was used either in the presence or absence of furafylline. However, in CYP1A2-fortified HLM, the inhibition of irosustat metabolism increased (for almost all metabolites) when furafylline was used together with the mix of P450-inhibitors.

Table 8. Investigation of the role of CYP1A2 in irosustat metabolism.

Matrix	Chemical Inhibitors	Inhibition (%)								
		M7	**M8**	**M9**	**M11**	**M13**	**M14**	**M16**	**M18**	**P-36**
Native HLM	**FU**	1.4	2.0	4.3	*-59.5*	1.7	2.7	1.2	2.4	1.9
	MIX	**66.2**	**100**	**74.6**	**100**	**65.0**	**49.5**	**70.3**	**64.4**	**47.7**
	MIX + FU	**65.6**	**100**	**81.3**	**100**	**66.5**	**54.6**	**81.3**	**68.0**	**54.6**
CYP1A2-fortified HLM	**FU**	-2.6	-8.2	-0.3	*-15.0*	7.0	**24.9**	12.1	0.8	-17.1
	MIX	**44.7**	**44.7**	**58.2**	**100**	**44.3**	**23.7**	**29.6**	**46.1**	**22.6**
	MIX + FU	**56.3**	**61.5**	**72.9**	**100**	**61.1**	**54.2**	**53.8**	**60.7**	**32.8**

Formation of irosustat metabolites in incubations with native and CYP1A2-fortified HLM. Results are expressed as percentage of inhibition for each separate metabolite and are the mean values from duplicate incubations.

Inhibitors: FU, 1 μM furafylline; MIX, 10 μM quercetin + 2 μM sulfaphenazole + 20 μM tranylcypromine + 0.5 μM ketoconazole. Microsomal protein concentration: 1 mg/mL ± 20 pmol/mL recombinant human CYP1A2. Incubation time: 15-min preincubation ± furafylline followed by 40-min incubation. Irosustat concentration: 50 μM. Bold numbers represent percentage of inhibition >20%. Italic values represent high variability for M11 because peak areas were close to the limit of detection.

Determination of the Phase II Enzymes Responsible for the Metabolism of Irosustat

To identify the relative contribution of specific human liver enzymes responsible for the formation of the phase II metabolites of irosustat, incubations were performed using cDNA-expressed human UGT and SULT enzymes in the presence of the

respective cofactors. The experimental approach consisted of incubating irosustat with recombinant CYP1A2 to induce the formation of most of the phase I in vitro metabolites (Table 7), followed by the addition of the different UGT and SULT enzymes and the required cofactors.

Table 9. Formation of irosustat metabolites in incubations with human cDNA-expressed UGT enzymes.

Enzyme	Mean Peak Area								
	G1*	**G2***	**G3***	**G4***	**M2**	**M4***	**G7***	**G8***	**M12****
UGT1A1	3426	4859	nd	nd	9573	3341	nd	nd	451831
UGT1A3	nd	nd	nd	nd	31109	11989	nd	nd	521544
UGT1A4	nd	nd	nd	nd	nd	nd	nd	nd	Nd
UGT1A6	nd	nd	nd	nd	nd	nd	nd	nd	15031
UGT1A7	nd	nd	nd	nd	3228	nd	nd	nd	68845
UGT1A8	nd	nd	nd	nd	7468	2584	nd	5038	330741
UGT1A9	nd	4860	6819	nd	11240	3141	nd	25835	228401
UGT1A10	nd	nd	nd	nd	nd	nd	nd	nd	86036
UGT2B4	nd	nd	nd	nd	3619	nd	nd	nd	210011
UGT2B7	nd	nd	nd	nd	6706	nd	nd	nd	510503
UGT2B15	nd	nd	nd	3135	24520	4696	nd	nd	541538
UGT2B17	nd	nd	nd	nd	nd	nd	12861	nd	320705

Results are expressed as mean of metabolite peak area units from duplicate incubations.
nd: not detected
** : Unidentified glucuronide conjugates*
***: Incubations performed with 667-coumarin*

As shown in Table 9, up to nine peaks corresponding to putative glucuronides were produced by the different UGTs. These metabolites were as follows: M12 and M2 (already detected in hepatocyte incubations; see Figure 10) and G1, G2, G3, G4, M4, G7, and G8 (newly detected metabolites). M12 was also formed when 667-coumarin was incubated directly with all UGTs except for UGT1A4, which, in turn, was the unique UDP-glucuronosyltransferase unable to form any of the glucuronides.

Table 10. Formation of irosustat metabolites in incubations with human cDNA-expressed SULT enzymes.

Enzyme	Mean Peak Area							
	M3	**S2***	**S3***	**S4***	**S5***	**S6***	**M17****	**S7***
SULT 1A1*1	12626	12773	2645	4299	6554	9783	99619	3040
SULT 1A1*2	4672	3753	nd	2521	nd	6892	59468	2835
SULT 1A2*1	2604	nd	nd	nd	nd	nd	17799	2802
SULT 1A3	nd	nd	nd	nd	nd	4066	nd	3950

Results are expressed as mean of metabolite peak area units from duplicate incubations.
nd: not detected
** : Unidentified sulfate conjugates*
***: Incubations performed with 667-coumarin*

As shown in Table 10, up to eight peaks corresponding to potential sulfate conjugates were found after incubation of irosustat phase I metabolites with different human SULTs (1A1*1, 1A1*2, 1A2*1, and 1A3), using the same experimental approach. The sulfate conjugates were named S2, S3, S4, S5, S6, and S7 (new peaks) and were formed in addition to M17 and M3, which had already been detected in hepatocyte incubations (Figure 10). M17 formation was also confirmed when 667-coumarin was incubated directly with all the SULTs. Sulfotransferases SULT1A1*1, 1A1*2, and 1A2*1, but not SULT1A3, were capable of forming M17. SULT1A1*1 was able to produce all the sulfate conjugates identified and also in the largest amounts.

INHIBITION OF DRUG-METABOLIZING ENZYMES BY IROSUSTAT

Inhibition of P450 Enzyme Activity

The inhibitory potential of irosustat for CYP1A2, CYP2A6, CYP2B6, CYP2C8, CYP2C9, CYP2C19, CYP2D6, CYP2E1, and CYP3A4/5 (CYP3A4/5 substrates were nifedipine, midazolam, and testosterone) was studied in HLMs by comparing the P450-specific activities at increasing concentrations of test compound with and without 30-min preincubation in the presence of irosustat and cofactor, to assess possible TDI.

Table 11. P450 enzyme activity inhibition results for irosustat.

P450	Activity	IC_{50} (CV)	
		Direct	TDI
CYP1A2	Phenacetin O-deethylase	7.6 (22%)	1.1 (8%)
CYP2A6	Coumarin 7-hydroxylase	NA	NA
CYP2B6	Bupropion hydroxylase	> 50	~ 50
CYP2C8	Paclitaxel 6α-hydroxylase	NA	NA
CYP2C9	Tolbutamide methylhydroxylase	> 50	> 50
CYP2C19	S-Mephenytoin 4-hydroxylase	40 (18%)	38 (13%)
CYP2D6	Dextromethorphan O-demethylase	> 50	> 50
CYP2E1	Chlorzoxazone 6-hydroxylase	NA	NA
CYP3A4/5	Nifedipine oxidase	NA	NA
CYP3A4/5	Midazolam 1-hydroxylase	> 50	~ 50
CYP3A4/5	Testosterone 6β-hydroxylase	~ 50	44 (9%)

Results are mean values from triplicate incubations. IC50 values are expressed in μM.
CV: coefficient of variation of the estimates in percentage
NA: not assessed (no inhibition found at any of the assayed concentrations, up to 50 μM)

As shown in Table 11, the results let us classify P450s into three categories as a function of the extent of enzyme activity inhibition by irosustat: i.e., 1) noninhibited P450 enzyme activities, including CYP2A6, CYP2C8, CYP2E1, and CYP3A4/5 (nifedipine substrate), which were not inhibited at any of the assayed irosustat concentrations; 2) mildly inhibited P450 enzyme activities, including CYP2B6, CYP2C9, CYP2D6, and CYP3A4/5 (midazolam and testosterone substrates), which were inhibited only at the highest tested irosustat concentrations and yielded estimated IC_{50} values of ≥ 50 μM; and 3) highly inhibited P450 enzyme activities, including CYP1A2 and to a lesser extent CYP2C19, for which IC_{50} values were estimated to be < 50 μM (the estimated IC_{50} values are presented in Table 11). For CYP1A2, CYP2B6, and CYP3A4 (with midazolam and testosterone as substrates), TDI was observed. All of the reference P450 inhibitors used (see material and methods section) showed the expected inhibitory effects, which validated the experiments.

Table 12. P450 enzyme activity inhibition results for 667-coumarin.

P450 Enzyme	IC_{50} (CV)		K_i (CV)	Inhibition Type
	Direct	TDI		
CYP1A2	0.65 (4%)	0.27 (5%)	0.77 (7%)	Competitive
CYP2C19	10 (6%)	13 (17%)	5.8 (10%)	Competitive

Results are mean values from triplicate incubations. IC50 and Ki values are expressed in μM.
CV: coefficient of variation of the estimates in percentage

The potential inhibitory effects of the irosustat derivative 667-coumarin on CYP1A2 and CYP2C19 were also investigated. The IC_{50} values presented in Table 12 show that 667-coumarin was more potent than irosustat in inhibiting both P450 enzyme activities. For CYP1A2, 667-coumarin showed an IC_{50} value > 10-fold lower than that of the parent compound without preincubation (0.65 versus 7.6 μM) and 4-fold lower after a 30-min preincubation with HLMs and cofactor (0.27 versus 1.1 μM). The remarkable differences between the two incubation conditions demonstrated TDI for both compounds for CYP1A2 activity. For CYP2C19, 667-coumarin showed an IC_{50} value 3- to 4-fold lower than that of irosustat. However, the potency of irosustat and 667-coumarin in the inhibition of CYP2C19 activity was remarkably lower than for CYP1A2, and preincubation did not enhance 667-coumarin-induced inhibition of CYP2C19 activity.

Because 667-coumarin was more potent than irosustat in inhibiting both CYP1A2 and CYP2C19 activities, additional incubations were performed to determine the K_i values and inhibition type for 667-coumarin for both P450 enzyme activities. The resulting K_i values are shown in Table 12. As expected, 667-coumarin was more potent in inhibiting CYP1A2 (K_i = 0.77 µM) than CYP2C19 (K_i = 5.8 µM), and the competitive inhibition model was the one that statistically best fit the inhibition data for 667-coumarin with both enzymes.

Table 13. Determination of NADPH dependence and irreversibility for P450 enzyme activity inhibition with irosustat and 667-coumarin.

P450	Test Compound	+ NADPH			- NADPH			With Dilution		
		0 min	15 min	30 min	0 min	15 min	30 min	0 min	15 min	30 min
		% remaining								
CYP1A2	**5 µM Irosustat**	73	48	31	69	53	43	99	94	94
	0.5 µM 667-Coumarin	65	44	37	61	55	58	104	96	95
	2 µM Furafylline	53	21	14	56	49	52	99	65	55
CYP2B6	**50 µM Irosustat**	77	69	62	*nd*	62	58	102	98	90
	5 µM 667-Coumarin	82	77	79	*nd*	75	76	113	102	91
	4 µM Thio-TEPA	70	47	<31	*nd*	79	74	90	47	39
CYP3A4/5[1]	**50 µM Irosustat**	86	76	67	*nd*	76	69	121	101	95
	5 µM 667-Coumarin	99	98	88	*nd*	101	104	111	104	103
	50 µM Mifepristone	30	11	10	*nd*	29	33	67	22	14
CYP3A4/5[2]	**50 µM Irosustat**	48	40	36	*nd*	46	38	89	98	86
	5 µM 667-Coumarin	74	69	67	*nd*	80	76	87	107	102
	50 µM Mifepristone	15	<11	<11	*nd*	17	13	73	12	<6

For irreversibility testing (dilution test), test compounds were preincubated with HLMs with 25-fold increased microsomal protein concentrations and with NADPH. Incubates were diluted 25-fold before the addition of P450 substrates. During incubations, the actual concentrations of irosustat and 667-coumarin were 2 µM irosustat and 0.2 µM 667-coumarin for CYP2B6 and CYP3A4/5 and 0.2 µM irosustat and 0.02 µM 667-coumarin for CYP1A2. Results are expressed as mean percentages of remaining P450 enzyme activity (n = 3).
CYP3A4/5 activities: midazolam 1'-hydroxylation[1] and testosterone 6β-hydroxylation[2]
nd :not done (samples not prepared). The same values as +NADPH (0 min) were assumed.

Because TDI was found for CYP1A2, CYP2B6, and CYP3A4/5 (with midazolam and testosterone as substrates), the NADPH dependence and the irreversibility of the inhibition of these P450 activities were assayed for both irosustat and 667-coumarin (Table 13). TDI for all of the assayed P450 enzymes was confirmed for irosustat, although the inhibition was not dependent on NADPH in any of the cases. When the effect of 667-coumarin was assessed, no differences were found among the preincubation times for CYP2B6 and CYP3A4/5, either in the presence or in the absence of NADPH. However, TDI of CYP1A2 activity was caused by 667-coumarin only when NADPH was present. The results of the dilution experiments showed that the CYP1A2, CYP2B6, and CYP3A4/5 inhibition by irosustat and 667-coumarin can be considered reversible. The reference mechanism-based P450 inhibitors (2 μM furafylline for CYP1A2, 4 μM Thio-TEPA for CYP2B6, and 50 μM mifepristone for CYP3A4/5) were able to produce time-dependent, NADPH-dependent, irreversible inhibition of their corresponding P450s, which validated the experimental procedure (Table 13).

Inhibition of UGT Enzyme Activity

The effect of protein concentration and incubation time on 7-hydroxy-4-methylcoumarin glucuronosyltransferase activity by UGT1A1 and UGT2B7 was studied in order to determine linear incubation conditions.

The 7-hydroxy-4-methylcoumarin glucuronide formation *vs* protein concentration and *vs* incubation time, showed a linear formation up to approximately 0.5 mg/mL for UGT1A1, 1 mg/mL for UGT2B7 and 60 minutes for both, respectively. Taking these results into account, the incubation conditions selected were 0.5 mg/mL protein concentration and 60 minutes incubation time for both enzymes.

The inhibitory potential of irosustat and 667-coumarin towards recombinant UGT1A1 and UGT2B7 was studied comparing 7-hydroxy-4-methylcoumarin glucuronosyltransferase activity. The inhibitory potential of irosustat and 667-coumarin towards recombinant UGT1A4 was studied comparing trifluoperazine glucuronosyltransferase activity. All activities were studied in the presence/absence of irosustat or 667-coumarin at increasing concentrations.

Table 14. Effect of irosustat and 667-coumarin on UGT1A1, UGT2B7 and UGT1A4 enzymes.

Compound	7-Hydroxy-4-methylcoumarin glucuronosyltransferase activity		Trifluoperazine glucuronosyl-transferase activity
	UGT1A1	**UGT2B7**	**UGT1A4**
CONTROL	100.0	100.0	100.0
Irosustat 0.05 µM	88.1	97.9	84.4
Irosustat 0.25 µM	96.3	99.1	102.3
Irosustat 2 µM	93.0	94.1	90.1
Irosustat 5 µM	86.5	89.9	99.6
Irosustat 50 µM	**37.7**	**68.2**	81.6
667-Coumarin 0.05 µM	97.5	88.6	96.5
667-Coumarin 0.25 µM	97.6	86.2	95.6
667-Coumarin 2 µM	94.1	81.9	90.8
667-Coumarin 5 µM	88.0	**78.1**	89.4
667-Coumarin 50 µM	**26.2**	**48.5**	**71.6**
Reference inhibitor*	**64.3**	**40.3**	**70.4**

Results are mean values from triplicate incubations and expressed as percentage remaining.
**Reference inhibitor: 50 µM diclofenac (for UGT1A1 and UGT2B7) or 1.6 mM quinidine (for UGT1A4)*

As shown in Table 14, both irosustat and 667-coumarin were able to inhibit almost all UGT enzyme activities at the highest concentration tested (50 µM), except for irosustat with UGT1A4 activity, for which no inhibition was observed in the working concentration range. In all assays, 667-coumarin showed greater inhibitory potential than did irosustat. UGT1A1 activity was inhibited to the greatest extent by both compounds. The IC_{50} parameters for UGT1A1 enzyme were estimated (see Table 15): 43 µM and 30 µM for irosustat and 667-coumarin, respectively.

Table 15. UGT Inhibition Results. Determination of IC_{50} Parameters.

UGT Enzyme	Activity	Direct IC_{50} (CV)	
		Irosustat	**667-Coumarin**
UGT1A1	7-Hydroxy-4-methylcoumarin glucuronosyltransferase	43 (9%)	30 (9%)
UGT1A4	Trifluoperazine glucuronosyltransferase	NA	> 50
UGT2B7	7-Hydroxy-4-methylcoumarin glucuronosyltransferase	> 50	~ 50

Results are expressed as μM and are the mean value from triplicate incubations.
CV: coefficient of variation of the estimates in percentage
NA: not assessed (no inhibition found at any of the assayed concentrations, up to 50 μM)

INDUCTION OF DRUG-METABOLIZING ENZYMES BY IROSUSTAT

Induction of P450 Enzymatic Activities

Irosustat at 0.25, 2.5, and 10 μM was incubated with freshly isolated human hepatocytes for 72 h (for assessment of CYP1A2 and CYP3A4 induction) or 96 h (for assessment of CYP2C9 and CYP2C19 induction). Hepatocytes corresponded to three separate donors. Cell viability after isolation was determined with the trypan blue exclusion method and ranged from 75 to 94%. The prototypical P450 inducers (50 μM omeprazole for CYP1A2 and 50 μM rifampicin for CYP2C9, CYP2C19, and CYP3A4) showed the expected results (≥2-fold induction), which validated the induction response of the three hepatocyte batches. Results for each donor are shown in Figure 18.

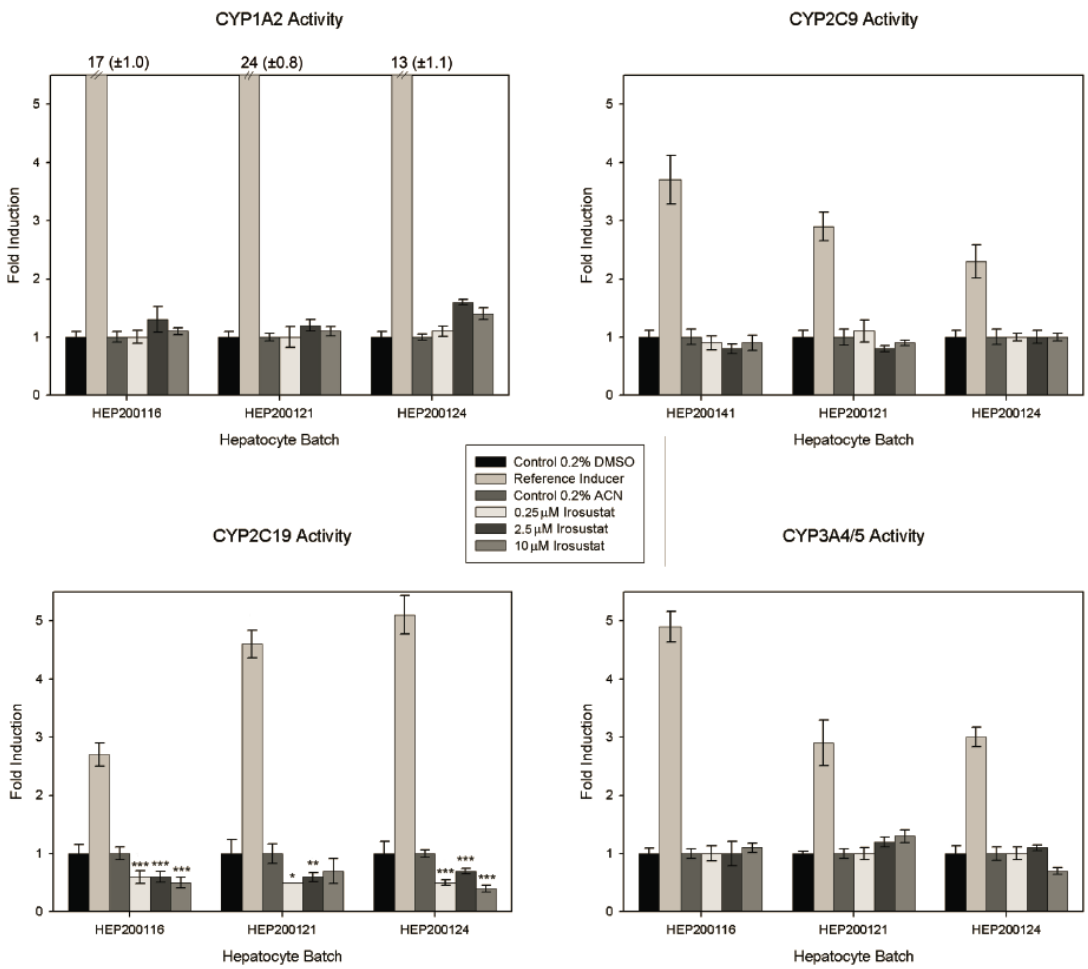

Figure 18. Induction potential of irosustat for CYP1A2, CYP2C9, CYP2C19 and CYP3A4/5 enzymatic activities in human hepatocytes (first experiment).

Results are expressed as fold induction (mean ± SD; n=4, three donors). Reference inducers were omeprazole for CYP1A2 and rifampicin for CYP2C9, CYP2C19 and CYP3A4. *, $p < 0.05$; **, $p < 0.01$; ***, $p < 0.001$, in comparison with vehicle control group. ACN, acetonitrile.

CYP1A2 enzyme activity. Phenacetin O-deethylase activity was not appreciably changed at any of the tested irosustat concentrations in two of the hepatocyte batches. In batch HEP200124, CYP1A2 enzyme activity was increased by factors of 1.6 and 1.4 (relative to solvent control) with 2.5 µM and 10 µM irosustat, respectively, but these values represented only 12.3% and 10.8% of the values obtained with the positive control omeprazole.

CYP2C9 enzyme activity. Tolbutamide methylhydroxylase activity was not noticeably changed with any of the tested concentrations of irosustat in any of the batches of hepatocytes used.

CYP2C19 enzyme activity. In the presence of irosustat, (S)-mephenytoin 4'-hydroxylase activity decreased significantly to 40% to 70% of the control values with

all tested concentrations of test compound (even the lowest concentration, 0.25 µM) with the three hepatocyte batches.

CYP3A4/5 enzyme activity. Nifedipine oxidase activity was not appreciably changed with any of the tested irosustat concentrations in one of the hepatocyte batches. In batch HEP200121, CYP3A4/5 enzyme activity was increased by factors of 1.2 and 1.3 (relative to solvent control) after exposure to 2.5 µM and 10 µM irosustat, respectively. In batch HEP200124, CYP3A4/5 enzyme activity decreased to 70% of control values after treatment with 10 µM irosustat.

Measurement of mRNA expression.

In a second induction experiment, 2.5 µM irosustat was incubated with human hepatocytes from two individual donors for 48 h for evaluation of *CYP1A2, CYP2C19*, and *CYP3A4* mRNA contents and for 96 h for assessment of CYP2C19 enzyme activity. Cell viability after isolation was determined with the trypan blue exclusion method and ranged from 96% to 98%. The prototypical inducers used to validate the qPCR results (see above) worked as expected. Results are shown in Figure 19.

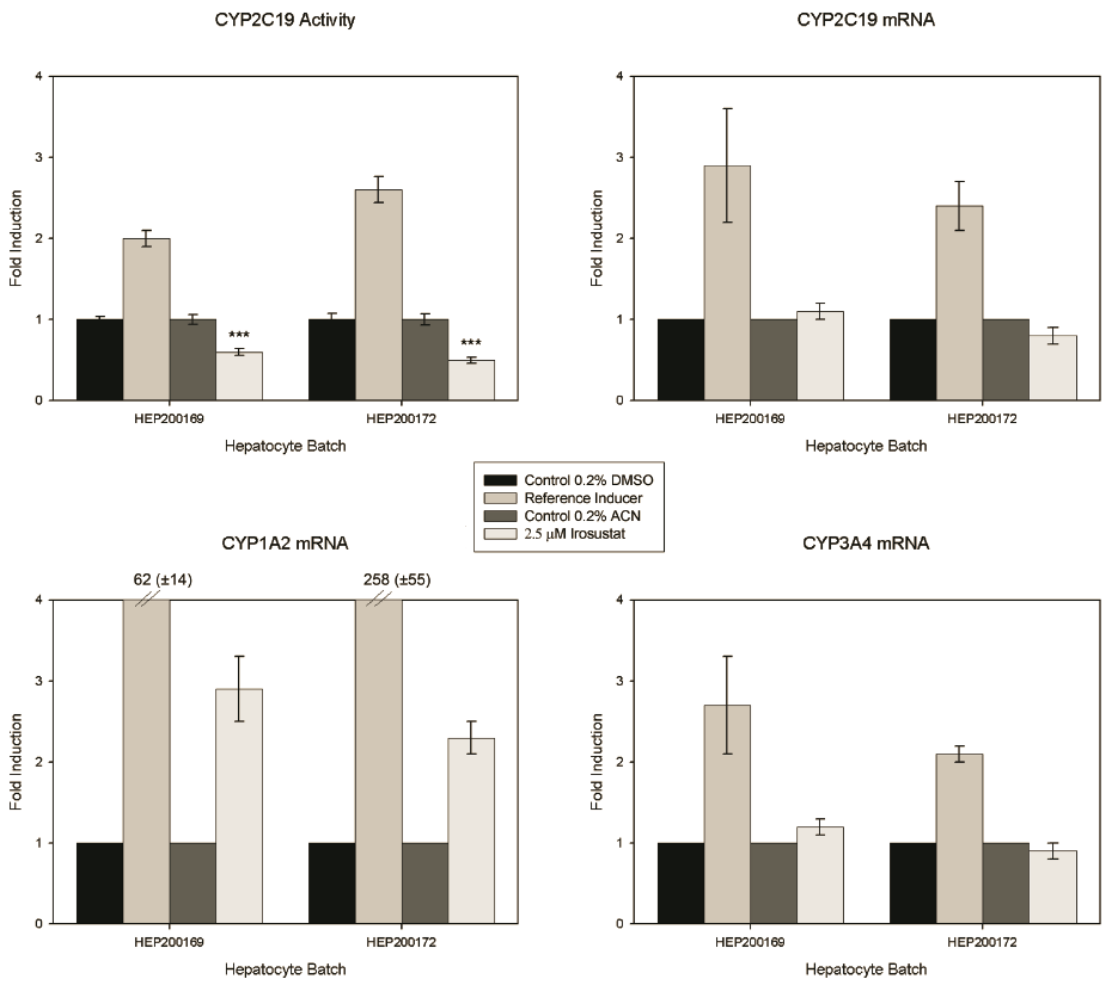

Figure 19. Induction potential of irosustat for CYP2C19 enzymatic activity and *CYP1A2, CYP2C19*, and *CYP3A4* mRNA expression in human hepatocytes (second experiment).

Results are expressed as fold induction (mean ± SD; n = 3, two donors). Reference inducers were omeprazole for CYP1A2 and rifampicin for CYP2C9, CYP2C19, and CYP3A4. ***, $p < 0.001$, in comparison with vehicle control group. ACN, acetonitrile.

As in the preceding experiments, CYP2C19 enzymatic activity decreased significantly to 50% to 60% of control values after exposure to 2.5 µM irosustat, whereas the reference inducer worked as expected. The expression of *CYP2C19, CYP1A2*, and *CYP3A4* mRNA was evaluated with the same hepatocytes. No considerable modification of *CYP2C19* and *CYP3A4* mRNA expression in cells exposed to irosustat for 48 h was detected in the two batches of hepatocytes (0.8 – 1.2-fold induction, relative to solvent control). In contrast, the expression of *CYP1A2* mRNA was increased to 2.9 and 2.3 times control values (0.2% acetonitrile) in hepatocytes from batches HEP200169 and HEP200172, respectively. However, these increases represented only 5 and 1%, respectively, of the responses to the positive inducer omeprazole.

EFFECT OF AROMATASE INHIBITORS ON THE IN VITRO METABOLISM OF IROSUSTAT

The inhibitory potential of the aromatase inhibitors (AIs) letrozole, anastrozole, and exemestane in the in vitro metabolism of irosustat was studied by using HLMs with and without preincubation of the AIs in the presence of cofactor.

The metabolite profile of irosustat in HLMs was characterized by the formation of 10 main phase I metabolites in addition to 667-coumarin, namely, M7, M8, M9, M11, M13, M14, M15, M16, M18, and P-36.

For letrozole, the inhibitory effect on the formation of irosustat metabolites never reached 50% in the concentration range tested (up to 100 μM); in particular, the formation of metabolites M14 and M15 was completely unaffected. Because of that, IC_{50} values were not estimated. Similar results were obtained with exemestane, which did not affect the formation of any irosustat metabolite in the concentration range tested (up to 20 μM). In contrast, anastrazole (from a 5 μM concentration) caused relevant inhibition of irosustat metabolism, either with or without 30-min preincubation in the presence of cofactor.

Table 16. Inhibition of irosustat metabolite formation by AIs letrozole, anastrozole, and exemestane.

Irosustat Metabolites	IC_{50} (CV)					
	Letrozole		Anastrozole		Exemestane	
	Direct	TDI	Direct	TDI	Direct	TDI
M7	>100	>100	78 (5%)	66 (5%)	NA	NA
M8	>100	NA	55 (5%)	44 (5%)	NA	NA
M9	>100	>100	75 (7%)	64 (7%)	NA	NA
M11	>100	>100	>100	83 (13%)	NA	NA
M13	>100	>100	38 (4%)	34 (4%)	NA	NA
M14	NA	NA	80 (4%)	58 (4%)	NA	NA
M15	NA	NA	78 (9%)	48 (10%)	NA	NA
M16	>100	NA	52 (4%)	42 (5%)	NA	NA
M18	>100	>100	42 (4%)	41 (4%)	NA	NA
P-36	>100	>100	74 (5%)	53 (4%)	NA	NA

Results are expressed as μM and are the mean value from triplicate incubations.
CV: coefficient of variation of the estimates in percentage
NA: not assessed (no inhibition found at any of the assayed concentrations, up to 100 μM letrozole and 20 μM exemestane)

Table 16 shows the estimated IC_{50} values for anastrozole corresponding to each irosustat metabolite. IC_{50} values ranged from 38 μM to 100 μM without preincubation and from 34 μM to 83 μM after the 30-min preincubation. Comparatively, M13 showed the most inhibited formation rate. The enzyme activity inhibitors specific for CYP2C8, CYP2C9, and CYP3A4/5, i.e., quercetin, sulfaphenazole and ketoconazole, respectively, worked as expected in inhibiting the formation of irosustat metabolites (see previous results of determination of the human P450 enzymes responsible for the metabolism of irosustat).

5. DISCUSSION

Irosustat, also known as BN83495, 667 COUMATE, or STX64, is a first-generation irreversible steroid sulfatase (STS) inhibitor for steroid hormone-dependent cancer therapy, and it is currently under clinical development. Irosustat structure is a tricyclic coumarin-based sulfamate, which undergoes desulfamoylation, leading to the formation of its main degradation product and also metabolite, 667-coumarin. 667-Coumarin is inactive because the sulfamate group is indispensable for its STS inhibitory activity.

During the development of new drugs, metabolism studies are performed to provide important data about the safety of a drug. The metabolism of a drug is understood as a set of biochemical reactions that produce changes on the drug chemical structure usually leading to facilitate its elimination. Most of these metabolic changes occur through two types of reactions called phase I and phase II reactions.

The knowledge of the enzymes involved in the metabolism of a drug, and the effect of this drug on enzymes that metabolize other drugs, enables us to make predictions about possible interactions with other concomitant medications. In addition, the comparative metabolite profile in different species in respect to man helps to determine the most suitable species for toxicological studies, and also to provide valuable foresight on metabolic pathways in humans.

In the first part of the present work, the metabolic profile, the preliminary metabolite identification, and the potential species differences in the in vitro metabolism of irosustat were characterized using pooled liver microsome preparations from rats, dogs, monkeys and humans; and hepatocytes from rats, dogs and humans. The use of liver microsomes allowed us to study phase I metabolism, whereas the incubations of irosustat with hepatocytes let us to study both phase I and phase II metabolic transformations.

In the second part of the present work, the enzymes participating in the irosustat metabolism and the in vitro inhibition / induction potential of irosustat on drug metabolism enzymes were evaluated in order to predict clinical drug-drug interactions between irosustat and other possible concomitant medications that may be used in the intended patient populations. The inhibition experiments were performed on the nine major human liver drug-metabolizing P450 isoforms: CYP1A2, CYP2A6, CYP2B6, CYP2C8, CYP2C9, CYP2C19, CYP2D6, CYP2E1, and CYP3A4/5, using incubations

of human liver microsomes (HLM) with CYP probe substrates. Moreover, the potential inhibitory effect of irosustat on the three main UDP glucuronosyltransferase (UGT) isoforms involved in drug metabolism: UGT1A1, UGT1A4, and UGT2B7 was also studied using recombinant enzymes. Finally, the induction study was performed on the four major inducible human P450 isoforms in the liver: CYP1A2, CYP2C9, CYP2C19, and CYP3A4/5, using freshly isolated human hepatocytes.

Aromatase and STS are considered as the key enzymes for the two main pathways of estrogen synthesis in peripheral tissues from postmenopausal women in whom breast cancer most frequently occurs. The aromatase pathway is already targeted in breast cancer treatment by widely prescribed aromatase inhibitors (AIs) such as letrozole, anastrozole, and exemestane. Since AIs are potential concomitant medications of irosustat in clinical use, the prediction of possible interactions between these drugs and irosustat was also assessed investigating the effect of these AIs on irosustat metabolism in HLM.

Irosustat was extensively metabolized in vitro in liver microsomes and hepatocytes. Its metabolite profile was similar among the species tested and between sexes. However, marked differences were found between both in vitro systems, meaning that phase I and phase II enzymes are involved in irosustat metabolism.

Various monooxidized metabolites of irosustat (primary metabolites) and of its desulfamoylated derivative 667-coumarin (secondary metabolites) were formed in liver microsomes; therefore, oxidation was the predominant route of irosustat phase I metabolism. The most abundant monooxidized metabolites were identified by NMR, showing hydroxyl groups at different carbon atoms of the cycloheptane ring. As shown in Table 3 and Figure 16, the main primary phase I metabolites were M7, M13, and M14 (10-hydroxy-, 8-hydroxy-, and 12-hydroxy-irosustat, respectively), and the corresponding secondary phase I metabolites were M8, M16, and M15 (10-hydroxy-, 8-hydroxy-, and 12-hydroxy-667-coumarin, respectively). On the other hand, the main metabolites in hepatocyte incubations were formed by phase II metabolic enzymes. This fact was further demonstrated by LC-MS analysis. Rat, dog, and human hepatocytes mainly converted irosustat to 667-coumarin and to 3-O-glucuronide and 3-O-sulfate conjugates of 667-coumarin (M12 and M17, respectively). In human hepatocytes, M1 and M2 derivatives were also formed and were identified as glucuronides of metabolites M11 and M16 (both 667-coumarin derivatives), respectively. However, the chemical

structures of M1 and M2 were not fully determined. Because hepatocytes are a more physiologically significant in vitro model, a high relevance of phase II metabolism is anticipated in vivo.

The comparison of the microsomal metabolites of irosustat allowed us to detect metabolic similarities between animal species and humans. These results were helpful in the selection of non-rodent species for toxicity evaluation. Qualitatively, all phase I human metabolites were formed by dog microsomes except for metabolite M11. Nevertheless, M11 was formed in rats, indicating that no unique human metabolites were formed in liver microsomes, and therefore no safety concerns were anticipated from the in vitro data. Quantitatively, the following rank order was established among species regarding irosustat $Cl_{int,app}$ (Table 4): monkey >> rat > dog ≥ humans. The fastest metabolism rate in monkeys was associated with increased production of metabolites M7 and M8 compared with those of the other species (see Table 3). As a conclusion, the dog was the species that showed the metabolic pattern closest to that of humans.

Under in vitro incubation conditions (at 37°C and pH 7.4), 667-coumarin was the major degradation product of irosustat formed by hydrolysis of the sulfamoyl ester group. Desulfamoylation in aqueous solution probably occurs via the E1cB elimination reaction, assisted by the extended conjugation present in the coumarin motif (Lloyd et al., 2005). However, the results of the present work showed how incubations of irosustat with microsomes in the absence of cofactor produced increased amounts of 667-coumarin compared with incubations of irosustat in buffer alone (Table 4), demonstrating that 667-coumarin can be also formed by non-NADPH-dependent enzymatic hydrolysis. Therefore, 667-coumarin may be considered as a metabolite and not only as a degradation product. Moreover, 667-coumarin was previously described to be a product resulting after STS inhibition by irosustat (Woo et al., 2000). Because the STS enzyme is present in liver microsomes (Kauffman et al., 1998), STS is a probable candidate for the enzymatic formation of 667-coumarin.

To support the clinical development of irosustat, we evaluated in vitro the enzymes capable of metabolizing irosustat, its inhibitory potential for the main drug-metabolizing P450s and UGTs, and its ability to induce CYP1A2, CYP3A4, CYP2C9, and CYP2C19. The desulfamoylated irosustat metabolite 667-coumarin was included in some of the investigations. The effects of the most-frequently prescribed aromatase inhibitors in breast cancer on irosustat metabolism were also studied.

Once the main metabolites of irosustat were identified and in consideration of the various phase I and phase II reactions involved, the enzymes capable of metabolizing irosustat were carefully evaluated. Figure 20 summarizes the in vitro metabolism pathways of irosustat including the enzymes considered to be most probably responsible for its primary metabolism (those showing positive results in the correlation, inhibition, and recombinant enzyme approaches): M7 was formed by CYP2C9 and CYP2E1, M9 by CYP2C8, M13 by CYP2C8, CYP2C9, and CYP3A4/5, M14 by CYP3A4/5, and M18 by CYP2C9.

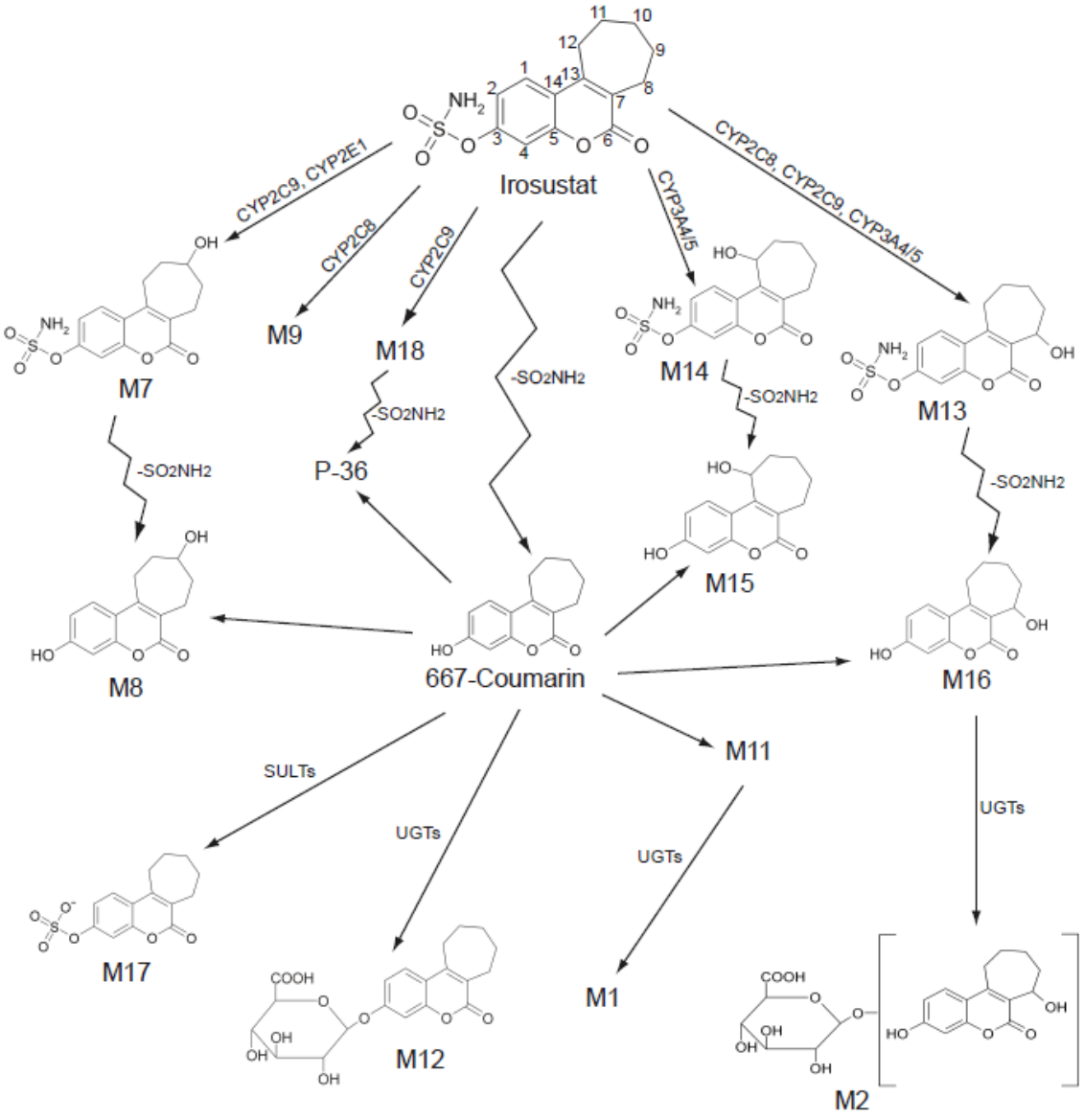

Figure 20. Structures of irosustat metabolites formed in vitro and proposed enzymatic pathways in humans.

Although the secondary metabolites M8, M11, M16, and P-36 were included in the phenotyping experiments, the enzymes involved in their formation should be considered as not fully elucidated because desulfamoylated derivatives can be formed by two sequential reactions: (1) Irosustat hydroxylation and further hydrolysis of the sulfamoyl group or (2) loss of the sulfamoyl group followed by hydroxylation. These two ways were demonstrated in the present work: first, by converting hydroxylated irosustat metabolites into their respective 667-coumarin counterparts by incubation at neutral pH and at 37°C; and second, by direct incubation of 667-coumarin with rat microsomes and hepatocytes (Figure 17) and with recombinant human P450s.

Because of the structural similarities between irosustat and 667-coumarin, it is likely that the same enzymes could be involved in the transformation of both compounds. From the correlation and chemical inhibition tests (Tables 5 and 6), no relevant differences in phenotyping between the primary metabolites and the respective secondary metabolites were obtained, except for CYP2E1, which is related to M7 formation but not to M8. In the recombinant P450s approach (Table 7), irosustat and 667-coumarin were transformed by almost the same enzymes. However, some main differences were found: (1) CYP2A6 was able to metabolize 667-coumarin but not irosustat; (2) CYP2C9 was able to metabolize irosustat but not 667-coumarin; and (3) CYP2B6 formed M16 from 667-coumarin but was not able to form M13 from irosustat. These different capabilities of CYP2A6, CYP2B6, and CYP2C9 to metabolize irosustat and 667-coumarin were considered as not relevant, given the high number of enzymes involved in the metabolism of both compounds.

Surprising results were obtained for CYP1A2 and CYP2C19 enzymes when the recombinant P450s approach was assessed. The incubation of irosustat with CYP1A2 Supersomes showed that this enzyme was able to produce a metabolite profile very similar to the one obtained by pooled HLM. However, the two specific CYP1A2 activities measured in the 16 individual HLM batches, 7-ethoxyresorufin O-dealkylation and phenacetin O-deethylation, did not correlate with the formation of any of the irosustat metabolites. In addition, the CYP1A2 mechanism-based inhibitor furafylline (1 μM) had no effect on inhibiting the metabolism of irosustat in pooled HLM. The inhibition was also assessed using a 10-fold increased furafylline and 10-fold reduced irosustat concentration with similar results (data not shown). Furthermore, the extent of inhibition of furafylline on irosustat metabolism was studied comparatively in incubations with native HLM and CYP1A2-fortified HLM in the additional presence of

other CYP-specific inhibitors (Table 8). As expected, irosustat metabolism was markedly decreased in both HLM models in the presence of a combination of P450-specific inhibitors, confirming that irosustat is metabolized by diverse P450 isoforms. In contrast, furafylline (either alone or in combination with the mix of P450-inhibitors) showed a negligible effect in native HLM, whereas in CYP1A2-fortified HLM, it essentially enhanced the inhibition induced by the other P450-inhibitors, meaning that several P450s must be affected at the same time to produce any potential metabolic interaction outcome. Concerning CYP2C19, the S-mephenytoin 4'-hydroxylation activity in 15 individual HLM batches (one was considered as an outlier) correlated with the formation of some of the irosustat metabolites in HLM. In addition, the incubation of irosustat with recombinant CYP2C19 also produced several irosustat metabolites. However, the two specific CYP2C19 inhibitors used, (+)-nootkatone and (+)-N-3-benzyl-nirvanol (Tassaneeyakul et al., 2000; Suzuki et al., 2002), did not inhibit the formation of any irosustat metabolite in the pooled HLM model. Overall, CYP1A2 and CYP2C19 enzymes were considered as not relevant in irosustat metabolism when other P450 enzymes are present and active, although a minor role cannot be completely discarded (i.e., a weak contribution of CYP1A2 in the case of overexpression or induction).

From the phenotyping results, we may conclude that, even if coadministered drugs inhibit one of the identified drug-metabolizing enzymes, the pharmacokinetics of irosustat is unlikely to be affected because of probable metabolic compensatory mechanisms produced by other P450 isoforms.

When irosustat phase I metabolites were incubated with different cDNA-expressed UGTs and SULTs (Tables 9 and 10), up to nine different glucuronides and eight sulfates were produced, respectively. Although the actual role of each phase II enzyme was not fully clarified, phase II metabolism is a secondary pathway in irosustat metabolism and can only occur after phase I transformation of the parent compound or after formation of 667-coumarin or any of its hydroxylated metabolites. Therefore, although highly involved in the overall drug disposition process, phase II enzymes would neither influence irosustat clearance nor be the target enzymes involved in possible drug-drug interaction processes, unless the biological activity of any of the phase I metabolites was demonstrated.

Once identified the enzymes capable of metabolizing irosustat, its inhibitory potential for the main drug-metabolizing P450s and UGTs was then evaluated. The hepatic P450s whose activity was inhibited most by irosustat were CYP1A2 and CYP2C19 (Table 11), for which the effect of 667-coumarin was also evaluated (Table 12).

667-Coumarin was a more potent inhibitor of CYP2C19 activity than irosustat. No differences appeared between conditions with and without preincubation, which indicated the absence of TDI. The metabolite profile for irosustat was determined in some samples with HPLC, which showed a decrease in the irosustat concentration after preincubation, whereas 667-coumarin levels remained nearly constant (results not shown); this finding is attributable to the fact that 667-coumarin is formed from irosustat through a non–NADPH-dependent process that is balanced by its own P450-mediated metabolism. These data indicate that 667-coumarin probably causes CYP2C19 inhibition in HLMs. In fact, 667-coumarin is a competitive inhibitor of CYP2C19 and exhibits a K_i of 5.8 μM (Table 12), a concentration approximately 40 times the highest 667-coumarin $C_{max,ss}$ in humans after administration of the recommended dose of irosustat (40 mg/day; Coombes et al., 2013). When irosustat was incubated with human hepatocytes, significant, non–dose-dependent inhibition of CYP2C19 enzyme activity was observed (30–60% inhibition at irosustat concentrations as low as 0.25 μM) (Figure 18). Therefore, the results obtained with HLMs are not sufficient to explain the remarkable effect on CYP2C19 in hepatocytes, even considering that all irosustat is transformed to 667-coumarin. Furthermore, the *CYP2C19* mRNA content in hepatocytes was not affected by exposure to irosustat, which indicates no repression of the *CYP2C19* gene (Figure 19). Because the metabolism of irosustat by hepatocytes is markedly different from the profile with HLMs, basically consisting of conjugation with glucuronic acid and sulfate, an inhibitory effect of any irosustat phase II metabolite might explain the strong inhibition of CYP2C19 activity. Moreover, hepatocytes represent a more-complex test system than microsomes, therefore the possibility of other mechanisms (e.g., involvement of hepatic drug transporters, leading to increased intracellular concentrations of test compounds or metabolites) cannot be excluded. Further studies are needed to investigate the mechanisms underlying CYP2C19 inhibition by irosustat or any of its metabolites.

The inhibition of CYP1A2 activity by irosustat and 667-coumarin in HLMs was remarkably higher than the inhibition showed for CYP2C19 (Tables 11 and 12). Again,

667-coumarin showed greater inhibition potential than its parent compound. In this case, clear differences were found between the two incubation conditions, which required additional experiments. As shown in Table 13, inhibition of CYP1A2 activity by irosustat increased with the preincubation time in an NADPH-independent manner, which suggests a role for 667-coumarin in CYP1A2 inhibition, because only 667-coumarin can be formed from irosustat in the absence of NADPH. This was further demonstrated by using HLMs incubated with 667-coumarin, which caused a 40% decrease in CYP1A2 activity in the absence of NADPH, regardless of the preincubation time. However, inhibition of CYP1A2 activity increased by 30% after a 30-min preincubation with NADPH, which was reversed by dilution. Therefore, we concluded that CYP1A2 inhibition is probably mediated by 667-coumarin and by its metabolites acting as reversible inhibitors (Ogilvie et al., 2008; Grimm et al., 2009). 667-coumarin is a competitive CYP1A2 inhibitor with a K_i value of 0.77 μM (Table 12), a concentration that exceeds by only 5-fold the highest $C_{max,ss}$ value measured in humans after administration of the recommended dose of irosustat. These data indicate that DDIs are possible in the clinical setting as a result of CYP1A2 inhibition, in cases of comedication of irosustat with CYP1A2 drug substrates (FDA, 2006). Moreover, the lower IC_{50} values for 667-coumarin observed when preincubated with NADPH (Table 12) strongly suggest that some 667-coumarin phase I metabolites are even more-potent CYP1A2 inhibitors. These results highlight the need for clinical evaluation of DDIs between irosustat and CYP1A2 drug substrates.

CYP2B6, CYP2C9, CYP2D6, and CYP3A4/5 activities were inhibited by irosustat only at the highest concentration assayed (50 μM) (Table 11). This inhibition is not clinically relevant, because 50 μM irosustat represents ~ 120 times the $C_{max,ss}$ in humans. As shown in Table 13, CYP2B6 and CYP3A4/5 activities were inhibited in a time-dependent manner, but the presence of NADPH did not enhance inhibition, meaning that no mechanism-based inhibition was involved. 667-coumarin is not likely to inhibit these enzymes in vivo in humans. The remaining P450s, i.e., CYP2A6, CYP2C8, CYP2E1, and CYP3A4/5 (nifedipine as substrate), were not affected by irosustat.

On the basis of UGT inhibition data (Tables 14 and 15), neither irosustat nor 667-coumarin are likely to affect the activity of the main drug-metabolizing UGTs (Williams et al., 2004). UGT1A1 was the most-inhibited enzyme, but the IC_{50} values for

irosustat and 667-coumarin for the inhibition of this enzyme were far from their clinically relevant plasma concentrations. The greater inhibitory potential of 667-coumarin towards UGT1A1 and UGT2B7 activities as compared with irosustat, could be explained by the fact that 667-coumarin is a relevant substrate of these enzymes which catalyse its glucuronide conjugation to form one of the main metabolites found in hepatocytes (M12).

The CYP induction potential of irosustat was also evaluated in the present work (Figure 18). Irosustat at up to 10 µM did not induce CYP1A2, CYP2C9, CYP2C19, or CYP3A4/5, following the criteria described in current guidelines [positive induction when enzyme activity or mRNA levels are >40% of positive control values (Food and Drug Administration, 2006) or positive induction when enzyme activity is >50% or mRNA levels are >20% of positive control values (European Medicines Agency, 2010)]. None of the results showed an increase in enzyme activity greater than 1.5-fold except for hepatocyte batch HEP200124 exposed to 2.5 µM irosustat, which exhibited 1.6-fold greater CYP1A2 activity, but this represented only 12.3% of the response to the positive control omeprazole. The inhibition of CYP2C19 activity found in human hepatocytes is discussed above.

Because AIs are expected to be potentially used in combination with irosustat for treatment of breast cancer, the prediction of possible DDIs between AIs and irosustat becomes a key factor in irosustat development. On the basis of literature reports, the three primarily prescribed AIs, i.e., letrozole (http://www.pharma.us.novartis.com/product/pi/pdf/Femara.pdf), anastrozole (Scripture and Figg, 2006), and exemestane (http://www.pfizer.com/files/products/uspi_aromasin.pdf) are metabolized mainly by CYP3A4. CYP2A6 also seems to contribute to letrozole biotransformation. A role for CYP1A enzymes has been suggested for exemestane metabolism, together with CYP4A11 and aldoketoreductases, in a process in which compensatory contributions of the various enzymes may occur (Kamdem et al., 2011). Data from the present work demonstrated neither inhibition of CYP3A4 and CYP2A6 activity nor induction of CYP3A4 by irosustat at clinically relevant concentrations. However, because AIs could theoretically inhibit P450s involved in irosustat metabolism, their effects were studied in incubations of irosustat with HLMs (Table 16). Letrozole showed almost no effect on irosustat metabolism (IC_{50} values were >100 µM for all irosustat metabolites), and

exemestane did not inhibit irosustat metabolism at up to 20 µM. In both cases, these concentrations exceed by 200-fold the respective $C_{max,ss}$ values in humans (Pfister et al., 2001; Groenewoud et al., 2010). By contrast, anastrozole was slightly more potent than the other two AIs in inhibiting irosustat metabolism, showing IC_{50} values between 34 and >100 µM, depending on the irosustat metabolite (Table 16). Taking into account the IC_{50} values, the K_i value for the inhibition of irosustat metabolism by anastrozole should be in the worst case approximately one half of the IC_{50} when the substrate concentration in the experiments is close to its K_M (Cheng and Prusoff, 1973), as in the present work. In a conservative estimation, our IC_{50} data indicate that the K_i would be not lower than 10 to 20 µM, a concentration 30-fold higher than the $C_{max,ss}$ of anastrozole after administration of a standard daily dose of 1 mg (Grimm and Dyroff, 1997). Together, these results indicate that no changes in irosustat pharmacokinetics are anticipated as a result of metabolism inhibition in the case of comedication with AIs.

To summarize, multiple irosustat metabolic pathways including desulfamoylation, primary and secondary metabolism, and phase I and phase II reactions were involved in the metabolism of irosustat in liver microsomes and hepatocytes from several species. Irosustat and 667-coumarin are primarily metabolized towards a number of hydroxylated derivatives detected in incubations with liver microsomes from preclinical species and humans. These metabolites and also 667-coumarin are further conjugated with sulfate and/or glucuronic acid. CYP2C8, CYP2C9, CYP3A4/5, and to a lesser extent CYP2E1, were identified as the main enzymes responsible for the primary transformation of irosustat. Although improbable, a minor contribution of CYP1A2 and CYP2C19 may not be fully discarded. Since a number of recombinant phase II enzymes were tested with positive results, their actual clinical relevance could not be clarified. However, glucuronide and sulfate conjugation reactions are secondary to phase I transformation of irosustat or 667-coumarin formation, and, therefore, they should not influence irosustat clearance. The data presented in this work strongly suggest that irosustat is not likely to inhibit or to induce most of the P450 enzymes involved in drug metabolism the clinical setting, except for inhibiting CYP1A2 and CYP2C19. The irosustat derivative 667-coumarin notably inhibited CYP1A2 activity in HLMs at clinically relevant concentrations. The inhibition was reversible and probably enhanced by 667-coumarin metabolites. Clinical interaction studies on CYP1A2 are recommended. Irosustat inhibited CYP2C19 activity in HLMs

in a lesser extent through the formation of 667-coumarin. Because CYP2C19 enzyme activity inhibition largely increased when assessed in human hepatocytes while *CYP2C19* gene expression was not affected, additional mechanistic and/or clinical follow-up studies are needed to explain CYP2C19 inhibition by irosustat. Irosustat did not show any inhibitory effect on the activity of UGT1A1, UGT1A4, and UGT2B7 enzymes. Finally, because the AIs letrozole, anastrozole, and exemestane are potential candidates for irosustat combination therapy, prediction of possible DDIs between AIs and irosustat was studied. On the basis of published data, no effect of irosustat on the pharmacokinetics of these drugs is anticipated. The results of the present work demonstrate that the aforementioned AIs are not able to inhibit the formation of the primary irosustat metabolites at clinically relevant concentrations. Consequently, no change in irosustat metabolism is expected to occur in vivo. The in vitro studies presented in this work have also been useful in identifying potential metabolites of irosustat and in obtaining valuable information for planning and interpreting future toxicology and in vivo metabolism of irosustat.

All these results have been recently published: Ventura et al., 2011 and Ventura et al., 2012.

6. CONCLUSIONS

CONCLUSIONS

1. Irosustat is extensively metabolized in vitro, both in liver microsomes and hepatocytes. Marked differences were found between both in vitro systems, meaning that phase I and phase II enzymes are involved in irosustat metabolism.

2. Although the metabolite profile of irosustat was similar among the species tested and between sexes, the dog was the species that showed the metabolic pattern closest to that of humans.

3. The main phase I metabolites were identified as mono-hydroxylations of irosustat and 667-coumarin. The main phase II metabolites were identified as glucuronide and sulfate conjugates of 667-coumarin or its monohydroxylated metabolites

4. 667-Coumarin was the major degradation product of irosustat formed by hydrolysis of the sulfamoyl ester group. 667-coumarin can be also formed by non-NADPH-dependent enzymatic hydrolysis. Therefore, 667-coumarin may be considered as a metabolite and not only as a degradation product.

5. The human enzymes considered to be responsible for irosustat primary metabolism are: CYP2C8, CYP2C9, CYP3A4/5 and to a lesser extent CYP2E1. CYP1A2 and CYP2C19 enzymes were considered as not relevant in irosustat metabolism when other P450 enzymes are present and active, although a minor role cannot be completely discarded. The formation of most of the primary metabolites can be catalyzed by two or more P450 enzymes, meaning that compensatory mechanisms in irosustat metabolism are likely to occur in vivo, minimizing the risk of interactions due to P450 inhibition by co-administered drugs or dietary constituents.

6. The hepatic P450s whose activity was inhibited most by irosustat were CYP1A2 and CYP2C19, for which 667-coumarin was a more potent inhibitor. The inhibition of CYP1A2 activity by irosustat and 667-coumarin in HLMs was

remarkably higher than that of CYP2C19 and the inhibition was reversible and probably enhanced by 667-coumarin metabolites. Clinical interaction studies on CYP1A2 are recommended. For CYP2C19, its inhibition exhibited large increases when assessed in human hepatocytes instead of HLM but *CYP2C19* gene expression was not affected. Further studies are needed to investigate the mechanisms underlying CYP2C19 inhibition by irosustat or any of its metabolites.

7. Neither irosustat nor 667-coumarin is likely to inhibit the activity of the main drug-metabolizing UGTs: UGT1A1, UGT1A4 and UGT2B7 enzymes.

8. Irosustat did not induce CYP1A2, CYP2C9, CYP2C19, or CYP3A4/5.

9. No changes in irosustat metabolism are anticipated as a result of irosustat metabolism inhibition in the case of comedication with the aromatase inhibitors letrozole, anastrozole and exemestane.

7. REFERENCES

REFERENCES

Baltes MR, Dubois JG, and Hanocq M (1998) Ethyl acetate extraction procedure and isocratic high-performance liquid chromatographic assay for testosterone metabolites in cell microsomes. *J Chromatogr B Biomed Sci Appl* 706:201-207.

Bohnert T and Gan LS (2010) The role of drug metabolism in drug discovery, in *Enzyme Inhibition in Drug Discovery and Development: The Good and the Bad* (Lu C and Li AP eds) pp 91-176, Wiley, New Jersey.

Bojarová P, Denehy E, Walker I, Loft K, De Souza DP, Woo LW, Potter BV, McConville MJ, and Williams SJ (2008) Direct evidence for ArO-S bond cleavage upon inactivation of Pseudomonas aeruginosa arylsulfatase by aryl sulfamates. *Chembiochem* 9(4):613-623.

Boxenbaum HG, Riegelman S, and Elashoff RM (1974) Statistical estimations in pharmacokinetics. *J Pharmacokinet Biopharm* 2(2):123-48.

Cheng YC and Prusoff WH (1973) Relationship between the inhibition constant (K_i) and the concentration of inhibitor which causes 50 per cent inhibition (I_{50}) of an enzymatic reaction. *Biochem Pharmacol* 22:3099–3108.

Coombes RC, Cardoso F, Isambert N, Lesimple T, Soulié P, Peraire C, Fohanno V, Kornowski A, Ali T and Schmid P (2013) A phase I dose escalation study to determine the optimal biological dose of irosustat – an oral steroid sulfatase inhibitor – in postmenopausal women with estrogen receptor-positive breast cancer. *Breast Cancer Research and Treatment (accepted for publication)*.

Curi-Pedrosa R, Daujat M, Pichard L, Ourlin JC, Clair P, Gervot L, Lesca P, Domergue J, Joyeux H, Fourtanier G, and Maurel P (1994) Omeprazole and lansoprazole are mixed inducers of CYP1A and CYP3A in human hepatocytes in primary culture. *J Pharmacol Exp Ther* 269(1):384-392.

Daujat M, Peryt B, Lesca P, Fourtanier G, Domergue J, and Maurel P (1992) Omeprazole, an inducer of human CYP1A1 and 1A2, is not ligand for the Ah receptor. *Biochem Biophys Res commun* 188: 820-825.

Dayer P, Leemann T, and Striberni R (1989) Dextromethorphan O-demethylation in liver microsomes as a prototype reaction to monitor cytochrome P450 db1 activity. *Clin Pharmacol Ther* 45(1):34-40.

Dekant W, Frischmann C, and Speerschneider P (1995) Sex, organ and species specific bioactivation of chloromethane by cytochrome P4502E1. *Xenobiotica* 25:1259-1265.

Distlerath LM, Reilly PE, Martin MV, Davis GG, Wilkinson GR, and Guengerich FP (1985) Purification and characterization of the human liver cytochromes P-450 involved in debrisoquine 4-hydroxylation and phenacetin O-deethylation, two prototypes for genetic polymorphism in oxidative drug metabolism. *J Biol Chem* 260: 9057-9067.

European Medicines Agency (2010) Guideline on the Investigation of Drug Interactions (Draft), European Medicines Agency, London.

Food and Drug Administration (2006) Guidance for Industry: Drug Interaction Studies: Study Design, Data Analysis, and Implications for Dosing and Labelling (Draft), Food and Drug Administration, Washington, DC.

Fasco MJ and Principe LM (1980) Vitamin K1 Hydroquinone Formation Catalyzed by a Microsomal Reductase System. *Biochem Biophys Res Commun* 97:1487-1492.

Fasco MJ and Principe LM (1982) R- and S-Warfarin Inhibition of Vitamin K and Vitamin K 2,3-Epoxide Reductase Activities in the Rat. *J Biol Chem* 257:4894-4901.

Fasco MJ, Hildebrandt EF, and Suttie JW (1982) Evidence that Warfarin Anticoagulant Action Involves Two Distinct Reductase Activities. *J Biol Chem* 257:11210-11212.

Fasco MJ, Preusch PC, Hildebrandt E, and Suttie JW (1983) Formation of Hydroxyvitamin K by Vitamin K Epoxide Reductase of Warfarin-resistant Rats. *J Biol Chem* 258:4372-4380.

Foster PA, Newman SP, Chander SK, Stengel C, Jhalli R, Woo LWL, Potter BVL, Reed MJ, and Purohit A (2006) In vivo efficacy of STX213, a second-generation steroid sulfatase inhibitor, for hormone-dependent breast cancer therapy. *Clin Cancer Res* 12:5543–5549.

Foster PA (2008) Steroid metabolism in breast cancer. *Minerva Endocrinol* 33:27-37.

Galetin A, Clarke SE, and Houston JB (2002) Quinidine and haloperidol as modifiers of CYP3A4 activity: multisite kinetic model approach. *Drug Metab Dispos* 30:1512-1522.

Gibson G and Skett P (2001) *Introduction to Drug Metabolism,* 3rd ed., Nelson Thornes, Cheltenham, United Kingdom.

Girault I, Rougier N, Chesné C, Lidereau R, Beaune P, Bieche I, and de Waziers I (2005) Simultaneous measurement of 23 isoforms from the human cytochrome P450 families 1 to 3 by quantitative reverse transcriptase-polymerase chain reaction. *Drug Metab Dispos* 33(12):1803-1810.

Goldstein JA, Faletto MB, Romkes-Sparks M, Sullivan T, Kitareewan S, Raucy JL, Lasker JM, and Ghanayem BI (1994) Evidence that CYP2C19 is the major (S)-mephenytoin 4'-hydroxylase in humans. *Biochemistry* 33(7):1743-1752.

Gomez-Lechon MJ, Donato MT, Ponsoda X, Jover R, and Castell JV (1992) Experimental in vitro models to evaluate hepatotoxicity, in In Vitro Alternatives to Animal Pharmaco-toxicology (Castell JV and Gomez-Lechon MJ eds) pp 92-107, Farmaindustria, Madrid.

Grimm SW and Dyroff MC (1997). Inhibition of human drug metabolizing cytochromes P450 by anastrozole, a potent and selective inhibitor of aromatase. *Drug Metab Dispos* 25(5):598-602.

Grimm SW, Einolf HJ, Hall SD, He K, Lim HK, Ling KH, Lu C, Nomeir AA, Seibert E, Skordos KW, Tonn GR, Van Horn R, Wang RW, Wong YN, Yang TJ, and Obach RS (2009) The conduct of in vitro studies to address time-dependent inhibition of drug-metabolizing enzymes: a perspective of the pharmaceutical research and manufacturers of America. *Drug Metab Dispos* 37(7):1355-1370.

Groenewoud G, Nell A, Potgieter L, Seiler D, and Wettmarshausen C (2010) Bioequivalence of exemestane in post-menopausal females. *Arzneimittelforschung* 60(2):96-100.

Guengerich FP, Martin MV, Beaune PH, Kremers P, Wolff T, and Waxman DJ (1986) Characterization of rat and human liver microsomal cytochrome P-450 forms involved in nifedipine oxidation, a prototype for genetic polymorphism in oxidative drug metabolism. *J Biol Chem* 261:5051-5060.

Ho YT, Purohit A, Vicker N, Newman SP, Robinson JJ, Leese MP, Ganeshapillai D, Woo LWL, Potter BVL, and Reed MJ (2003) Inhibition of carbonic anhydrase II by steroidal and non-steroidal sulphamates. *Biochem Biophys Res Commun* 305:909-914.

Huizing MT, Sparreboom A, Rosing H, van Tellingen O, Pinedo HM, and Beijnen JH (1995) Quantification of paclitaxel metabolites in human plasma by high-performance liquid chromatography. *J Chromatogr B Biomed Appl* 674:261-268.

Ireson CR, Parish D, Purohit A, Woo LWL, Potter BVL, Chander SK, and Reed MJ (2003) Development of a sensitive high performance liquid chromatography method for the detection of 667-Coumate in vivo. *J Steroid Biochem Mol Biol* 84(2-3):337-342.

Ireson CR, Chander SK, Purohit A, Parish DC, Woo LWL, Potter BVL, and Reed MJ (2004) Pharmacokinetics of the Nonsteroidal Steroid Sulphatase Inhibitor 667 COUMATE and its sequestration into Red Blood Cells in Rats. *Br J Cancer* 91(7):1399-404.

James VHT, McNeill JM, Lai LC, Newton CJ, Ghilchik MW, and Reed MJ (1987) Aromatase activity in normal breast and breast tumor tissues: in vivo and in vitro studies. *Steroids* 50:269–279.

Jeong S, Woo MM, Flockhart DA, and Desta Z (2009). Inhibition of drug metabolizing cytochrome P450s by the aromatase inhibitor drug letrozole and its major oxidative metabolite 4,4'-methanol-bisbenzonitrile in vitro. *Cancer Chemother Pharmacol* 64(5):867-875.

Kamdem LK, Flockhart DA, and Desta Z (2011) In vitro cytochrome P450-mediated metabolism of exemestane. *Drug Metab Dispos* 39:98-105.

Kauffman FC, Sharp S, Allan BB, Burchell A, and Coughtrie MWH (1998) Microsomal steroid sulfatase: interactions with cytosolic steroid sulfotransferases. *Chem Biol Interact* 109(1-3):169-182.

Kawano S, Kamataki T, Yasumori T, Yamazoe Y, and Kato R (1987) Purification of human liver cytochrome P-450 catalyzing testosterone 6 beta-hydroxylation. *J Biochem* 102(3):493-501.

Kenworthy KE, Bloomer JC, Clarke SE, and Houston JB (1999) CYP3A4 drug interactions: correlation of 10 in vitro probe substrates. *Br J Clin Pharmacol* 48:716-727.

Lake BG (1987) Preparations and Characterization of Microsomal Fractions for Studies on Xenobiotics Metabolism, in Biochemical toxicology: a practical approach (Snell K and Mullock B eds) pp 183-215, IRL Press, Oxford, Washington DC.

Li T, Chang CY, Jin DY, Lin PJ, Khvorova A, and Stafford DW (2004) Identification of the Gene for Vitamin K Epoxide Reductase. *Nature* 427:541-544.

Lin JH (2006) CYP Induction-Mediated Drug Interactions: in Vitro Assessment and Clinical Implications. *Pharmaceutical Research* 23:1089-1116.

Lloyd MD, Pederick RL, Natesh R, Woo LWL, Purohit A, Reed MJ, Acharya KR, and Potter BVL (2005) Crystal structure of human carbonic anhydrase II at 1.95 Å resolution in complex with 667-coumate, a novel anti-cancer agent. *Biochem J* 385:715-720.

Lowry OH, Roserbrough NJ, Farr AL, and Randall RJ (1951) Protein measurement with the Folin phenol reagent. *J Biol Chem* 193: 265-275.

Meunier V, Bourrié M, Julian B, Marti E, Guillou F, Berger Y, and Fabre G (2000) Expression and induction of CYP1A1/1A2, CYP2A6 and CYP3A4 in primary cultures of human hepatocytes: a 10-year follow-up. *Xenobiotica* 30(6):589-607.

Michaelis L and Menten M (1913) Die Kinetik der Invertinwirkung, *Biochem Z* 49:333-369.

Miles JS, McLaren AW, Forrester LM, Glancey MJ, Lang MA, and Wolf CR (1990) Identification of the human liver cytochrome P-450 responsible for Coumarin 7-hydroxylation activity. *Biochem J* 267(2):365-371.

Miners JO, Smith KJ, Robson RA, McManus ME, Veronese ME, and Birkett DJ (1988) Tolbutamide hydroxylation by human liver microsomes. Kinetic characterisation and relationship to other cytochrome P-450 dependent xenobiotic oxidations. *Biochem Pharmacol* 37:1137-1144.

Morel F, Beaune PH, Ratanasavanh D, Flinois JP, Yang CS, Guengerich FP, and Guillouzo A (1990) Expression of cytochrome P-450 enzymes in cultured human hepatocytes. *Eur J Biochem* 191(2):437-444.

Mouridsen H, Gershanovick M, Sun Y, Perez-Carrion R, Boni C, Monnier A, Apffelstaedt J, Smith R, Sleeboom HP, Jaenicke F, Pluzanska A, Dank M, Becquart D, Bapsy PP, Salminen E, Snyder R, Chaudri-Ross H, Lang R, Wyld P, and Bhatnagar A (2003) Phase III study of letrozole versus tamoxifen as firstline therapy of advanced breast cancer in postmenopausal women: Analysis of survival and update of efficacy from the international letrozole breast cancer group. *J Clin Oncol* 21:2101–2109.

Nabholtz JM, Bonneterre J, Buzdar A, Robertson JFR, Thurlimann B (2003). Anastrozole (Arimidex) versus tamoxifen as first-line therapy for advanced breast cancer in postmenopausal women: survival analysis and updated safety results. *Eur J Cancer* 39:1684–1689.

Nassar AF, Hollenberg PF and Scatina JA (2009) *Drug Metabolism Handbook: Concepts and Applications,* Wiley, New Jersey, USA.

Nussbaumer P and Billich A (2004) Steroid Sulfatase Inhibitors. *Medicinal Research Reviews* 24(4):529-576.

Ogilvie B, Usuki E, Yerino P and Parkinson A. (2008) Chapter 7: In vitro approaches for studying the inhibition of drug-metabolizing enzymes and identifying the drug-metabolizing enzymes responsible for the metabolism of drugs (reaction phenotyping) with emphasis on cytochrome P450, in Drug-Drug Interactions, (Drugs and the Pharmaceutical Sciences), (Rodrigues D. eds) pp 231-358, Informa Healthcare, Second edition. Xenotech LLC, Lenexa, KS, USA.

Ohnishi ST and Barr JK (1978) A simplified method of quantitating proteins using the biuret and phenol reagents. *Anal Biochem* 86:193.

Omura T and Sato R (1964) The carbon monoxide-binding pigment of liver microsomes. I.-Evidence for its hemoprotein nature. *J Biol Chem* 239(7):2370-2385.

Palmieri C, Januszewski A, Stanway S, and Coombes RC (2011) Irosustat: a first-generation steroid sulfatase inhibitor in breast cancer. *Expert Rev Anticancer* Ther 11(2):179-183.

Paridaens R, Dirix L, Lohrisch C, Beex L, Nooij M, Cameron D, Biganzoli L, Cufer T, Duchatea L, Hamilton A, Lobelle JP, and Piccart M (2003) Mature results of a randomized phase II multicenter study of exemestane versus tamoxifen as first-line hormone therapy for postmenopausal women with metastatic breast cancer. *Ann Oncol* 14:1391–1398.

Pearce RE, McIntyre CJ, Madan A, Sanzgiri U, Draper AJ, Bullock PL, Cook DC, Burton LA, Latham J, Nevins C, and Parkinson A (1996) Effects of freezing, thawing, and storing human liver microsomes on cytochrome P450 activity. *Arch Biochem Biophys* 331(2):145-169.

Pearson PG and Wienkers LC (2009) *Handbook of Drug Metabolism,* 2nd ed., Informa Healthcare, New York, USA.

Pelkonen O, Mäenpää J, Taavitsainen P, Rautio A, and Raunio H (1998) Inhibition and induction of human cytochrome P450 (CYP) enzymes. *Xenobiotica* 28(12):1203-1253.

Peters MM, Walters DG, van Ommen B, van Bladeren PJ, and Lake BG (1991) Effect of inducers of cytochrome P-450 on the metabolism of [3-14C]Coumarin by rat hepatic microsomes. *Xenobiotica* 21(4):499-514.

Peterson GL (1979) Review of the Folin phenol protein quantitation method of Lowry, Rosebrough, Farr, and Randall. *Analytical Biochemistry*, 100: 201-220.

Pfister CU, Martoni A, Zamagni C, Lelli G, De Braud F, Souppart C, Duval M, and Hornberger U (2001) Effect of age and single versus multiple dose pharmacokinetics of letrozole (Femara®) in breast cancer patients. *Biopharm Drug Dispos* 22:191–197.

Pichard L, Fabre I, Fabre G, Domergue J, Saint Aubert B, Mourad G, and Maurel P (1990) Cyclosporin A drug interactions. Screening for inducers and inhibitors of cytochrome P-450 (cyclosporin A oxidase) in primary cultures of human hepatocytes and in liver microsomes. *Drug Metab Dispos* 18(5):595-606.

Purohit A, Woo LWL, Potter BVL, and Reed MJ (2000) In vivo inhibition of estrone sulfatase activity and growth of nitrosomethylurea-induced mammary tumors by 667-COUMATE. *Cancer Res* 60:3394–3396.

Purohit A, Woo LWL, Chander SK, Newman SP, Ireson C, Ho Y, Grasso A, Lees MP, Potter BVL, and Reed MJ (2003) Steroid sulphatase inhibitors for breast cancer therapy. *Journal of Steroid Biochemistry and Molecular Biology* 86:423-432.

Raucy JL, Mueller L, Duan K, Allen SW, Strom S, and Lasker JM (2002) Expression and induction of CYP2C P450 enzymes in primary cultures of human hepatocytes. *J Pharmacol Exp Ther* 302: 475-482.

Reed MJ, Purohit A, Woo LWL, Newman SP, and Potter BVL (2005) Steroid sulfatase: molecular biology, regulation, and inhibition. *Endocr Rev* 26:171–202.

Santner SJ, Feil PD, and Santen RJ (1984) In situ estrogen production via the estrone sulfatase pathway in breast tumors: relative importance vs. the aromatase pathway. *J Clin Endocrinol Metab* 59:29–33.

Scripture CD and Figg WD (2006). Drug interactions in cancer therapy. *Nature Reviews* 6:546-558.

Seglen PO (1976) Preparation of isolated rat liver cells. *Methods Cell Biol* 13:29-83.

Selcer KW, Kabler H, Sarap J, Xiao Z, and Li PK (2002) Inhibition of steryl sulfatase activity in LNCaP human prostate cancer cells. *Steroids* 67(10):821-6.

Stanway SJ, Purohit A, Woo LWL, Sufi S, Vigushin D, Ward R, Wilson RH, Stanczyk FZ, Dobbs N, Kulinskaya E, Elliott M, Potter BVL, Reed MJ, and

Coombes RC (2006) Phase I study of STX 64 (667 Coumate) in breast cancer patients: the first study of a steroid sulfatase inhibitor. *Clin Cancer Res* 12:1585–1592.

Stanway SJ, Delavault P, Purohit A, Woo LWL, Thurieau C, Potter BVL, and Reed MJ (2007) Steroid Sulphatase: A New Target for the Endocrine Therapy of Breast Cancer. *Oncologist* 12:370-374.

Suzuki H, Kneller MB, Haining RL, Trager WF, and Rettie AE (2002) (+)-N-3-benzyl-nirvanol and (-)-N-3-benzyl-phenobarbital: new potent and selective in vitro inhibitors of CYP2C19. *Drug Metab Dispos* 30(3):235-239.

Suzuki T, Nakata T, Miki Y, Kaneko C, Moriya T, Ishida T, Akinaga S, Hirakawa H, Kimura M, and Sasano H (2003) Estrogen sulfotransferase and steroid sulfatase in human breast carcinoma. *Cancer Res* 63:2762-2770.

Tassaneeyakul W, Guo LQ, Fakuda K, Ohta T, and Yamazoe Y (2000) Inhibition Selectivity of Grapefruit juice components on human cytochromes P450. *Arch Biochem Biophys* 378(2):356-363.

Tishler M, Fieser LF, and Wendler NL (1940) Hydro, Oxido and Other Derivatives of vitamin K1 annd Related Compounds. *J Am Chem Soc* 62:2866-2871.

Turpeinen M, Nieminen R, Juntunen T, Taavitsainen P, Raunio H, and Pelkonen O (2004) Selective inhibition of CYP2B6-catalyzed bupropion hydroxylation in human liver microsomes in vitro. *Drug Metab Dispos* 32:626-631.

Uchaipichat V, Mackenzie PI, Elliot DJ, and Miners JO (2006) Selectivity of substrate (trifluoperazine) and inhibitor (amitriptyline, androsterone, canrenoic acid, hecogenin, phenylbutazone, quinidine, quinine, and sulfinpyrazone) “probes” for human UDP-glucuronosyltransferases. *Drug Metab Dispos* 34:449-456.

Uchaipichat V, Mackenzie PI, Guo XH, Gardner-Stephen D, Galetin A, Houston JB, and Miners JO (2004) Human UDP-glucuronosyltransferases: isoform selectivity and kinetics of 4-methylumbelliferone and 1-naphthol glucuronidation, effects of

organic solvents, and inhibition by diclofenac and probenecid. *Drug Metab Dispos* 32:413-423.

Ventura V, Sola J, Celma C, Peraire C, and Obach R (2011) In Vitro Metabolism of Irosustat, a Novel Steroid Sulphatase Inhibitor: Interspecies Comparison, Metabolite Identification, and Metabolic Enzyme Identification. *Drug Metab Dispos* 39:1235-1246.

Ventura V, Sola J, Peraire C, Brée F, and Obach R (2012) In Vitro Evaluation of the Interaction Potential of Irosustat with Drug-Metabolizing Enzymes. *Drug Metab Dispos* 40:1268-1278.

Venkatakrishnan K, von Moltke LL, and Greenblatt DJ (1998) Human cytochromes P450 mediating phenacetin O-deethylation in vitro: validation of the high affinity component as an index of CYP1A2 activity. *J Pharm Sci* 87: 1502-1507.

von Moltke LL, Greenblatt DJ, Schmider J, Duan SX, Wright CE, Harmatz JS, and Shader RI (1996) Midazolam hydroxylation by human liver microsomes in vitro: inhibition by fluoxetine, norfluoxetine, and by azole antifungal agents. *J Clin Pharmacol* 36(9):783-791.

Wallin R and Martin LF (1985) Vitamin K-dependent Carboxylation and Vitamin K Metabolism in Liver. *J Clin Invest* 76:1879-1884.

Weaver RJ (2001) Assessment of drug-drug interactions: concepts and approaches. *Xenobiotica* 31(8-9):499-538.

Whitlon DS, Sadowski JA, and Suttie JW (1978) Mechanism of Coumarin Action: Significance of Vitamin K Epoxide Reductase Inhibition. *Biochemistry* 17:1371-1377.

Wienkers LC and Heath TG (2005) Predicting in vivo drug interactions from in vitro drug discovery data. *Nat Rev Drug Discov* 4:825-833

Williams JA, Hyland R, Jones BC, Smith DA, Hurst S, Goosen TC, Peterkin V, Koup JR, and Ball SE (2004) Drug-Drug Interactions for UDP

Glucuronosyltransferase substrates: a Pharmacokinetic Explanation for Typically Observed Low Exposure (AUCI/AUC) Ratios. *Drug Metab Dispos* 32:1201-1208. Referencia Importancia UGT 1A1, 1A4 and 2B7

Woo LWL, Purohit A, Malini B, Reed MJ, and Potter BVL (2000) Potent active site-directed inhibition of steroid sulphatase by tricyclic Coumarin-based sulphamates. *Chem Biol* 7:773–791

Woo LWL, Purohit A, and Potter BVL (2011) Development of steroid sulfatase inhibitors. *Mol Cell Endocrinol* 340(2):175-85.

Zhang D, Chando TJ, Everett DW, Patten CJ, Dehal SS, and Griffith Humphreys W (2005) In vitro inhibition of UDP glucuronosyltransferases by atazanavir and other HIV protease inhibitors and the relationship of this property to in vivo bilirubin glucuronidation. *Drug Metab Dispos* 33:1729-1739.